Design Of A High Pressure Ratio Transonic Compressor Stage With Active Boundary Layer Control

by

Willy Steve Ziminsky

S.B. Aeronautics and Astronautics, Massachusetts Institute of Technology, 1994

Submitted to the Department of Aeronautics and Astronautics
in partial fulfillment of the requirements for the degree of

Master of Science

at the

MASSACHUSETTS INSTITUTE OF TECHNOLOGY

May 1996

Author..... .....
Department of Aeronautics and Astronautics
May 7, 1996

Certified by..... .....
Professor Jack Kerrebrock
Richard Maclaurin Professor of Aeronautics and Astronautics
Thesis Supervisor

Accepted by..... .....
Professor Harold Y. Wachman
Chairman, Department Graduate Committee

Design Of A High Pressure Ratio Transonic Compressor Stage With Active Boundary Layer Control

by

Willy Steve Ziminsky

Submitted to the Department of Aeronautics and Astronautics
on May 7, 1996, in partial fulfillment of the
requirements for the degree of
Master of Science

Abstract

A design of a high pressure ratio stage with boundary layer suction suitable for a modern gas turbine high pressure spool. Description of parallel experimental research being conducted at the MIT Gas Turbine Lab and details of quasi 3D design methodology used to develop the design. Results indicating that suction levels on the order of 8.5% of inlet mass flow for the stage can conceivably allow operating stagnation pressure ratios higher than 3.

Thesis Supervisor: Professor Jack Kerrebrock
Title: Richard Maclaurin Professor of Aeronautics and Astronautics

Acknowledgments

It's been two years and many projects... And I certainly could not leave the GTL without thanking the many people who were there throughout: from working on the plug-valve with Durali, Guenette and Chris; to working on the BDC with Duncan and JB; to modifying the code with Ali and Prof. Drela; to setting up the reverse flow cascade with Victor and Jimmy. I'd also like to the thank the people that helped make the day to day a little sweeter: from the daily lunch with the wit of Ken and Greg; to ice hockey with Don and Luc; to battling the computers with Dave T. and Ish; to sharing a test cell with Brian C. and Fouzi; to playing basketball with Maverick and Brian T. And of course, how can I not thank the "Old Guard", together since our sophomore year: Julian S. screening the latest comic; Sonia E. taking time to swing or tango; and John K., through classes and projects to rock climbing, diving and sailing. On the home front, I'd like to thank my mom, my dad and my sister; always there and ready to help. Finally I'd like to thank my advisor, Prof. Kerrebrock: his office door never closed and his patience never ran out. Always willing to roll up his sleeves and lend a hand; an engineer, a scientist, a marathon runner, a climber, a diver, a sailor and more. To him my thanks, respect and admiration.

Contents

List of Figures

List of Tables

Chapter 1

Introduction

The axial compressor is a series of ducted bladed discs and wheels whose collective function is to bring the gas up the first leg of the engine's thermodynamic cycle. However the metric of a successful design transcends basic notions of overall pressure ratio and efficiency; for, as a part of an engine that is ultimately designed to be carried aloft, the compressor must satisfy global requirements of length and weight as well. Once the target pressure rise set by the cycle analysis has been obtained and the device exhibits an acceptable range of stable operation, the measure of success becomes the number of stages taken to get there. The direction to be taken then, is to rethink the individual components of the compressor in an effort to enhance their performance and reduce overall system length, weight and cost.

1.1 Loading Limits On Current Designs

The number of stages is subject to the desired thermodynamic efficiency set for the engine and a function of the ability of each stage to deliver a reliable pressure rise. Controlling the pressure rise attainable per stage is the so called loading limit of both rotor and stator; a limit that captures the complex interactions of boundary layer growth and separation, and the ability of the blade to turn the flow [3]. Hence, expanding this limit would revolve around the possibility of influencing the development of the viscous layer in an effort to enhance the capabilities of the foil.

Current designs operate at or near separation, with transonic designs particularly sensitive to the impingement of the passage shock on the boundary layer of the blade [10]. These highly loaded designs are an attempt to reduce the number of stages, as well as the number

of blades per stage in an effort to cut costs. The cost of these aggressive configurations is a limited range of stable operation and an increased sensitivity to airfoil shape. However, beyond simply optimizing airfoil shape, a more robust and far reaching enhancement may be possible by redesigning the blades entirely with a new system for boundary layer suction.

1.1.1 Boundary Layer Control

Suction techniques have been demonstrated computationally as well as experimentally on a variety of devices, ranging from wind tunnel walls to aircraft wings [11] [8]. In most cases, a moderate level of mass removal from the boundary layer flow -on the order of a couple of percent of the free stream flow- results in a significant reduction in boundary layer thickness profile and an associated delay of the onset of separation. These suggestive trends invite the possibility of implementing similar techniques in the design of airfoils for turbomachinery.

However the unique demanding environment of the transonic axial compressor makes direct application of non-rotating subsonic trends highly suspect. It may very well be that suction provides the desired results; but it is unclear what levels must be pursued for a successful application, nor is there an obviously optimal location on the blade. These issues are at the heart of boundary layer control for turbomachinery and must be specifically answered within the context of an actual design. Ultimately however, and perhaps somewhat beyond the physics of controlling boundary layer growth, remains the question of whether or not it is practical to implement such a system.

It is natural to require that the implementation of a boundary layer scheme to increase the loading on the blade should in turn introduce no new disturbances into the flow. Nevertheless, this requirement may prove to be a stumbling block of singular and upsetting difficulty. Previous idealizations have envisioned systems that are not only intrusive, but suffer from severe non-uniformities and losses. Thus addressing the unique aspects of actual implementation must necessarily round out any serious proposal to increase loading limits by means of boundary layer suction.

The boundary layer scoop may be the answer to "how". As will be discussed in the next chapter, the Gas Turbine Lab is currently immersed in a two pronged approach to tie down all primary aspects of boundary layer suction. The computational study outlined in this document is the complement to the experimental investigation of implementing a scoop-like intake to ingest a fraction of the high entropy flow. The convergence of both tests and

simulations should ultimately result in a system capable of surpassing the performance of any conventional design.

Chapter 2

Preliminary Work And Background

The ability to control boundary layer growth on airfoils for axial compressors is under continuous investigation at the MIT Gas Turbine Laboratory (GTL). This program of study bears on all aspects of a wide yet concerted effort to bring about the next step in turbomachinery, including numerical simulations, experimental setups and continuous analysis. Amongst the major milestones are the design of a high pressure ratio fan stage to take advantage of boundary layer suction and the testing of a transonic rotor with a group of blades modified to ingest a fraction of the high entropy viscous flow.

2.1 High Pressure Ratio Fan Stage

Increasing the pressure ratio of the fan stage can be instrumental in raising the propulsive efficiency of the modern high bypass engine [4]. Analysis of the ratio of the power delivered to the vehicle to that imparted to the engine flow reveals an optimal trend as the exit velocity of the core flow approaches that of the bypass stream. Moving towards matching these two velocities has lead designers to either reduce the speed of the core flow -while increasing the mass flow to preserve the level of thrust; hence, the high bypass ratios- or raise the exit velocity of the bypass flow by increasing the pressure ratio of the fan. Global design constraints -such as overall engine weight and length- and fan noise regulations dominate engine layout despite the desirability of a high pressure ratio fan, restricting the forward section to a single stage; and, as the diameter of the fan increases to accommodate the high

bypass ratios, structural considerations place a limit on the rotational speed of the blades, effectively capping the attainable pressure rise of a single stage fan. It is in this framework of design constraints and trade offs that the idea of active boundary layer control creates a new opportunity to raise the propulsive efficiency of the engine by allowing a higher pressure rise per stage without an increase in the blade tip speed.

This was the motivation behind the Quasi 3D computational design of a high pressure ratio fan stage. A precursor to the work presented here, this exercise provided encouraging results while demonstrating the latent potential of the boundary layer scoop. Evaluating the design against a conventional baseline design, possible gains of up to 16% in both specific impulse and thrust per unit airflow were computed. Yet the details of this advanced stage suggest that a significant percentage of the inlet mass flow -on the order of 10% - must be removed from the boundary layer flow to enable the target stagnation pressure rise of 2.0 [9].

The promise of the high pressure fan is in its ability to deliver an increased amount of work to the flow [9]. Taking the blades to a higher loading limit allows a larger amount of turning to be introduced into the stream. Yet there is a another more elusive effect resulting from the boundary layer scoop that links the stage to the rest of the compressor; for the removal of the high entropy fluid not only inhibits boundary layer separation, it reduces in turn, the work required to further compress the gas. The impact on the cycle, however, has not yet received full scrutiny.

2.2 Experimental Facilities

Parallel to the design study reported here is the experimental setup that is used to implement and investigate the boundary layer scoop. At the heart of these arrangements is the MIT Blowdown Compressor Facility (BDC), whose established history of independently corroborated results, provides the necessary backing to fully accredit the information obtained. This versatile, low cost facility allows the exploration of a test matrix no other test bed could possibly fill in the same period of time. Thus flexibility and speed are combined to continuously fuel the advance, as all concepts move steadily towards their true form.

The Blowdown Compressor

The BDC is in principle a very simple facility made up of two large vessels connected by a sizeable tube that serves as the test section. One vessel is "charged" with the operating gas whilst the other is pumped down to a vacuum. At the appropriate moment the charged supply tank is opened through the test section and "blown down", allowing the gas to flow into the evacuated dump tank. Placing the rotor in the gas path with the appropriate instrumentation completes the functional layout of the BDC (see figure 2-1).

However, the actual workings of this blowdown wind tunnel require an elaborate set of prescribed matching procedures to ensure the operating point of the rotor. The gas mixture must be controlled for gamma and the speed of sound; the back pressure of the rotor must be fixed to bring it to the design point during the run; and the inertia of the wheel must be matched to compensate for deceleration as the rotor is unpowered during the test. In the past, these rather numerous and subtle details were further exacerbated by the inability to conveniently adjust them; fine tuning between runs was controlled by the frequency of tunnel operation, and this could easily translate into month long delays.

These delays arose primarily from the explosive diaphragm system that was used to open the supply tank and initiate the run. The stringent precautions that surround the use of explosives made for innumerable complications; and, compounding the additional logistics, the sheer violence of the event had pronounced adverse effects on both test conditions and duration. A new controlled, non-explosive opening mechanism was consequently envisioned, designed and installed to replace the original system.

The Fast Acting Plug Valve

The Fast Acting Plug Valve is the latest improvement to the blow down facility. This clever pneumatic device controls the opening and closing of the supply tank in a safe, repeatable and practical manner. The valve consists of two simple components linked by a drive shaft that spans the length of the supply tank. The first of these two elements, the external drive piston, is located to the rear of the tank (see figure2-2).

The drive piston is the actuator of the valve and it comprises four separate chambers. The two chambers located towards the front of the piston serve to trigger and power the driver during the initial phases of operation, while the third and fourth chambers serve to

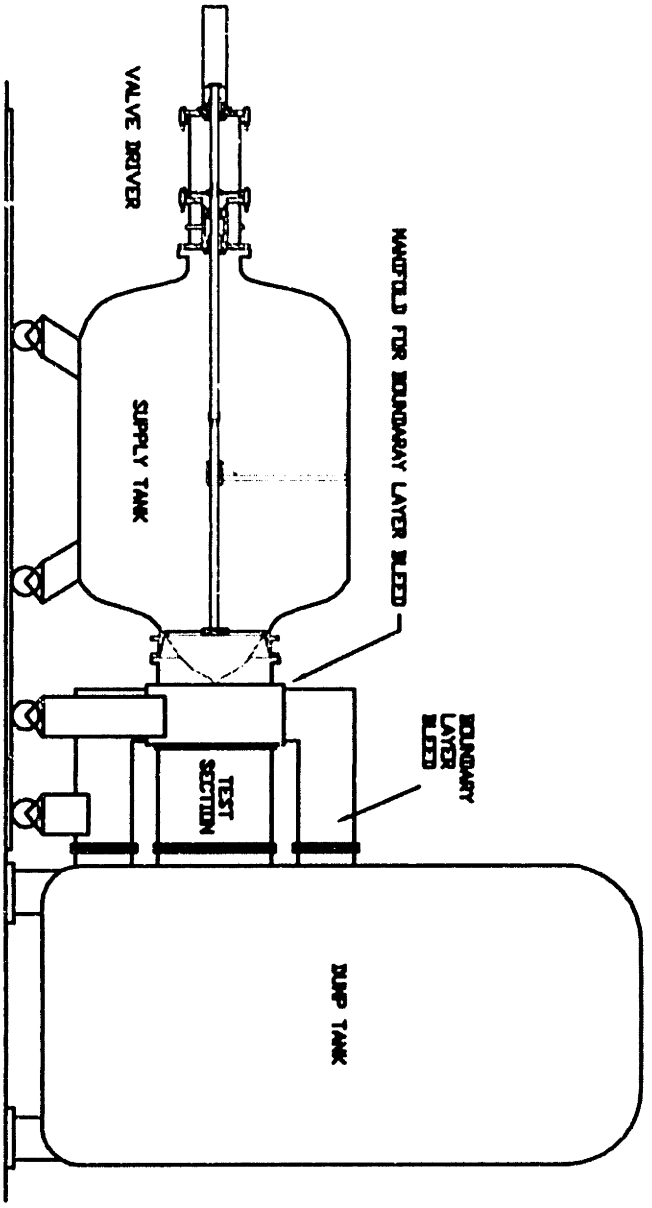

Figure 2-1: Blowdown compressor schematic layout

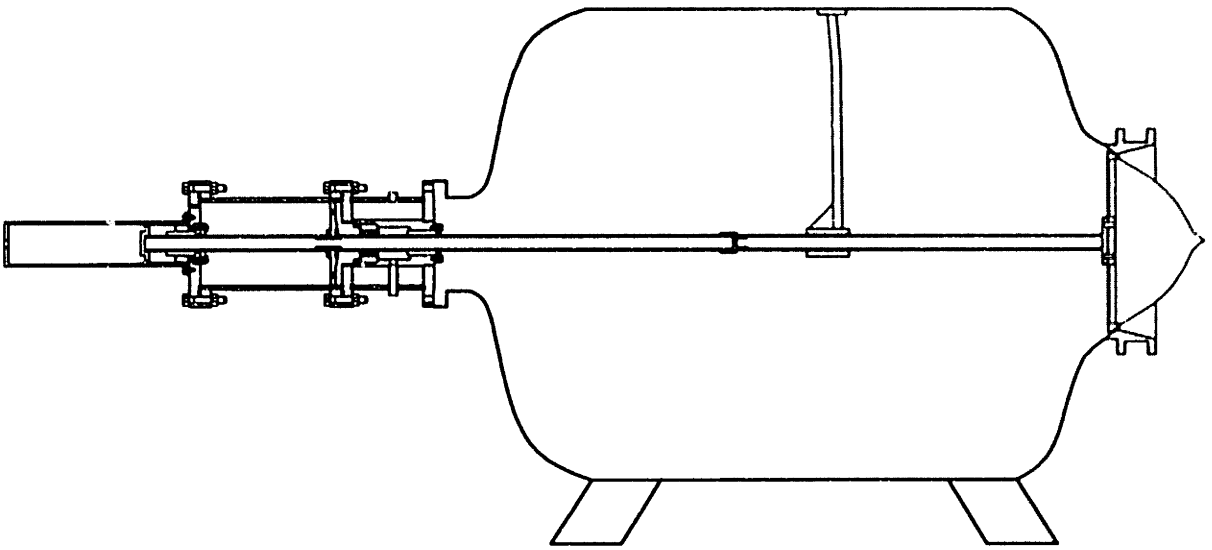

Figure 2-2: Plug valve and supply tank schematic

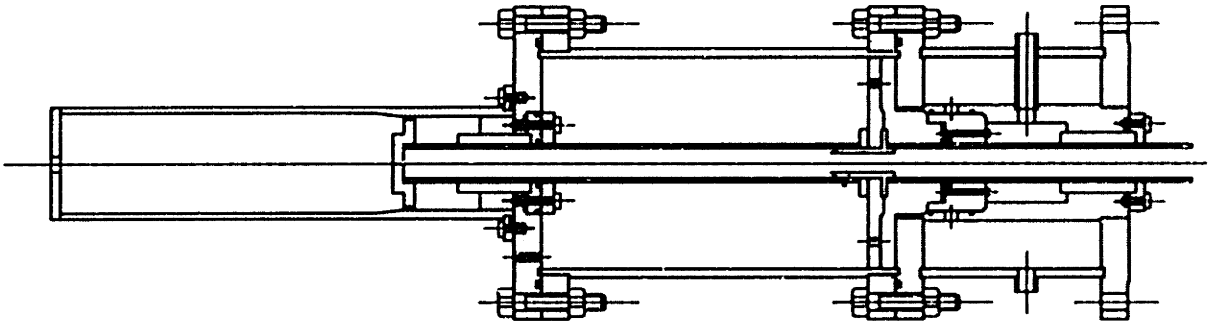

Figure 2-3: Fast acting plug valve schematic layout

dampen and reset the piston, in that order. Details of the internal layout together with a schematic of the drive piston's operation and use can be seen in diagrams 2-3 and 2-4 through 2-6.

The forward component of the valve, seals the supply tank from the mouth of the test section. This "plug" is nothing more than an aluminum plate, in the manner of a truncated cone, that creates its seal by compressing an o-ring on the face of a contraction ring tapered to match the angle of the plate. A fiber glass faring completes the make up of the plate, providing the blowdown flow with a smooth contraction into the mouth of the test section. The entire plug assembly was designed for minimum weight so as to enhance the performance characteristics of the valve.

The key challenge for this device is to be able to rival the opening time of the explosive aluminum diaphragm. Computer simulations and extensive calibration runs were undertaken to optimize the operating pressures governing the behavior of the valve (see figure2-7).

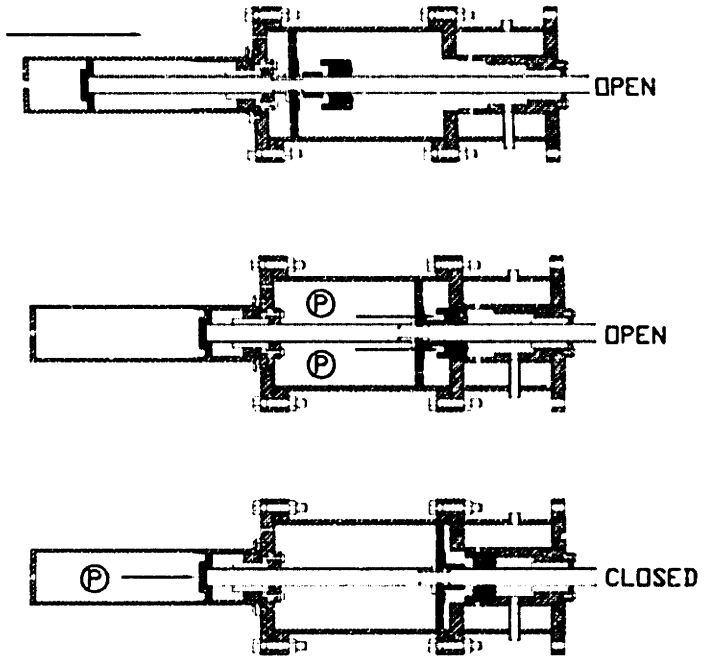

1_ PNEUMATICALLY MOVE ASSEMBLY AND SEAT FREE PISTON SEAL.

2_ PRESSURIZE MAIN CYLINDER AND FORCE FREE PISTON INTO PLACE.

3_ PRESSURIZE REAR PISTON AND SEAT MAIN SEAL.

Figure 2-4: Fast acting plug valve operation: steps 1-3

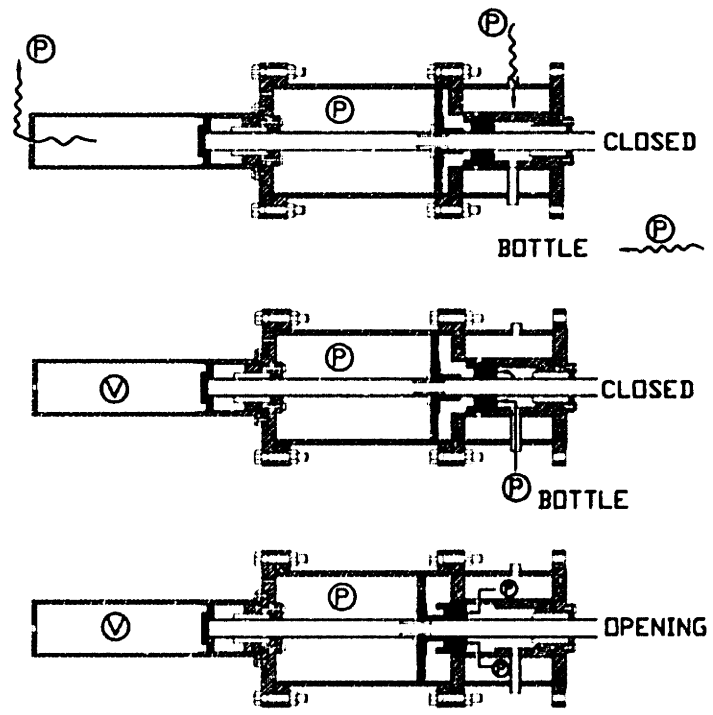

4_ PRESSURIZE RESERVOIR AND BOTTLE. EVACUATE REAR PISTON. PRESSURIZE/VENT MAIN CYLINDER TO DESIRED LEVEL.

5_ OPEN VALVE AND FIRE POWER SHOT FROM BOTTLE.

6_ FREE PISTON UNCOVERS RESERVOIR HOLES WHICH SETS FIXED PISTON MOVING.

Figure 2-5: Fast acting plug valve operation:steps 4-6

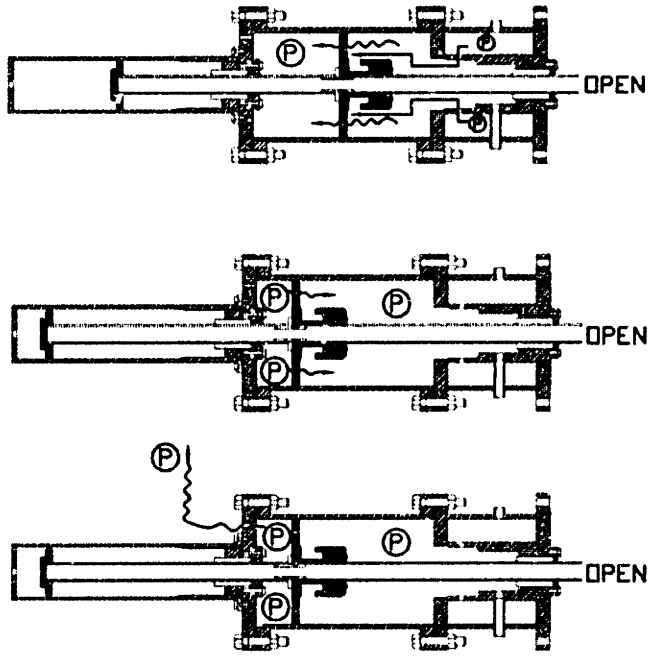

7_ FIXED PISTON ACCELERATES WHILE GAS LEAKS PAST. BACK END OF MAIN CYLINDER IS COMPRESSED BY PISTON MOTION.

8_ PRESSURE IN THE BACK END OF MAIN CYLINDER DECELERATES PISTON WHILE GAS LEAKS AWAY EQUALIZING PRESSURE IN THE ENTIRE MAIN CYLINDER. PISTON MOTION STOPS.

9_ GAS IN MAIN CYLINDER IS VENTED TO ATMOSPHERE.

Figure 2-6: Fast acting plug valve operation: steps 7-9

The results were extremely satisfying, placing the opening time somewhere between 45 to 50 milliseconds (see figure2-8). However, it was the controlled nature of the stroke that truly placed the valve beyond the performance of the aluminum diaphragm, by significantly reducing the settling time of the blowdown stream.

It is extremely important that the signature of the startup event be virtually imperceptible by the time the data is acquired. Yet, given the constrained time frame of the blow down run, ensuring steady conditions is tantamount to simply reducing the available test time; and since the violent history of the explosion is slow to die down, the aluminum diaphragm severely restricted the usable run time of the BDC. In stark contrast, the opening of the valve leaves a significantly weaker foot print that decays quickly, effectively extending the available test time. This increase in usable test time, when compared to the original startup mechanism, is on the order of 30% to 50%.

Thus a longer test time; the ability to produce consecutive runs; and the opportunity to do multiple surveys using the same operating mixture (the valve permits "recycling" by providing a means to re-seal the supply tank without venting the gas); combine to make the improved BDC an appropriate platform from which to study the effects of active boundary layer control. Hence, this unique facility and the singular opportunity it provides have become the focus of the experimental study currently under way.

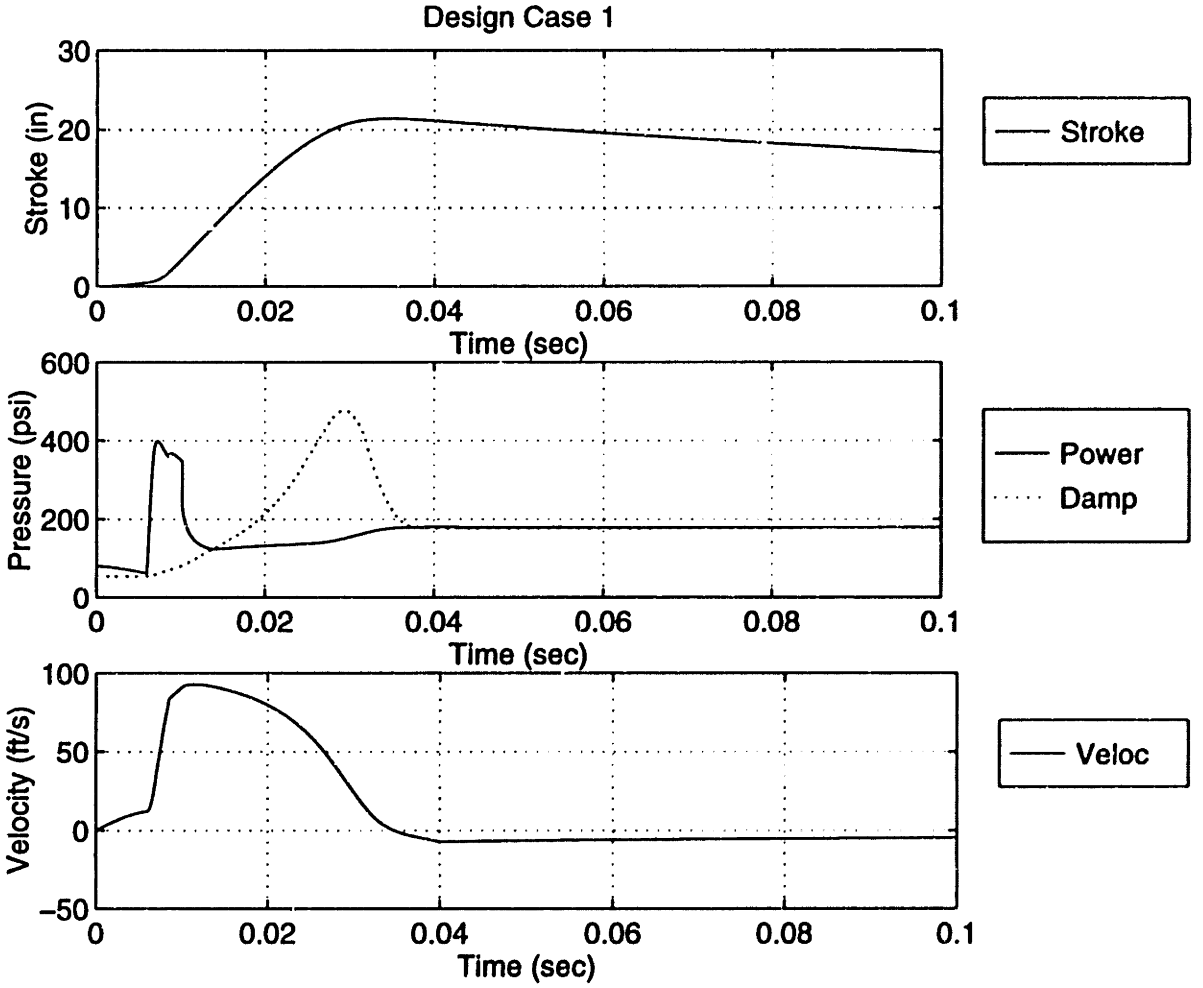

Figure 2-7: Fast acting plug valve computer simulation

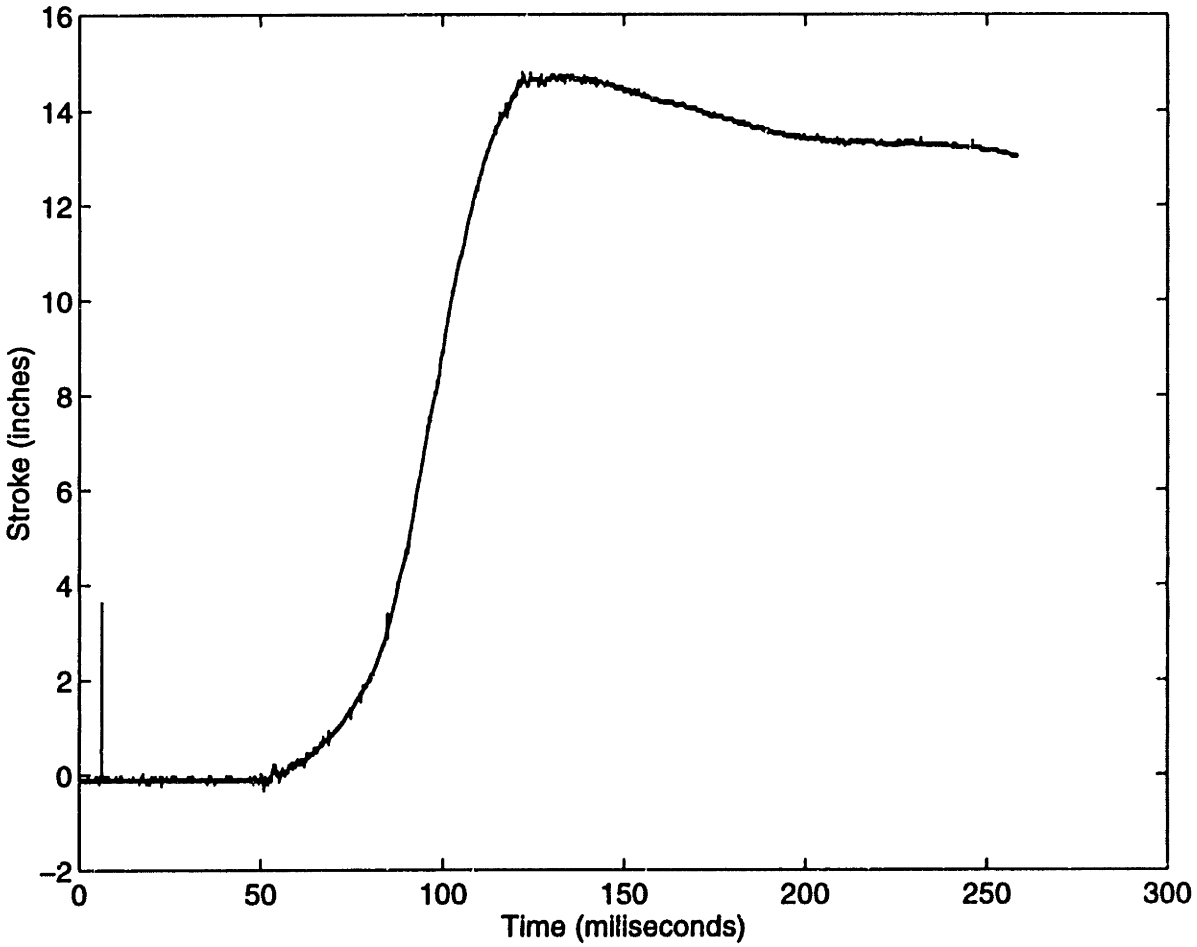

Figure 2-8: Fast acting plug valve test data

2.3 Experimental Development

Two experimental phases have been formulated to study and develop the advanced high pressure compressor stage. The initial phase, being carried out by D. Reijnen, was devised as a comparative study that takes an existing rotor and evaluates the effect of modifying a group of blades to ingest a fraction of the high entropy viscous flow. The second phase will be the culmination of the comparative study and the analytical design presented in the body of this document; it will mark the high point of the project and yield the performance results for a complete rotor designed around the concept of boundary layer control for maximum pressure rise.

Modifying an existing rotor demands a unique amalgam of craftsmanship and science to ensure the survival of both blade and disc in what is a most rigorous environment. Nevertheless, after a series of tentative trials, five of twenty seven blades were successfully produced to remove a fraction of the boundary layer flow, amounting to something on the order of 1% of total inlet mass flow. These blades have hollowed out passages that help to pump the fluid sucked in by a graphite composite scoop that completes the blade profile on the suction side of the foil. This modified rotor has already demonstrated its ability to survive in the demanding conditions typical of a transonic stage. (see figures 2-9 and 2-10)

Preliminary results seem to suggest that suction has a significant impact on the performance of the rotor, with marked effects on all aspects of operation, ranging from stability characteristics, to shock structure, pressure rise and efficiency. Yet despite the wealth of information obtained and the suggestive trends observed thus far, the lack of a complete analysis of the data precludes the exposition of any definitive conclusions at this time.

The objective then, for the final phase of the experimental approach, will be to design and build a high pressure ratio transonic stage that incorporates the boundary layer scoop as an integral part of the blade geometry; and is equipped with a pumping system suitable for conducting tests in the MIT Blowdown Compressor Facility.

This thesis comprises a feasibility study for a high pressure-ratio stage; overall geometric specifications of solidity and hub-tip absolute dimensions; operational parameters specifying rotational speed and axial mach number; along with the blade coordinates for both rotor and stator foils. Aerodynamics of blade passages are provided along with boundary layer projections and summary of suction design, including mass fraction removed, as well as the

Figure 2-9: Modified rotor blade with composite scoop

Figure 2-10: Modified rotor blade with composite scoop

position of the scoop as a percentage of blade chord.

Chapter 3

The Quasi 3D Method

The numerical codes used to estimate the performance of the stage are essentially two dimensional. The coordinates of the blade or vane together with the desired solidity, provided as an input to the code, serve to define the geometry of the passage that the program will use in its calculations for the cascade. These computations are then fully prescribed by specifying the conditions upstream of the blade while appropriately constraining the downstream characteristics of the flow. If a solution to the system can be found, detailed information regarding the flow within the passage and the overall performance of the cascade are then made available to the designer.

Modeling an inherently 3-D system with a 2-D cascade, however, is certainly less than satisfactory as the basis for any serious design [1]. Hence a more accurate description is obtained by including the effects of rotation on an axisymmetric base flow. This additional refinement is known as the "quasi 3-D" solution. In this mode, the numerical solution tracks the radial displacement and contraction of the streamtubes as they flow through the passage. Thus a quasi 3-D description requires a second set of coordinates, that specify the streamtube radius and location, to be fully prescribed. These coordinates can be easily obtained by what is known as the streamline-curvature through flow method.

The final design of the blade can thus be grown as the spanwise assembly of the solutions obtained for blade slices taken from hub to tip, the only constraint being the results of the streamline curvature calculation. Combining in this fashion an analysis of the blade-to-blade flow with a mean flow through flow calculation has been shown to provide satisfactory results [6].

3.1 The Mean Flow Through-Flow Calculation

The streamline curvature code solves the radial momentum equation, as constrained by continuity, along a meridional plane. The radial momentum equation is a simplified version of the general equations of motion for an axial compressor and its solution requires that the entropy, enthalpy, and tangential velocity distributions be prescribed [9] [4]. Performing this calculation is sufficient to specify the radial displacement and contraction of the streamtubes as they flow through the stage. Albeit an inviscid approach, this method has been widely used for many years with considerable success.

The analysis begins by defining the geometry of both the hub and the casing, along with the axial positions of the rotor and stator (see figure 3-1). Once a particular configuration is selected the numerical solver generates the grid that will be used to evaluate the equation. The next step is to specify the inlet flow conditions into the duct as well as the desired pressure rise and tangential velocity changes of the stage. The solver then marches downstream, iterating on the results until an acceptable solution has been found (see figure 3-2). These results not only provide a constraint to connect the solutions of the blade to blade flow but allow a first cut generation of the airfoil "shape" required to perform the desired level of turning (see figure 3-3). By computing the velocity triangles for the streamlines in the stage, the code generates simple cross sections by fairing a curve between the lines tangent to the computed inlet and exit angles of the rotor or stator [9]. These sections are merely used to visually evaluate the level of turning required by the stage; more complete sections for computation in MISES were constructed as MCA or J-blade sections and are further discussed in chapter 5.

3.2 Blade to Blade Flow

The blade to blade flow was computed with a Multiple Interacting Streamtube Euler Solver (MISES). This is fundamentally a coupled viscous/inviscid numerical solver built around the Newton-Raphson method and supplied with appropriate models for turbulence and transition [12]. MISES provides numerous amenities to the airfoil designer by facilitating grid generation and refinement as well as a variety of plotting routines for quick and easy viewing of results. However, for supersonic inlet flows, the flexibility of the solver is somewhat limited and great care has to be taken when specifying the pertinent parameters, so

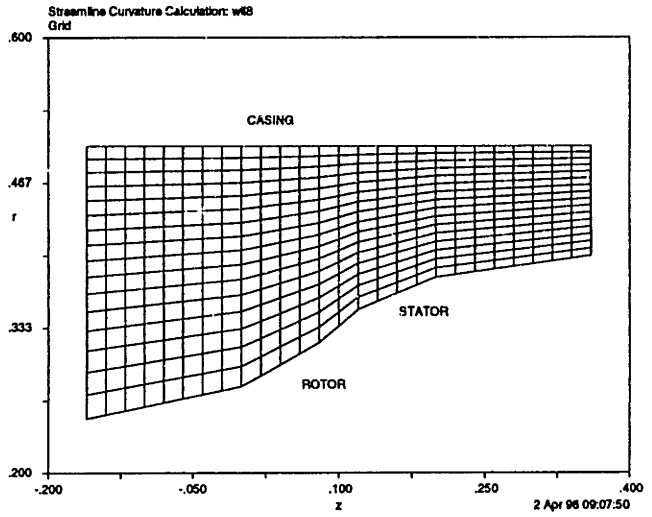

Figure 3-1: Duct geometry and grid

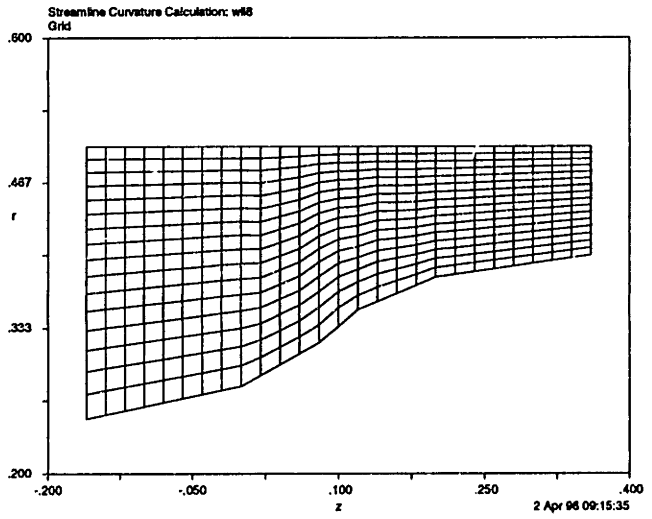

Figure 3-2: Solution streamlines

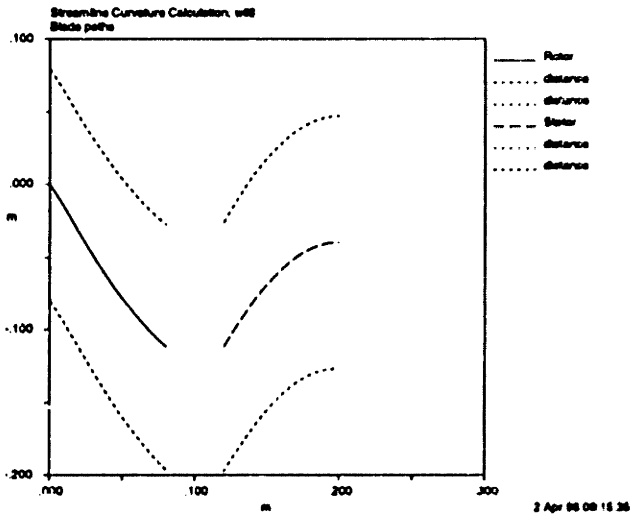

Figure 3-3: Primitive airfoil shape

as to avoid an ill posed problem.

Analysis begins by providing MISES with the three input files that specify the case to be considered: BLADE.xxx; ISES.xxx; and, STREAM.xxx. The BLADE file supplies the airfoil coordinates along with the inlet and outlet angles for the cascade. Two additional coordinates, specifying the location of the "inlet" and "outlet" planes, serve to reference the position of the upstream and downstream "mixed out" conditions.

Flow characteristics and constraints are detailed for the solver in the ISES file. Parameters such as the pressure ratio, inlet Mach number, Reynolds number and so forth are listed to reflect both the conditions that are to be enforced, as well as the ones allowed to be varied, when solving a particular case. Examples of the input files can be found in the MISES documentation and references [9] and [12].

Finally, for operation in Quasi 3D mode, a third input file is necessary to compute the flow. This file contains the coordinates for the location and radii of the streamtube as it progresses through the passage. Designated the STREAM file, this additional input must provide in turn a suitably nondimensionalized wheel speed for the stage. Supplied with all three input files, the case is then fully prescribed.

Computation, as with most numerical methods, requires a certain level of skill that revolves in particular around the issue of grid generation. Special attention must be paid to avoid excessive "shearing" of grid cells in regions of extreme curvature, such as around

the leading edge of the blade, or the solution will be plagued with numerical errors. Similar precautions are required when considering the location of the shock structure in the passage; for in addition to cell shape, node density is critical for adequate resolution and placement of shocks. Refining the grid and specifying flow conditions that are close to the final computed results is strongly advised when analyzing designs with a relative supersonic inlet [2].

3.3 Boundary Layer Control

The ability to represent removal of the boundary layer in MISES was devised as an additional feature to enable modeling the design of a high pressure ratio stage with active boundary layer control. Two independent sets of modifications were considered and attempted to simulate the effects of removing a fraction of the high entropy fluid. However, only one of these approaches, provided acceptable results within the original framework of the program.

There are two basic effects -regardless of the particulars of implementation- that must be captured by the model: a sharp localized decrease in the value of the displacement thickness; and the shifting of the external streamlines associated with the removal of mass from the flow [9]. The structure of the solver is such, that these effects can be treated as independent problems that simply "communicate" their results.

MISES can be thought of as two individual solvers linked through an information bridge. Any given case, is broken down into two different camps that share, compute and compare results while searching for an answer that can be neatly pieced together as the final solution. This convenient "division of labor" is achieved along the lines of viscous/inviscid solvers, the results of one being the effects on the other and vice a versa, until it converges.

The viscous solver handles the boundary layer calculations and therefore must be made to represent the sudden reduction in the displacement profile associated with suction (see figure 3-4). One approach is to directly influence the array containing the values of delta star by simply multiplying some of the nodes -where the scoop would be, for example- by a predetermined fraction. This "controlled" version of the boundary layer profile would then serve as the input to the normal 2D momentum equation, resulting in a displacement growth marked by the desired discontinuity at the suction nodes. An alternate approach and the one adopted here, is to model the scoop as a "normal wall velocity" that pulls the profile down through the body (see figure 3-5). Mass removal in this manner is controlled

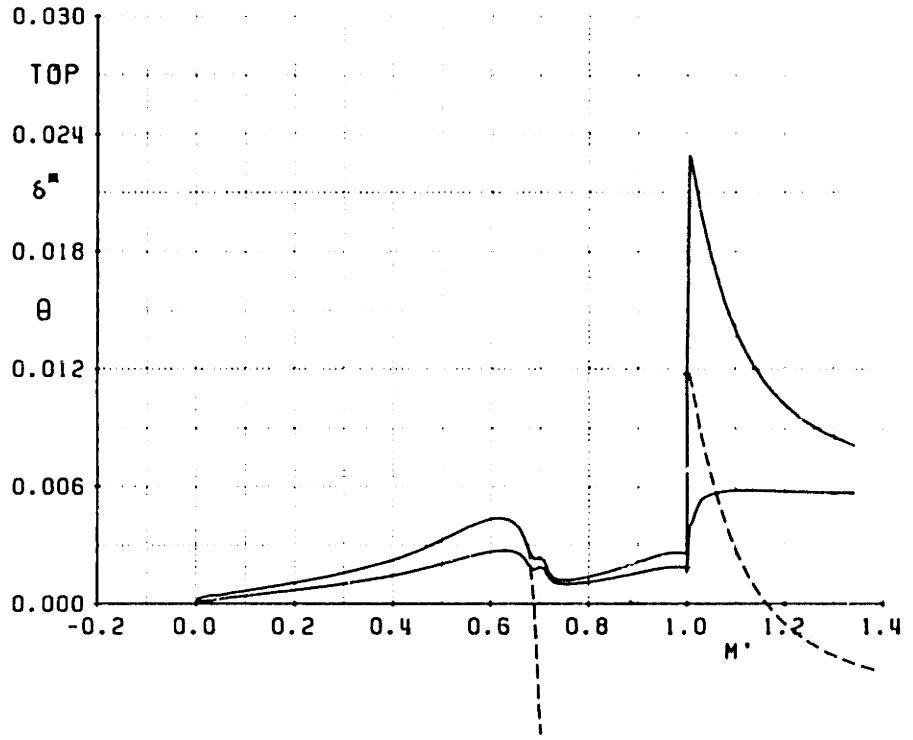

Figure 3-4: Profile reduction associated with boundary layer suction

by specifying the length and location of the segment over which the wall is "porous", and the amount of mass to be removed. Hence, a highly localized effect on the boundary layer thickness profile -so as to model a boundary layer scoop- can be had by reducing the suction length to values on the order of 3 to 5 percent of chord. Modifying the solid wall boundary condition in this fashion is not as artificial as multiplying delta star by a fraction and has been used with considerable success as part of the related airfoil code MSES [7]. Although this second method requires a more involved set of changes -additional sensitivities in the Newton-Raphson method and so forth- it is by far the most robust version of the modified code. This robustness stems from the fact that by modifying the airfoil boundary, it directly communicates the effects of the scoop to the inviscid solver.

It is the task of the inviscid solver to compute the flow through the passage, and it is thus this analysis that should reflect the mass removal associated with boundary layer suction. The "normal wall velocity" incorporates this effect immediately by allowing the

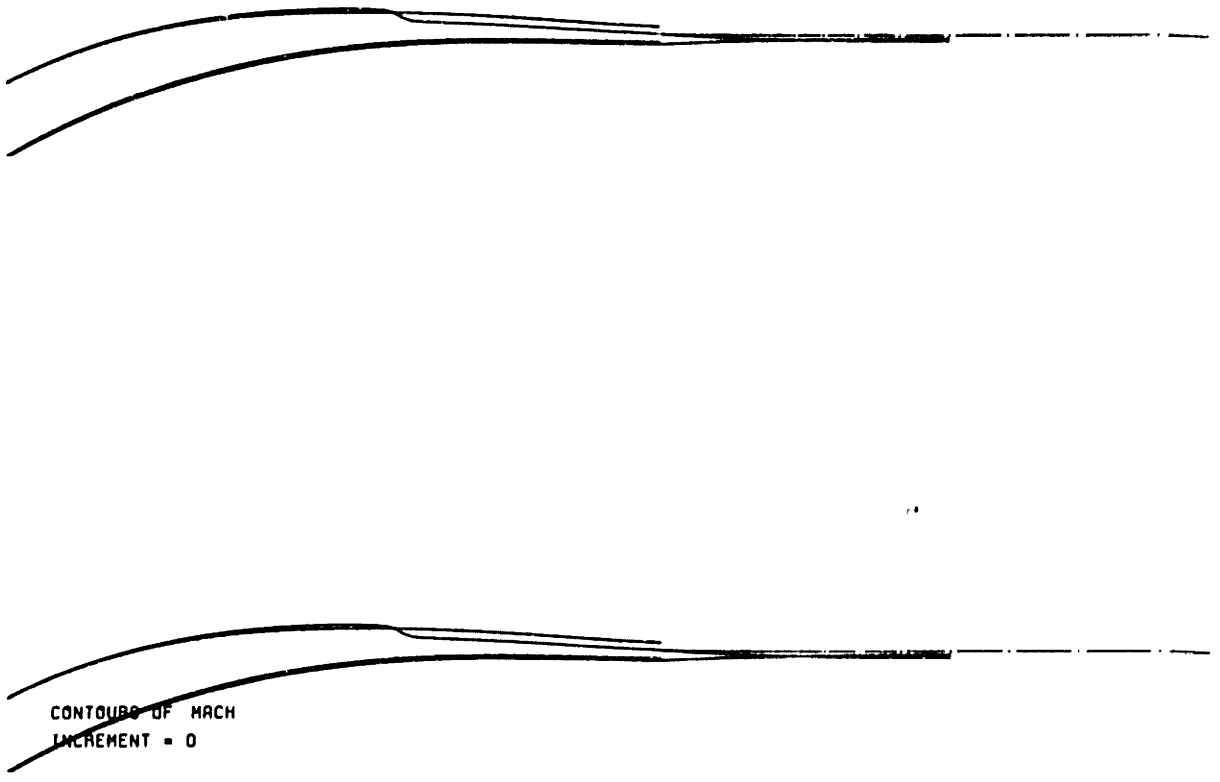

Figure 3-5: Streamline displacement to model mass removal

streamlines to be dipped beneath the surface of the blade to represent the expansion of the flow characteristic of the mass deficit behind the scoop. The simpler approach of multiplying the displacement array by a fraction leaves the solid wall intact and a special "fish tail" blade is required to model the removal of mass. The "fish tail" blade is more cumbersome to generate, requiring a match between displacement thickness deficit and increased camber of the blade suction surface. However, the most intrusive change introduced by this special geometry is its disruption of the MISES grid generator. Creating the node arrays for the solver is no small task and this fact alone should quickly discredit the "fraction-fish tail" alternative to modeling boundary layer suction, leaving the second approach as the only one that is compatible with the original architecture of the MISES code.

Chapter 4

Numerical Design Process

Two computational steps were used to arrive at a working configuration. The initial step consisted of a series of inviscid calculations primarily concerned with establishing the geometry of the blade and layout of the diffusing passage. The second step served to establish the location of the boundary layer "scoop" together with the width of the simulated slot and the amount of mass removed.

4.1 The Inviscid Analysis

Given an initial geometry, a quick coarse grid inviscid computation was performed to obtain a preliminary estimate of shock location, exit angle, inlet slope and pressure distribution for the blade. A low density grid of 40 to 45 distributed points is enough to capture the overall geometry of the section and yield reasonable results; additional nodes should only be used to target specific areas, as suggested by the initial run, that seem to require a higher spatial resolution. This economy of grid points allows for a very fast first computation, generating the initial results over twenty to forty iterations in a matter of minutes.

These preliminary mach number and pressure distribution plots for the blade were scrutinized primarily for shock losses. Five different geometric parameters were then explored in an effort to minimize the inefficiencies of the compression: the leading edge radius, the camber, the thickness, the incidence angle and the solidity. The first four were varied with the help of the airfoil package Xfoil; the geometric redesign capabilities of this program are simple and easy to use, facilitating rapid changes. The fifth parameter, changes in solidity, was explored within MISES by varying the circumferential pitch of the cascade, contained

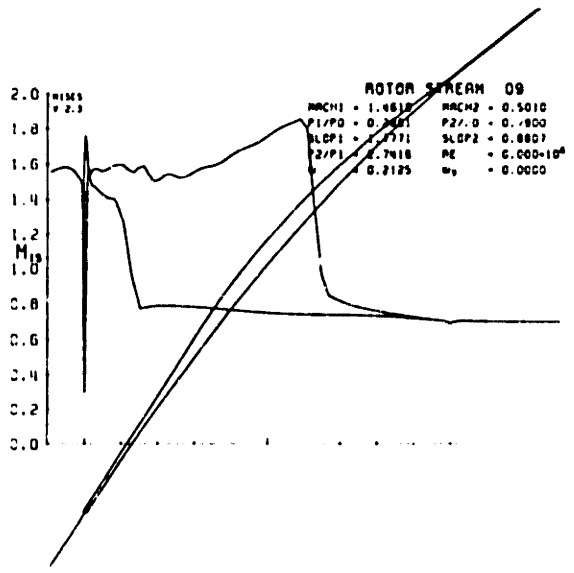

Figure 4-1: Low solidity solution showing supersonic turning

as an input within the BLADE.xxx file.

The initial rotor sections suffered from shock losses higher than those associated with a normal shock for the given inlet mach number and pressure rise over the blade. This was due primarily to the supersonic turning of the flow; the expansion of the supersonic stream raised the mach number before the shock well above that of the inlet, leading to a very costly compression (see fig.4-1). To address this problem, the sections were redesigned with a suction surface consisting of a precompression ramp and subsonic turning arc. A new series of runs with increasing solidity was then performed to establish the location of the shock towards the end of the ramp and before the turning. The most favorable computed configuration placed the shock at the entrance to the passage.

After establishing the location of the passage shock a second series of computational runs was made on a much finer grid, placing additional nodes around the leading edge and over the segment of the precompression ramp where the shock impinges on the suction side of the blade. This secondary analysis served to scrutinize the acceleration over the nose and to stabilize the position of the shock (on the coarse grid, the shock has a tendency to oscillate between grid nodes). The new grids consisted of 80 to 100 points, clustered by adjusting the stagnation-point spacing ratio and the upper surface spacing refinement options in MISES. These runs required anywhere between 60 to 100 iterations to converge; a computing time on the order of tens of minutes.

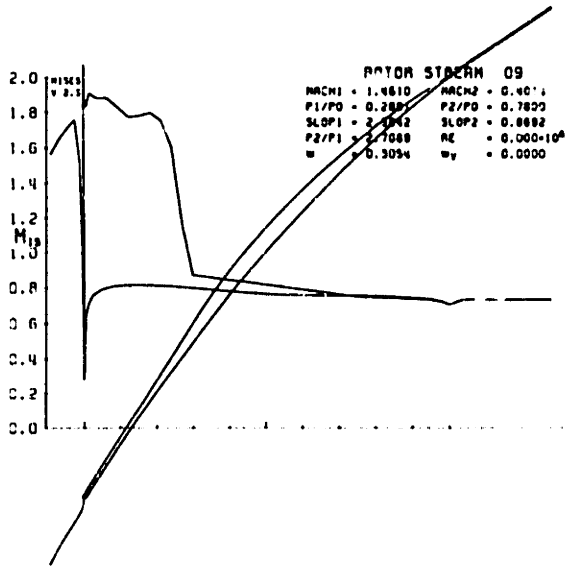

Figure 4-2: Leading edge expansion with associated losses

The results made evident an unnecessarily high acceleration of the flow over the leading edge leading to significant losses. As in the case of supersonic diffusion, the expansion over the nose raised the mach number before the shock to a value higher than that of the incoming flow (see fig.4-2). This particular issue was corrected by sharpening the leading edge and adjusting the incidence of the rotor blade so as to line up the section with the incoming stream. Both changes were performed in Xfoil by respecifying the leading edge radius and angle of attack for the section (see fig.4-3).

Once the issue of losses had been addressed by the redesigned sections, a third set of computations on the finer grids was performed to establish the outlet angle of the cascade. Matching this value to the exit angle prescribed by the streamline curvature code is at the heart of the quasi 3D design. And although MISES provides a modal redesign mode that drives the exit angle to a prescribed value, it is necessary for a well behaved solution that these changes be small. For sections computed to be far off the mark, the exit angle was adjusted coarsely by changing the camber and exit angle prescribed when generating the blade and only then fine tuned by making use of the modal redesign. The combination of both options brought all sections to within 1 to 2 degrees of the angle computed by the streamline curvature code.

The final step of the inviscid analysis concerned the spanwise assembly of the analyzed sections. This is of particular importance for the rotor sections designed, for most of the

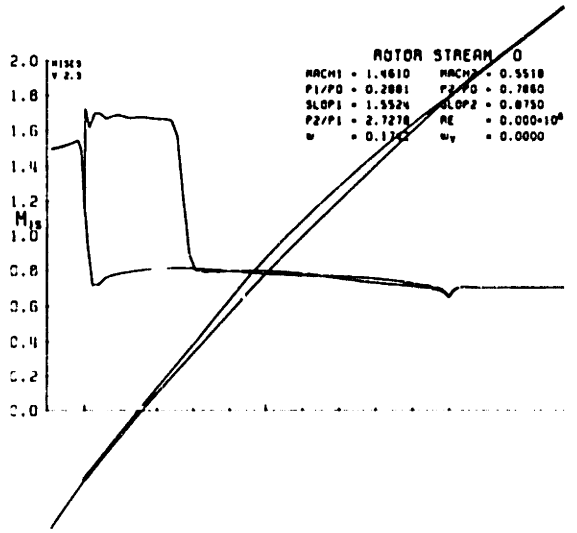

Figure 4-3: Rotor section illustrating appropriate incidence

pressure rise across the rotor is to due to the shock in the passage, which was computed as though normal to the flow. That is to say, the passage shock for all rotor sections is normal in two dimensions, implying that the results obtained would only hold if the incoming flow is normal to the shock plane in all three dimensions. This requirement posed a particular problem when trying to piece together the sections computed towards the tip of the blade with those at midspan and closer to the hub.

The amount of turning required to achieve the prescribed pressure rise across the blade decreases with increasing radius. This results in diffusing passages towards the tip that are in two dimensions of nearly constant area -the suction surface being nearly flat. Hence the point of minimum area is controlled by streamtube contraction, placing the "throat" of the passage, and thus the passage shock, at the exit of the diffuser (see fig.4-4). To correct the area distribution through the cascade and place the shock at the entrance of the passage, allowing a stack line radial through the nose of each section, radical thickness and camber distributions were attempted (see fig.4-5). However, these sections were deemed unsatisfactory. Though beyond the scope of this analysis, the three dimensional assembly of the blade based on the computed results with the shock receding into the passage towards the tip, would require a forward sweep to preserve the shock normal to the flow in all three dimensions.

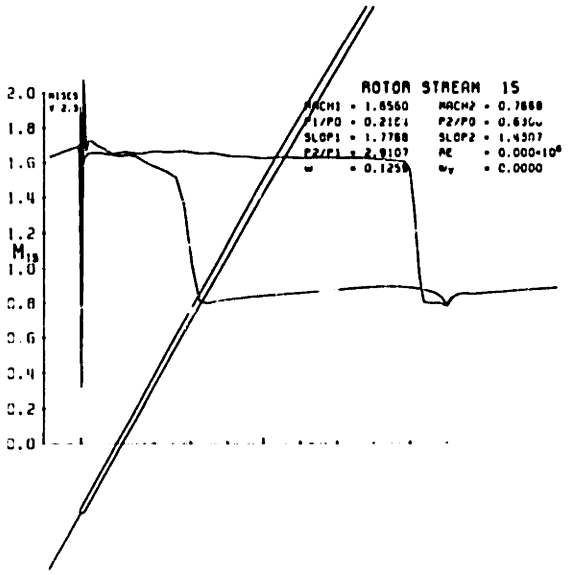

Figure 4-4: Tip section with passage shock at the exit of the diffuser

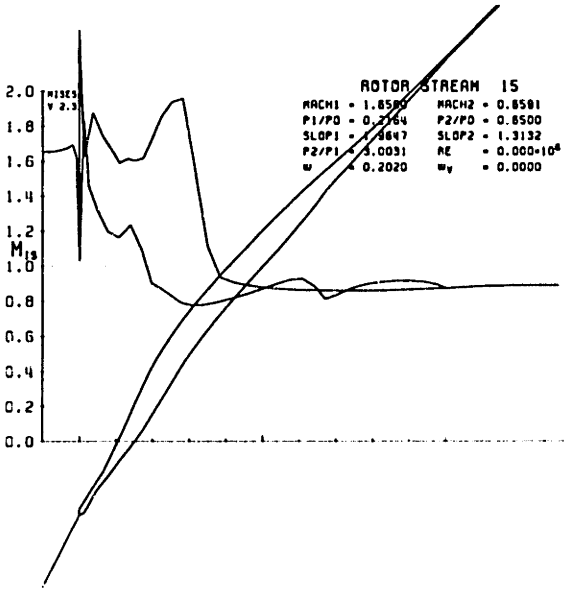

Figure 4-5: Coarse grid radical solution with shock at the entrance to the passage

4.2 Viscous Analysis

The starting point of all viscous computations was a converged inviscid case; using an inviscid solution eases the work of the solver, by making its initial guess closer to the final solution. In this manner, starting from the 80 or so iterations of the previous computational run, an additional 10 to 20 iterations were performed to estimate the development of the boundary layer without suction. It is not necessary -or depending on the case, it may not be possible- to do more iterations. The loading for all sections was extremely high, leading to separated regions that would disrupt the solver, producing spurious results and a high level of numerical error. These initial runs were performed merely to estimate the region were the onset of separation would occur and not to arrive at a converged solution.

Three parameters govern the boundary layer suction incorporated in the model: a suction coefficient and slot length, controlling the amount of mass removed, and a slot location. These governing parameters were thus explored in an effort to produce a solution where the boundary layer remains attached throughout, while removing a relatively small amount of mass -on the order of 1 to 5 percent.

The first viscous computations with suction were performed by placing the suction-slot at a chord location based on the rough results of the preliminary iterations. For these runs a very high amount of mass removal was specified -around 7% of inlet flow- together with a relatively wide slot -10% of chord. The high level of mass removal was expected to behave as an upper bound; if more than 7% of inlet mass flow had to be removed, the case was impractical and a new slot location would be selected for analysis. The wide slot served to ease the behavior of the solver by relaxing the discontinuity in the boundary layer. These early suction runs provided enough information to tune the location of the slot by illuminating the problems associated with "suction too soon" and "suction too late".

The forward boundary for slot placement was set for the rotor sections by the location of the passage shock; and for the stator sections by the point of minimum slope for the curve defining the suction side of the vane; suction forward of these two locations -15 to 20 percent of blade chord- resulted in separation towards the trailing edge or required levels of mass removal in excess of 7%. The aft boundary for slot placement was determined again by the location of the shock for the rotor sections and anything beyond 90% chord for the stator; the first limit being set by the inability to recover the boundary layer once separated

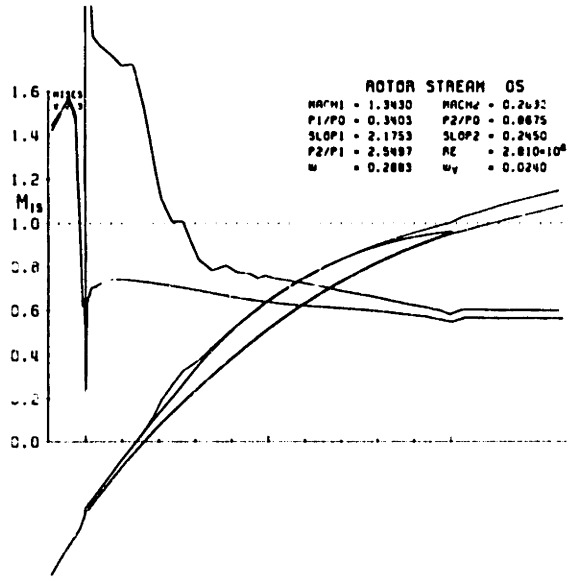

Figure 4-6: Mach plot for suction post separation

(see fig.4-6 and 4-7), and the second by simply being impractical to place the slot so far back.

Once a satisfactory slot location had been computed, additional runs were performed while successively reducing the level of mass removed. If the simulation failed for the new low level of suction, more iterations at this reduced level of suction would be performed on the slot location, in essence repeating the previous step. The final step of the process involved running simulations while narrowing the width of the slot, driving the effect of suction towards a concentrated step in an effort to represent the effect of the boundary layer scoop.

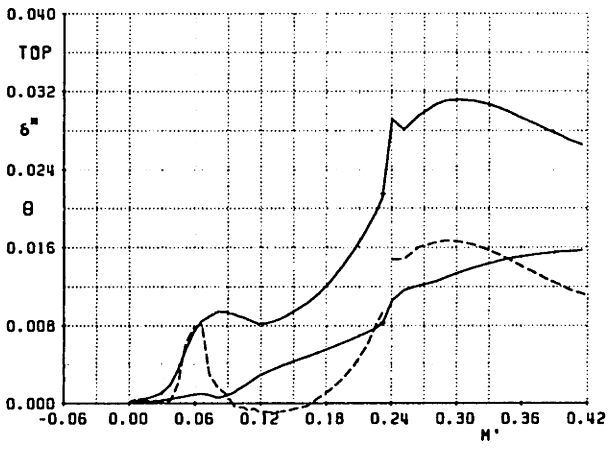

Figure 4-7: Boundary layer profile for suction post separation. The displacement thickness continues to grow despite mass removal.

Chapter 5

Results

The design presented here represents one possible solution to the proposed problem of the high pressure ratio stage. It is by no means an optimum design nor is it necessarily a working design; it is simply a workable configuration that demonstrates the aerodynamic feasibility of increased loading through boundary layer control. The results obtained, if perhaps lacking in an absolute sense -as all model predictions necessarily do-, are strong enough to put the numbers behind the idea and roll the concept on towards production.

5.1 Rotor and Stator Foils

Two baseline shapes were used as starting points for the design of the rotor and stator foils. A simple J-blade section was selected for the rotor blade whereas a basic Multiple Circular Arc (MCA) section was chosen for the stator vane. The J-blade section, consisting of a suction side precompression ramp and turning arc, is well suited for supersonic blading, for the ramp decreases the mach number before the passage shock. On the other hand, the MCA blade suction side, made up of two arc segments chosen to accommodate the inlet and outlet angles respectively, produces a more distributed loading across the blade and is preferred in the high subsonic regime. These initial shapes were then redesigned in MISES to appropriately match calculated outlet angles, optimize shock placement and remove any abrupt expansions.

The final shapes for the rotor blade sections differ very little from their basic J-blade design. MISES computations for supersonic blading are extremely sensitive and it is paramount that the input geometry be very close to the desired solution. Most redesigns

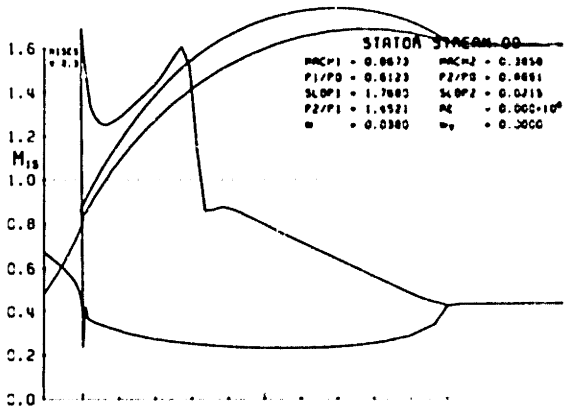

Figure 5-1: Original inviscid solution for MCA stator

performed in MISES consisted primarily of using the modal redesign option that imposes the exit angle as a constraint. All gross geometric changes were performed with the help of an airfoil program entitled Xfoil. This package features a variety of window driven redesign options that allow the user to quickly manipulate the airfoil shape. Rotor results can be seen in the appendix.

The stator vane sections, on the other hand, are much more the product of the MISES redesign options available to the user. Once the loading profile of the MCA blade had been computed by MISES, the inverse design mode was used to generate a pressure distribution that gradually loaded the blade from leading edge to trailing edge (see fig 5-1). However, the inverse redesign is a harsh option, and somewhat discontinuous geometric shapes are produced as a result. This accountants for the "droopy" leading edge noticeable on stator sections 5 and 9. However, the trend is clear and a sharper leading edge radius should be pursued in the final mechanical design of the vane. All sections can be seen in the provided appendices.

5.2 Rotor Blade and Stator Vane

The geometry and operating point of the rotor blade were chosen as being representative of the first stage of a modern high pressure axial compressor. An average hub to tip ratio of .6

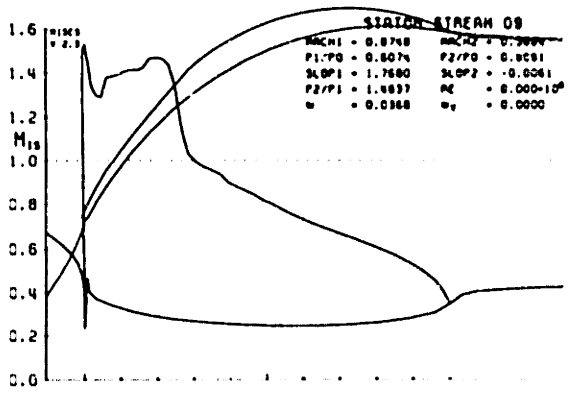

Figure 5-2: Redesigned inviscid solution for MCA stator

and a tip speed of 1500 feet per second were selected as inputs to the design. The solidity of the rotor, however, was primarily set by the desired location of the passage shock.

Most of the pressure rise across the rotor is due to the passage shock, with comparatively little turning being introduced. However, due to the high mach numbers through the diffuser it is essential that the desired exit angle be approached gradually along the chord of the blade. This constraint implies a relatively forward passage shock, for it is extremely inefficient to turn the flow before the throat of the diffuser; such a design would result in an unnecessary expansion before the shock and the severe losses associated with an even higher mach number compression. Consequently, after several iterations to minimize shock losses on the mean profile of the rotor, an acceptable solidity was arrived at by "assembling" the disc with fifty blades. Nevertheless, the location of the passage shock recedes into the diffuser as the sections analyzed move towards the tip of the blade.

The overall configuration of the stator vane was determined primarily on the basis of the geometry of the duct. Thus the hub to tip ratio was set by the gradual extension of the hub, the casing being held at a constant radius. As for the solidity of the stator, it was chosen as low as feasible, while maintaining the desired exit angle of the flow. The vanes, having been selected to return the flow to axial, required a very high degree of turning, which in turn resulted in a configuration of thirty two vanes to reduce deviation. All analyzed sections can be seen in fig 5-3.

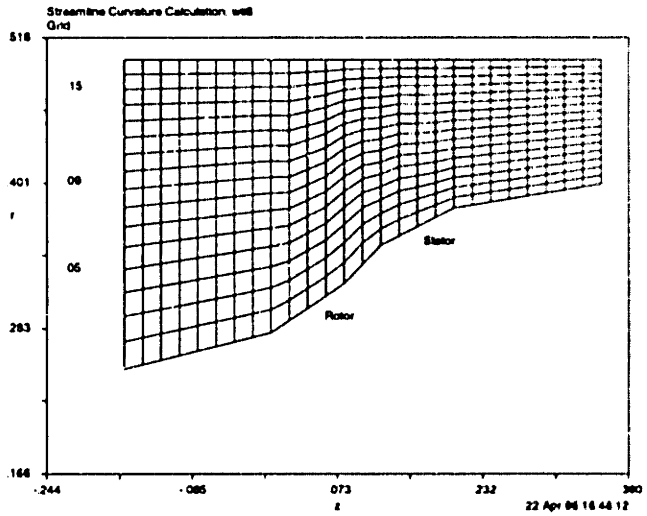

Figure 5-3: Rotor and stator analyzed sections

Casing Radius	0.5 m
Hub Radius (inlet)	0.25 m
Hub Radius (exit)	0.40 m
Inlet Mach	0.65
Exit Mach	0.364
Inlet Pressure	101325 Pa
Inlet Temperature	300 K
Rotor Angular Speed	1000 rad/sec
Rotor blades	50
Stator blades	32

Table 5.1: Summary of duct, rotor and stator parameters

5.3 Duct Geometry and Inlet Conditions

The design of the duct was conducted by choosing a set of absolute dimensions characteristic of a high pressure spool. These selected parameters, while sufficient in themselves to define the inlet of the duct, were then used with the streamline curvature program to arrive at the full geometry of the hub-casing configuration, including exit area, location of rotor and stator, and radial extension of the hub. All pertinent parameters for the duct, rotor and stator are summarized in table 5.1.

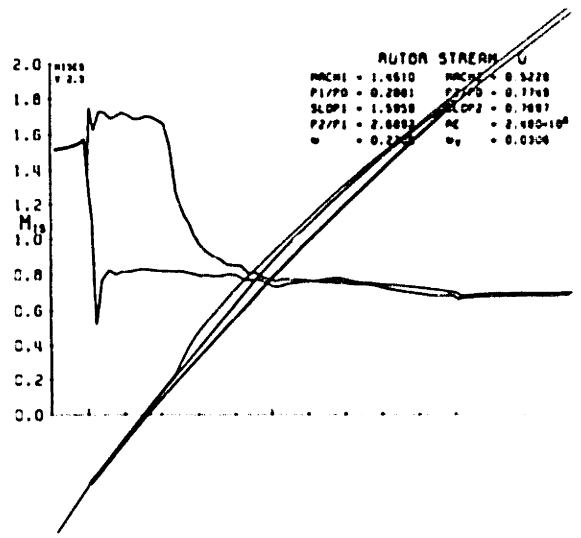

Figure 5-4: Rotor section 9 without suction

5.4 Boundary Layer Control

No solution could be found for any one of the rotor or stator sections analyzed without the use of boundary layer suction. The viscous behavior at mid-span without suction is represented in figures 5-4 and 5-5, showing the characteristic region of separation, indicative of an untenable level of loading. Thus the operating point of the stage is completely contingent upon the ability to control boundary layer dynamics. This somewhat obvious statement (considering the very high pressure ratio set for the stage) leads however, to a set of not so obvious considerations: if suction is a must, then how much and where?

5.4.1 Rotor Blade Boundary Layer Control

Analysis of the flow at midspan of the rotor blade revealed a single failure point on the suction side of the airfoil; the adverse pressure gradient across the passage shock induced an early separation. In contrast, the lightly loaded pressure side evinced very little viscous growth and posed no problem. Consequently, suction was applied to the suction surface of rotor section 9, approximately beneath the separation bubble. In this analysis, it was found that a very moderate level of mass removal, on the order of 2 to 3 percent of inlet streamtube, was required to reattach the boundary layer and converge a solution with minimal viscous loss. Requirements and conditions at both hub and tip however, differ significantly from

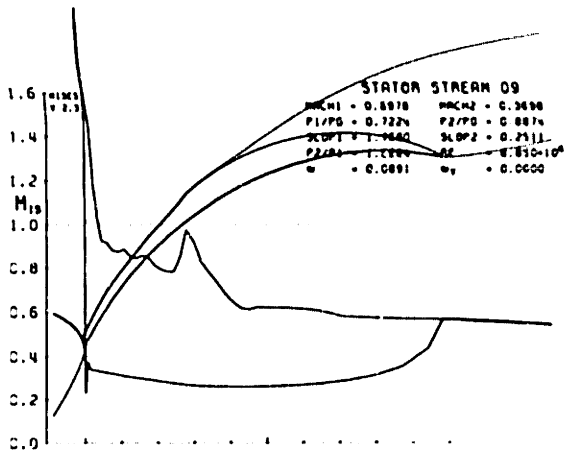

Figure 5-5: Stator section 9 without suction

midspan and hence, each in turn presented its own unique set of problems.

Closer to the hub, the rotor sections have a larger degree of turning given the fact that the relative velocity is significantly less than that at mid-span (constant work being prescribed across the annulus). This particular situation gave rise to two distinct failure points across the suction side of the foil; one associated with the passage shock as described for midspan and one tied to the turning of the flow. This second point however, was brought under control by simply increasing the amount of mass removed at the first failure point on the profile. A relatively large amount of suction -as compared to midspan- was required to keep the boundary layer attached throughout. Despite the difficulties encountered with the suction side, the pressure side of rotor section 5 presented no new problems and its boundary layer shows very little growth.

In contrast to both hub and mean, the pressure side of the section computed in proximity to the tip displayed separation problems similar to those described for the suction surface of all lower radii. As was mentioned previously in section 4.2, the passage shock recedes into the diffuser, exacerbating the boundary layer growth on the pressure side of the foil. However, by iterating on the geometry of the airfoil and carefully selecting the level of mass removal on the suction side of the blade, a solution was found in which the pressure side boundary layer reattaches with minimal viscous loss.

Section	Location	Slot length	Mass percentage removed
r05	0.28	0.05	14.4
r09 (midspan)	0.248	0.05	2.25
r15	0.55	0.05	2.57
s05	0.6	0.03	2.0
s09 (midspan)	0.7	0.05	4.41
s15	0.75	0.05	3.0

Table 5.2: Suction parameters for both rotor and stator

5.4.2 Stator Vane Boundary Layer Control

Stator vane viscous solutions with suction presented very little problem. All three sections analyzed displayed similar characteristics requiring an almost identical level of mass removal at virtually the same location. The gradual diffusion across the entire length of the passage presented no single localized failure, and it was rather the combination of loading and turning that would lead to separation. Final results for the stator show minimal losses along the entire span.

A summary of suction levels and location for both rotor and stator can be found in table 5.2. The position and length of the suction region along the airfoil are given as a percentage of chord in the meridional-theta coordinates used by MISES; the amount of mass removed is expressed as a percentage of inlet streamtube. The mass averaged amount of mass removed for both rotor and stator is 5.4% and 3.15% respectively, making the total percentage of mass removed from the inlet flow for the stage 8.55%.

Chapter 6

Conclusion

The simulations conducted in this study support the practicability of controlling boundary layer growth through suction. The possibility of enhancing the loading limit of airfoil performance by delaying separation should come as no surprise; however, it is the low level of mass removal required and the prospect of stagnation pressure ratios higher than three for a single stage that make the study not only revealing but extremely enticing.

The stage design proposed would be suitable for a first stage for a modern high pressure spool. Both rotor and stator airfoils make use of a "suction scoop" to ingest a fraction of the high entropy fluid and preserve a favorable boundary layer profile despite the high loading. The level of mass removal required to maintain the operation of the rotor blade under these conditions increases significantly towards the hub, whereas that for the stator vane remains fairly constant throughout the span. Stator and rotor alike present minimal viscous losses; shock losses in the rotor passages account for most of the inefficiencies.

All results were obtained by implementing a quasi 3D design. The approach consists of combining a streamline curvature code with a blade to blade viscous/inviscid coupled Euler solver known as MISES. MISES was successfully modified to incorporate the effects of boundary layer suction. The methodology is both robust and expedient; however, sensitive and tedious in the high Mach number regime. The design obtained is thus at the limit of what this particular approach can deliver; all further enhancements and analysis performed on this configuration should strive towards a more inclusive and integrated process.

6.1 Recommendations

Most recommendations for further study simply stem from the approximate nature of the model used to deliver the design. The aerodynamics of turbomachinery, though tractable to first degree under approximate conditions, evince a variety of truly three dimensional features not captured by the present approach. Not to be forgotten amongst the subtleties of compressor flows, the effects of both hub and casing boundary layers, perhaps exacerbated by the high pressure ratio of the stage, deserve a careful analysis as well.

Spanwise flows within the diffusing passages are one of the significant effects neglected by the model. As discussed in the chapter on methodology, the design was constructed by assembling a spanwise aggregate of essentially two dimensional slices. The nature and strength of the spanwise flow has been shown to be significant in previous studies completed at MIT [5] and, the proposed removal of boundary layer flow could have marked effects on this secondary flow. It is possible to speculate on repercussions throughout the various aspects of performance, ranging to tip clearance flows and uniformity conditions downstream, to stability and stall characteristics for the stage.

Yet perhaps the single most important recommendation for future work stems from the feasibility of implementing a boundary layer suction scheme. The results of the study indicate that the level of performance sought can be had for levels of suction as low as 8.5% of the inlet mass flow. Hollow compressor blades are already an option, and the opportunity to exploit this architecture in the pursuit of a higher pressure rise per stage should not be neglected.

Bibliography

[1] N. Cumpsty. *Compressor Aerodynamics.* The MIT Press, 1992.

[2] M. Drela. *Personal communication.* 1995.

[3] L. Fottner. Review on turbomachinery blading design problems. Technical Report AGARD-LS-167, AGARD, 1989.

[4] J. L. Kerrebrock. *Aircraft Engines and Gas Turbines.* The MIT Press, 1992.

[5] P. Kotidis. *Unsteady Radial Transport in a Transonic Compressor Stage.* PhD thesis, Massachusetts Institute of Technology, 1989.

[6] G. Meauze. Overview on blading design methods. Technical Report AGARD-LS-167, AGARD, 1989.

[7] A. Merchant. Design and analysis of supercritical airfoils with boundary layer suction. Master's thesis, Massachusetts Institute of Technology, 1996.

[8] H. Schlichting. *Boundary-Layer Theory.* McGraw-Hill, Inc., 1955.

[9] L. Smilg. Design of a high pressure ratio fan stage to take advantage of boundary layer suction. Master's thesis, Massachusetts Institute of Technology, 1994.

[10] H. Starken. Design criteria for optimal blading design. Technical Report AGARD-LS-167, AGARD, 1989.

[11] F. M. White. *Viscous Fluid Flow.* McGraw-Hill, Inc., 1974.

[12] H. Youngren. Analysis and design of transonic cascades with splitter vanes. Master's thesis, Massachusetts Institute of Technology, 1991.

Appendix A

Rotor

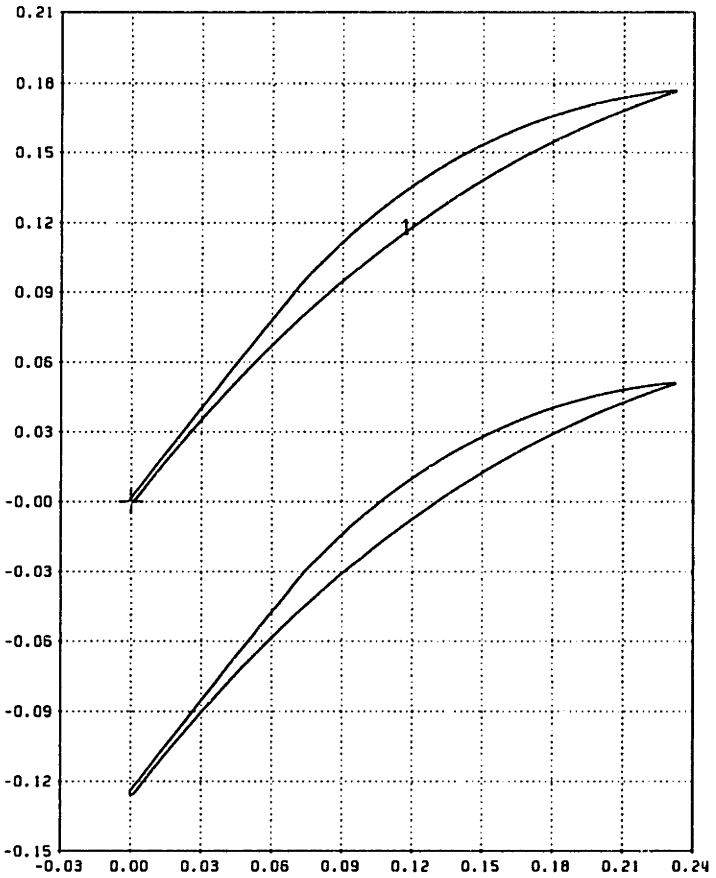

Figure A-1: Rotor Section 5 MISES Coordinates

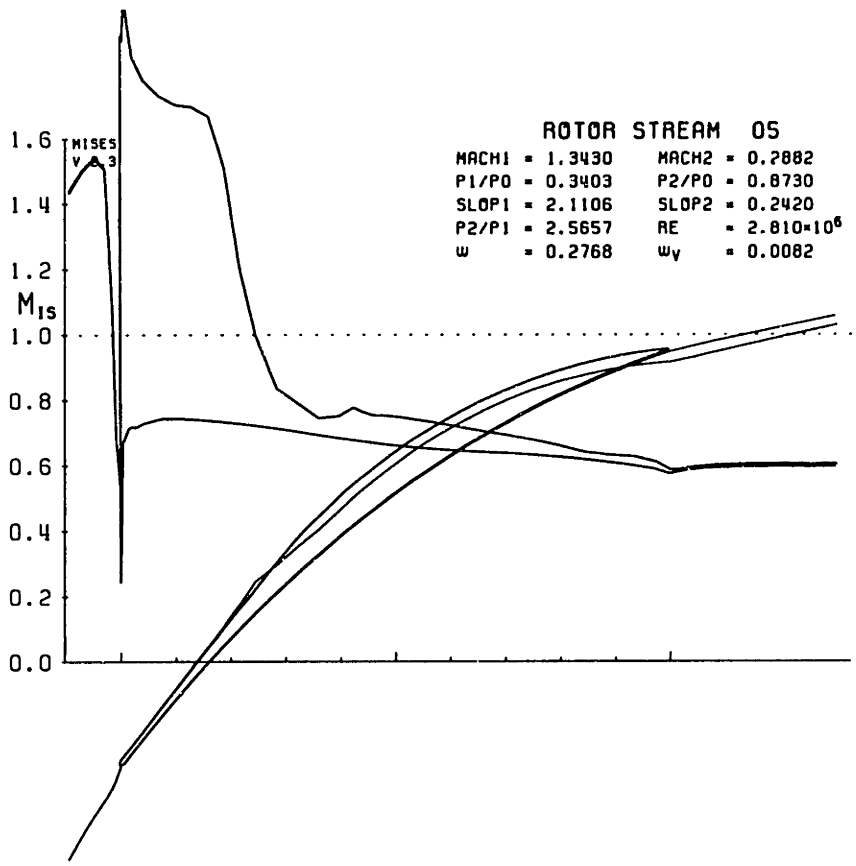

Figure A-2: Rotor Section 5 Mach Contour Viscous Projection

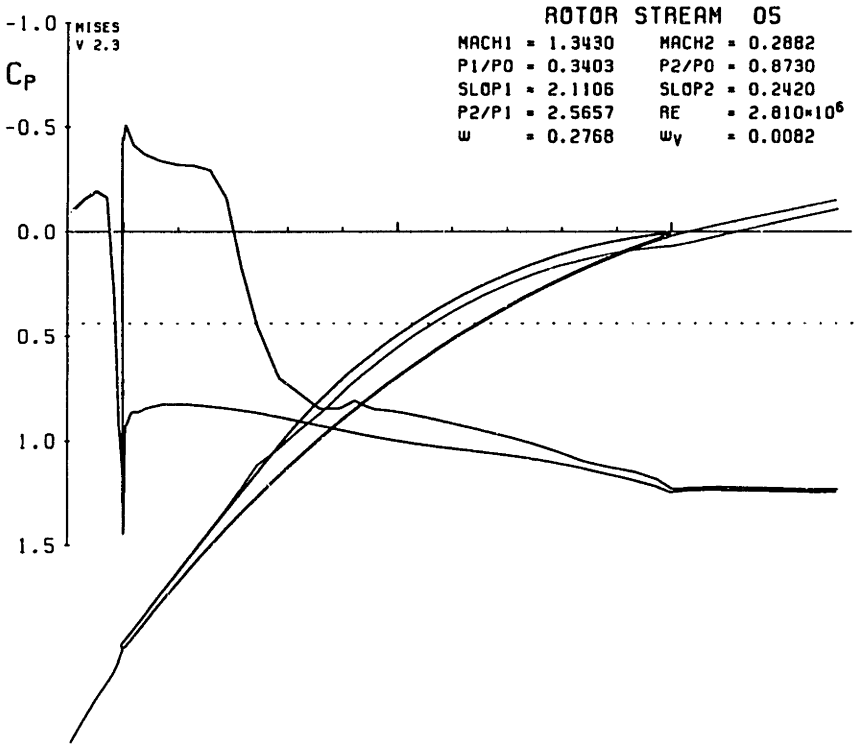

Figure A-3: Rotor Section 5 Coefficient of Pressure Viscous Projection

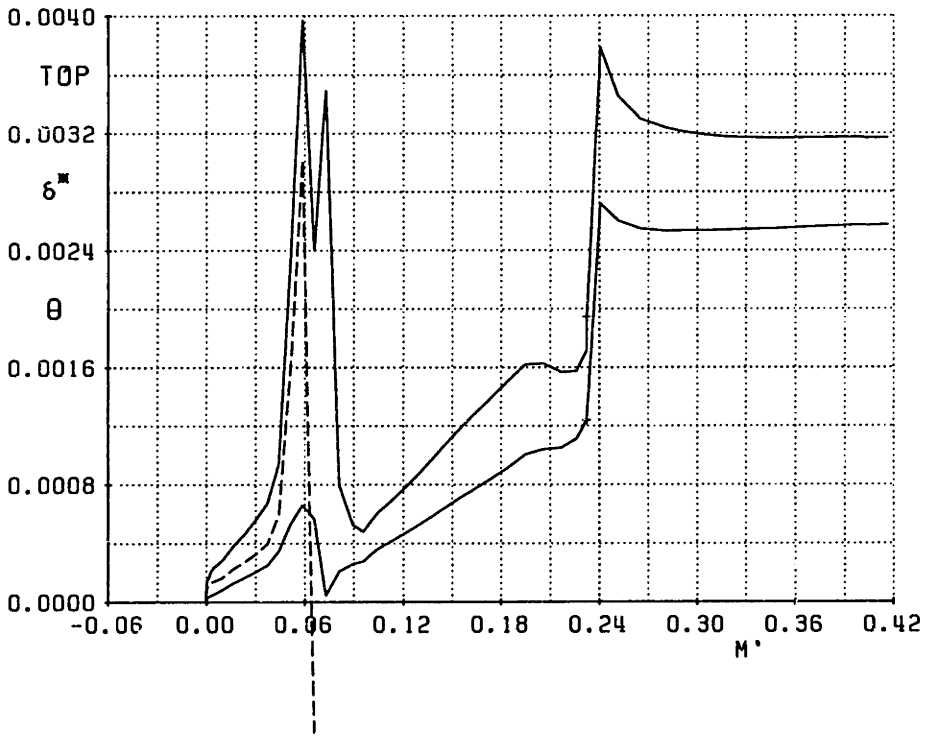

Figure A-4: Rotor Section 5 Suction Surface Boundary Layer Profile Projection

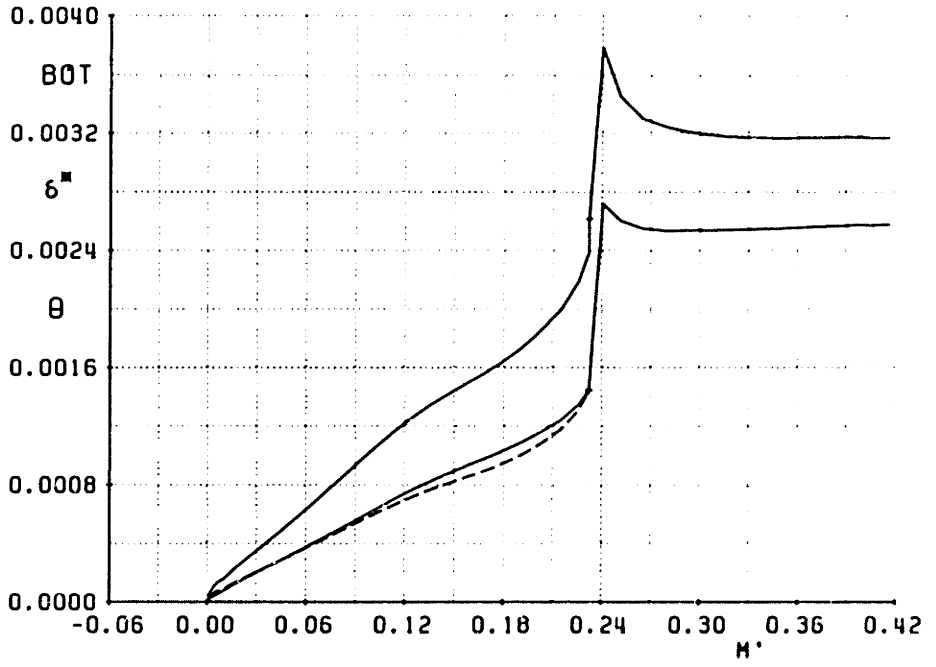

Figure A-5: Rotor Section 5 Pressure Surface Boundary Layer Profile Projection

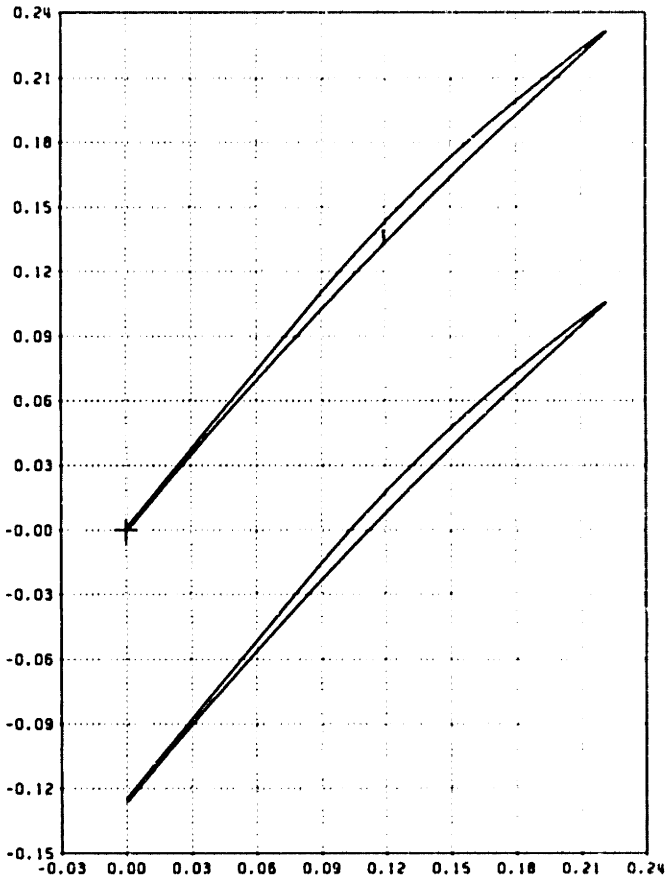

Figure A-6: Rotor Section 9 MISES Coordinates

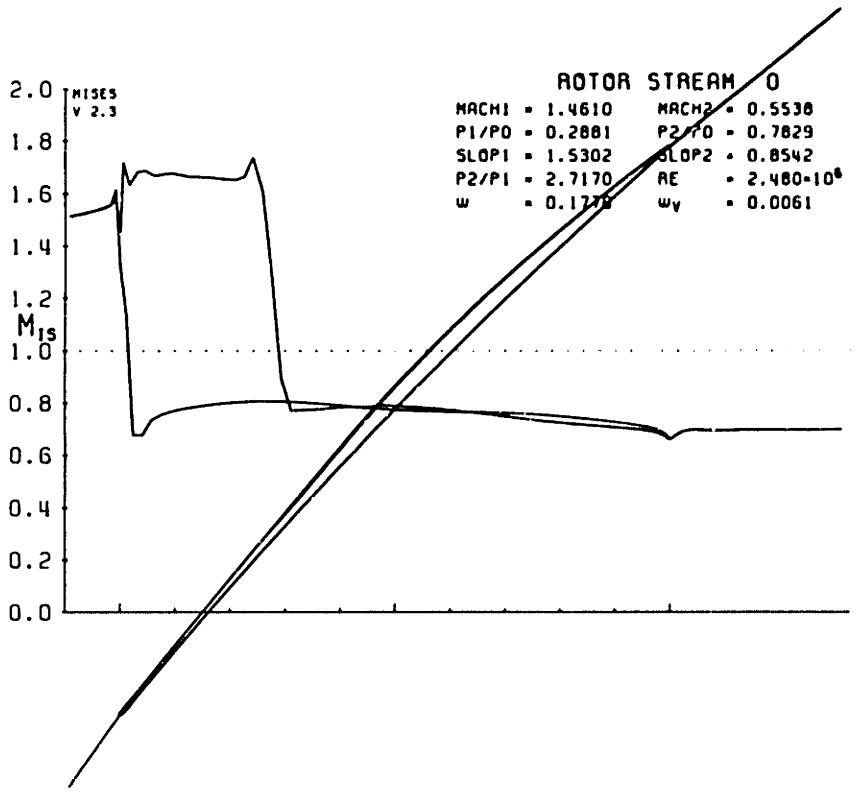

Figure A-7: Rotor Section 9 Mach Contour Viscous Solution

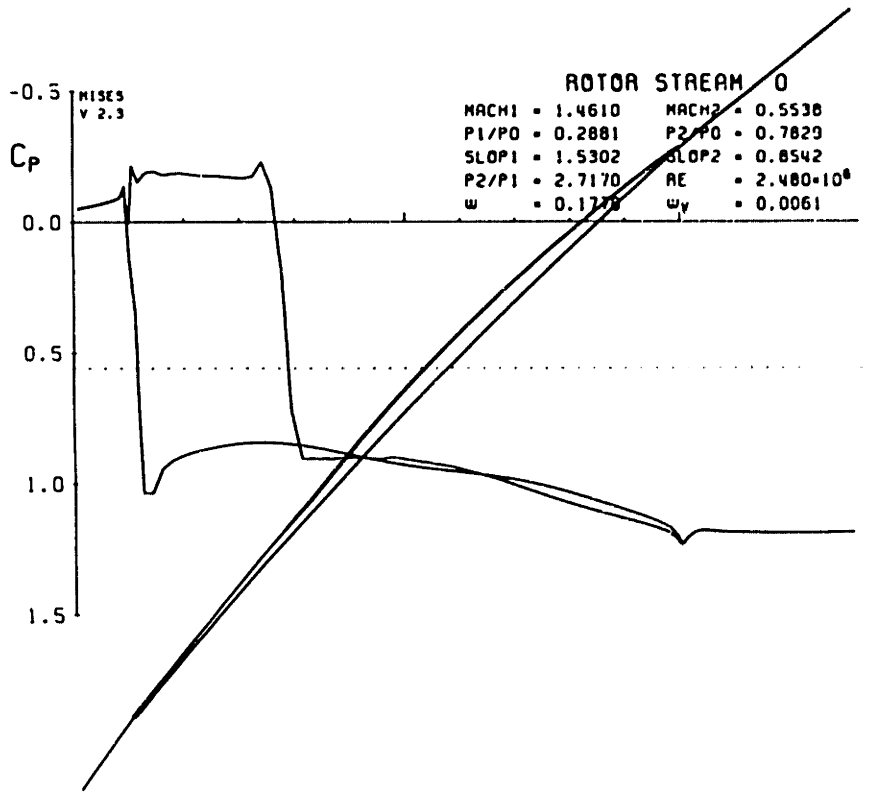

Figure A-8: Rotor Section 9 Coefficient of Pressure Viscous Solution

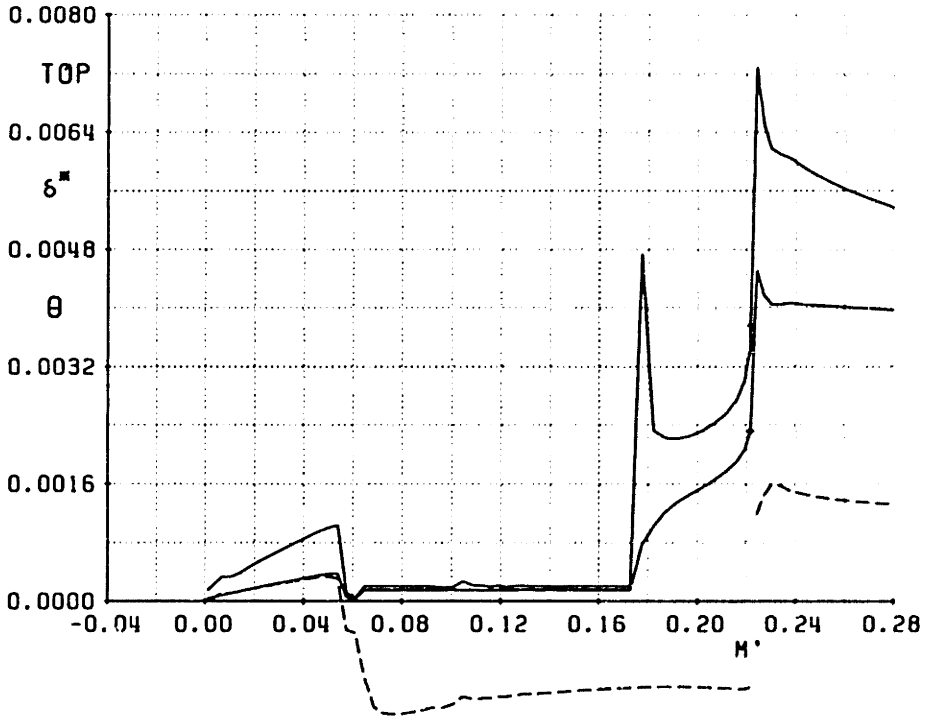

Figure A-9: Rotor Section 9 Suction Surface Boundary Layer Profile

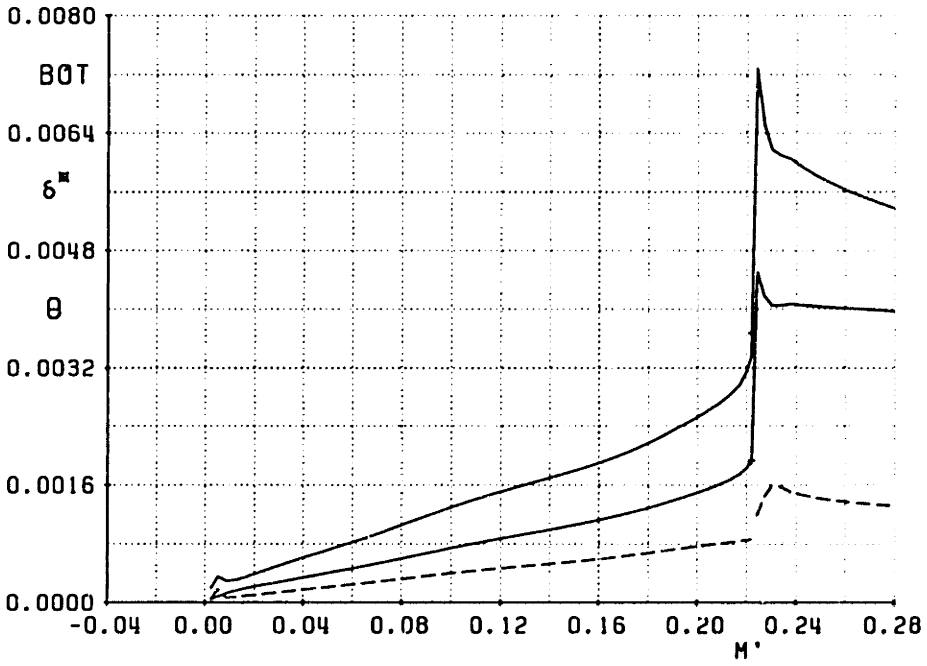

Figure A-10: Rotor Section 9 Pressure Surface Boundary Layer Profile

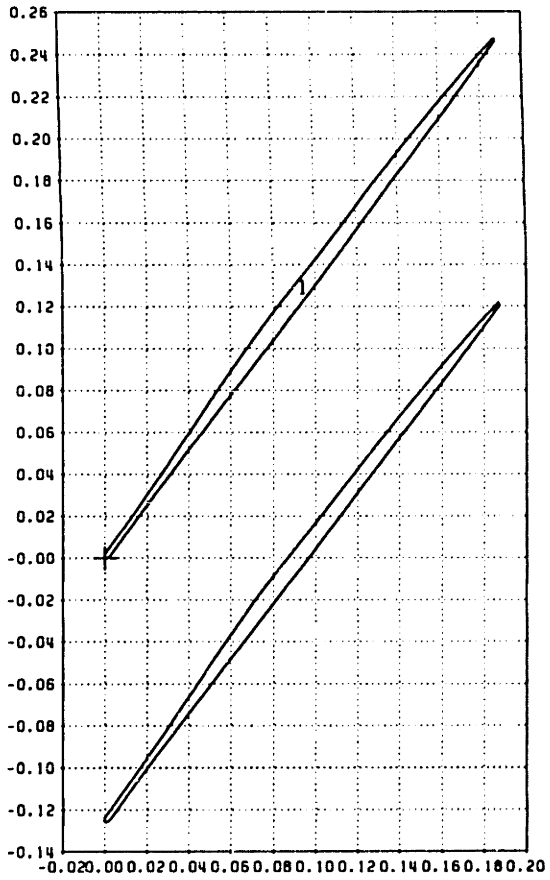

Figure A-11: Rotor Section 15 MISES Coordinates

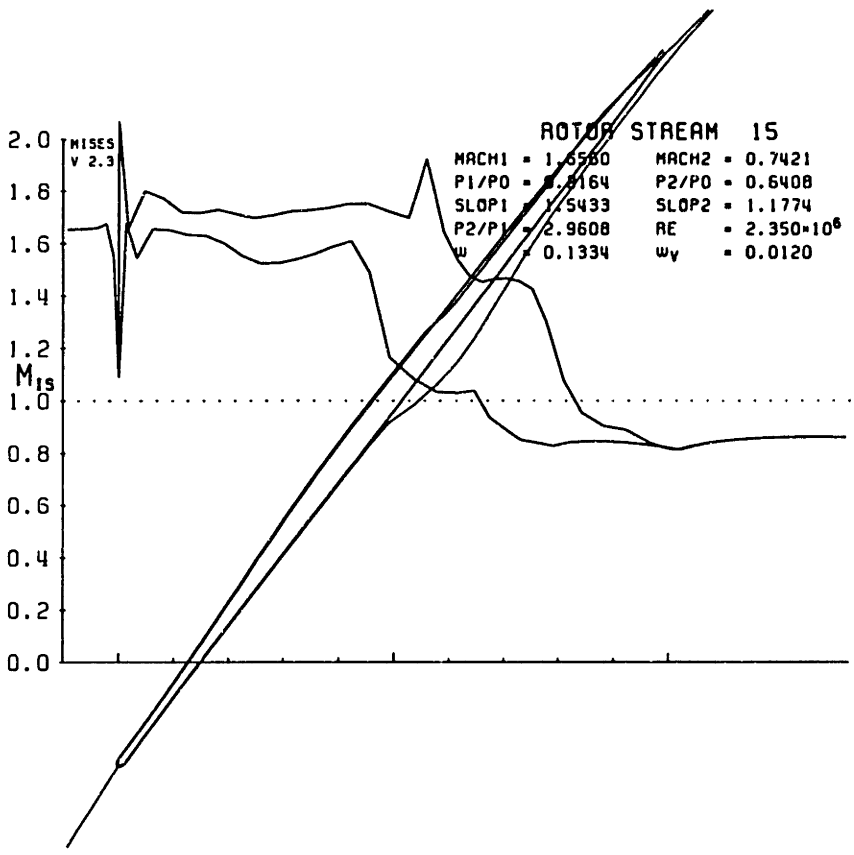

Figure A-12: Rotor Section 15 Mach Contour Viscous Projection

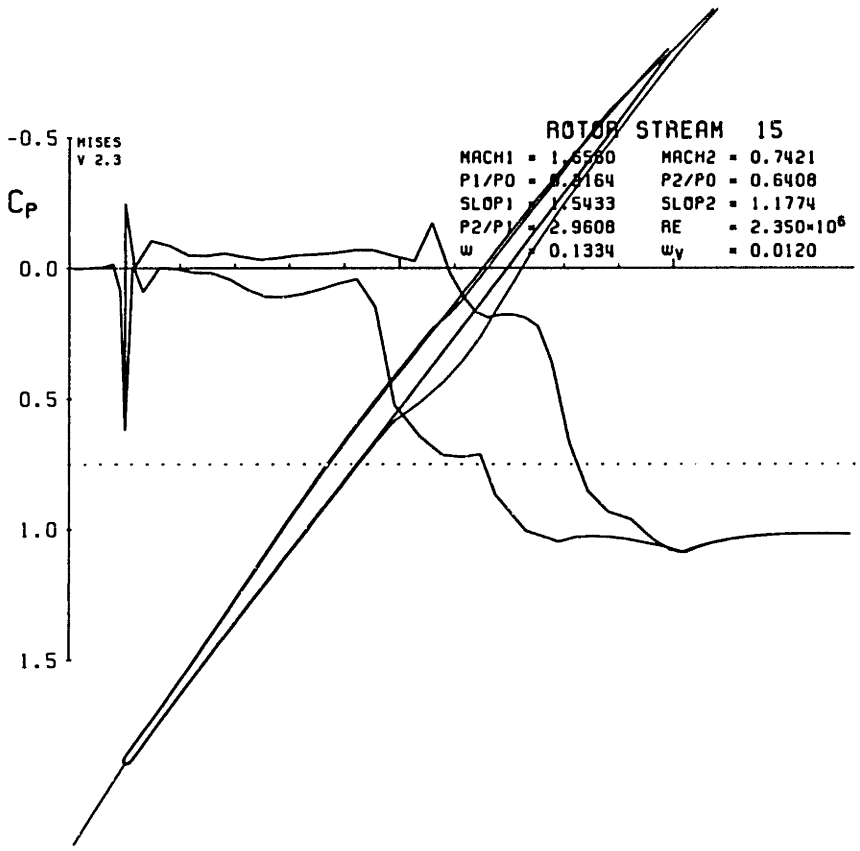

Figure A-13: Rotor Section 15 Coefficient of Pressure Viscous Projection

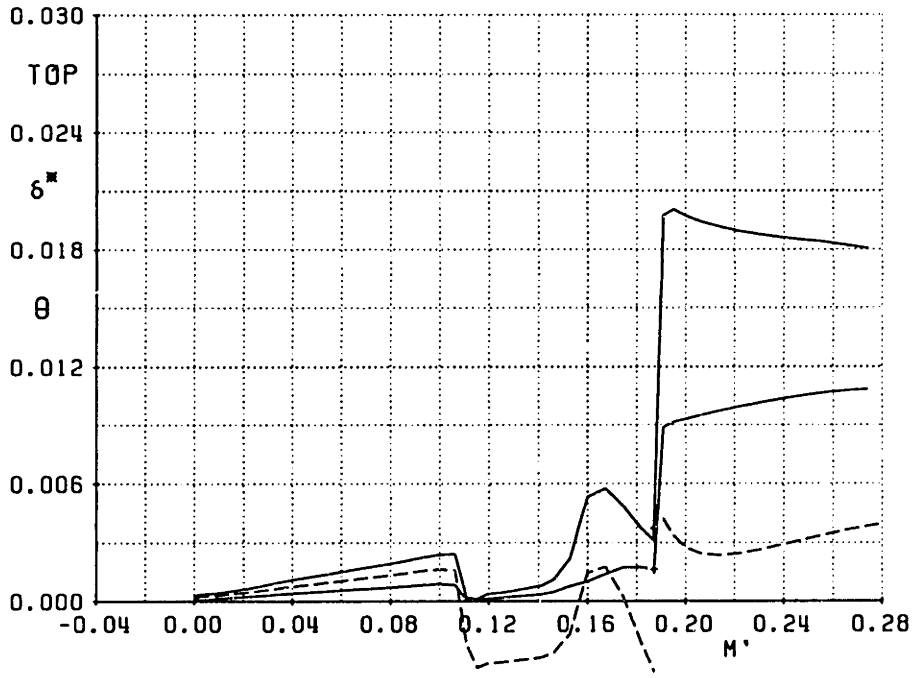

Figure A-14: Rotor Section 15 Suction Surface Boundary Layer Profile Projection

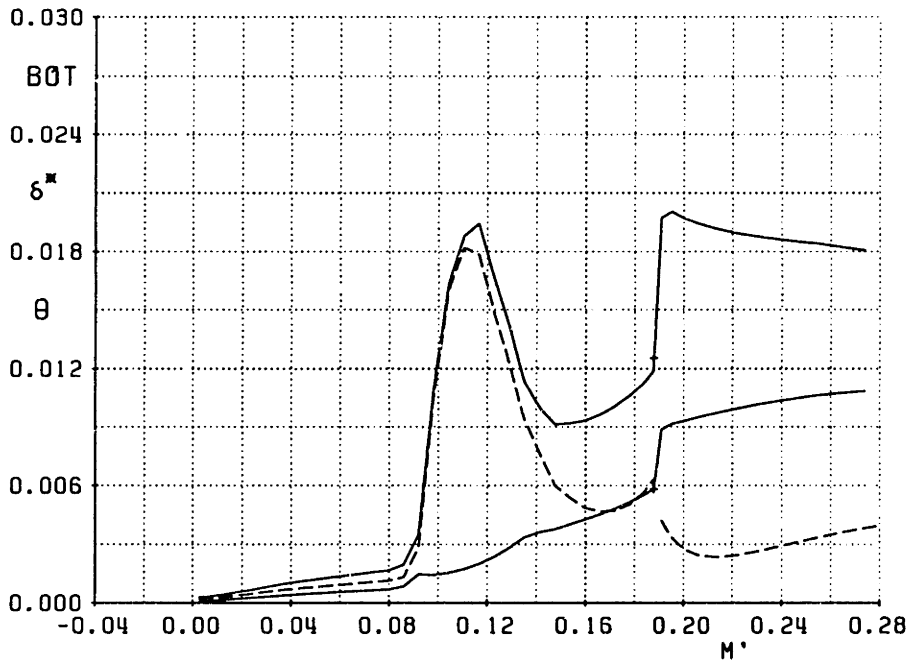

Figure A-15: Rotor Section 15 Pressure Surface Boundary Layer Profile Projection

Appendix B

Stator

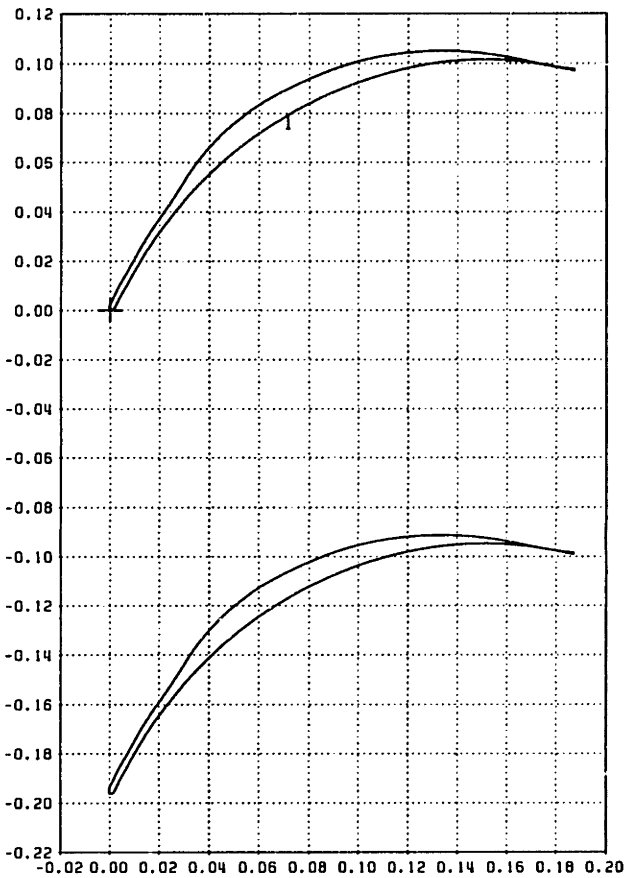

Figure B-1: Stator Section 5 MISES Coordinates

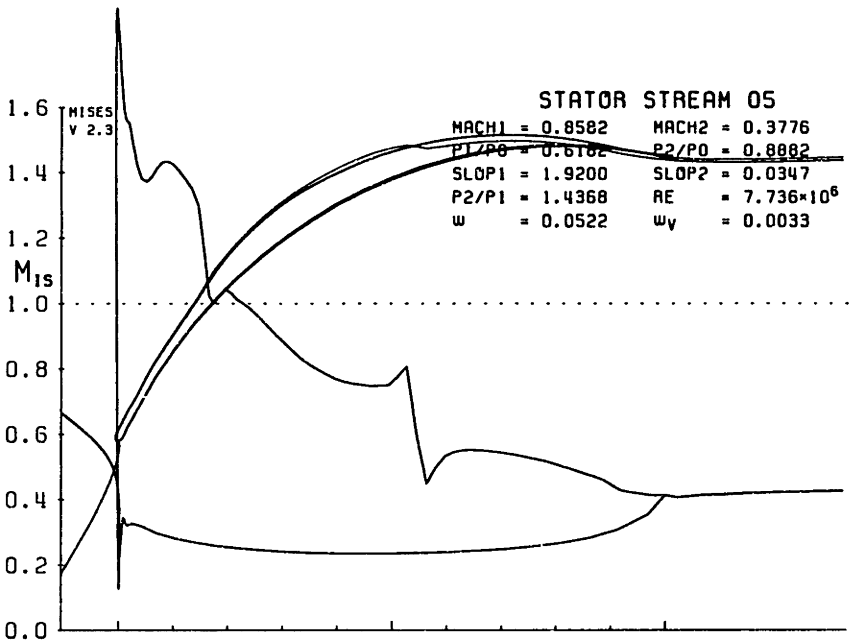

Figure B-2: Stator Section 5 Mach Contour Viscous Solution

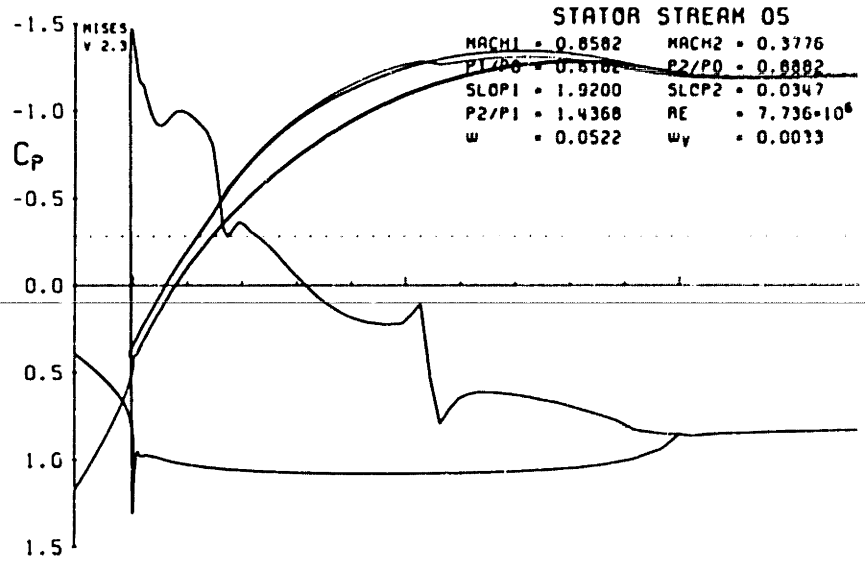

Figure B-3: Stator Section 5 Coefficient of Pressure Viscous Solution

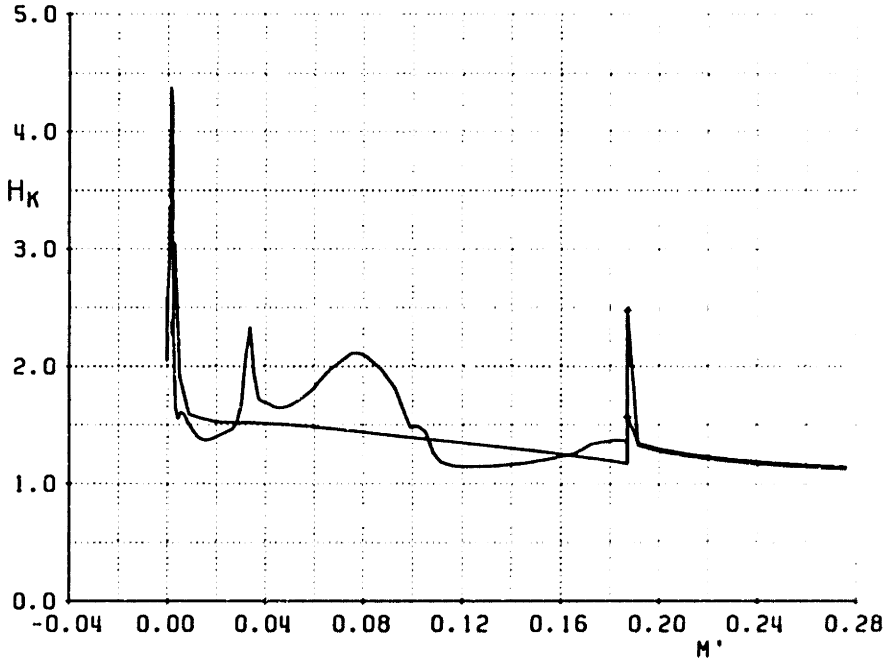

Figure B-4: Stator Section 5 Shape Factor

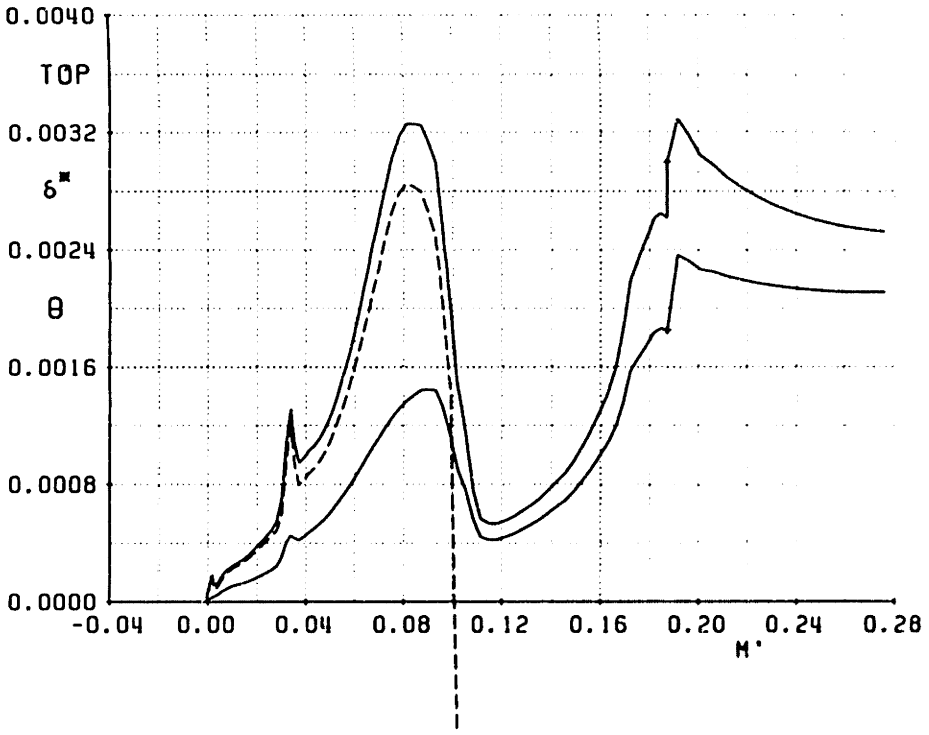

Figure B-5: Stator Section 5 Suction Surface Boundary Layer Profile

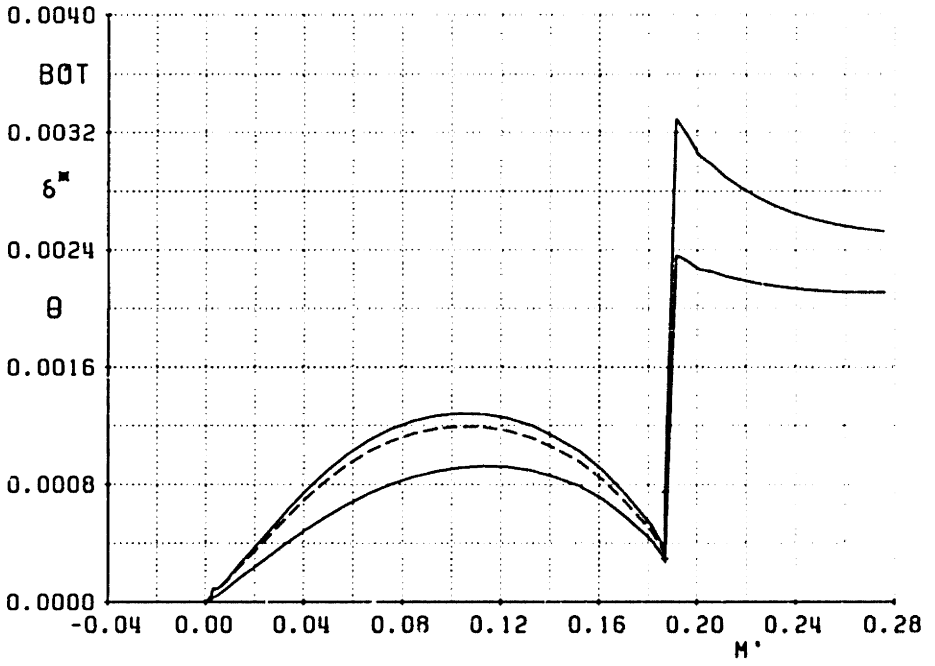

Figure B-6: Stator Section 5 Pressure Surface Boundary Layer Profile

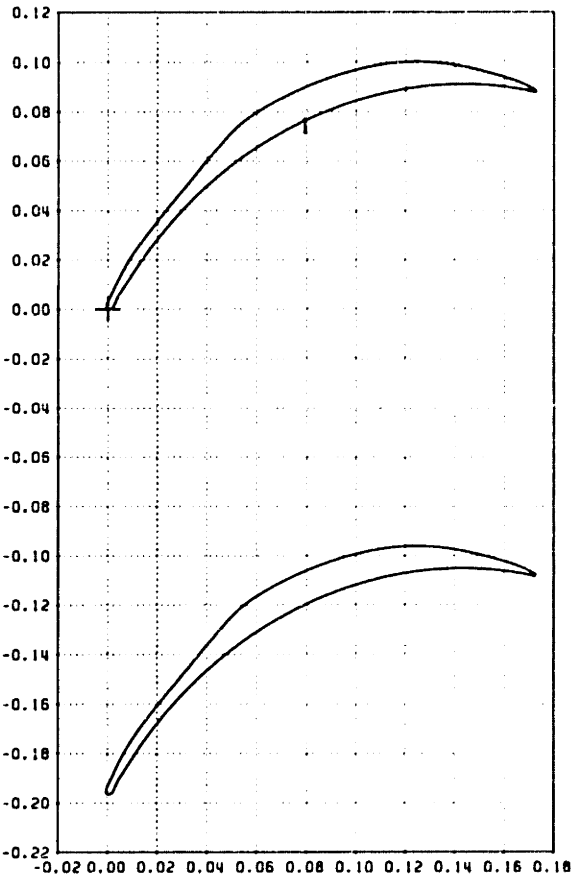

Figure B-7: Stator Section 9 MISES Coordinates

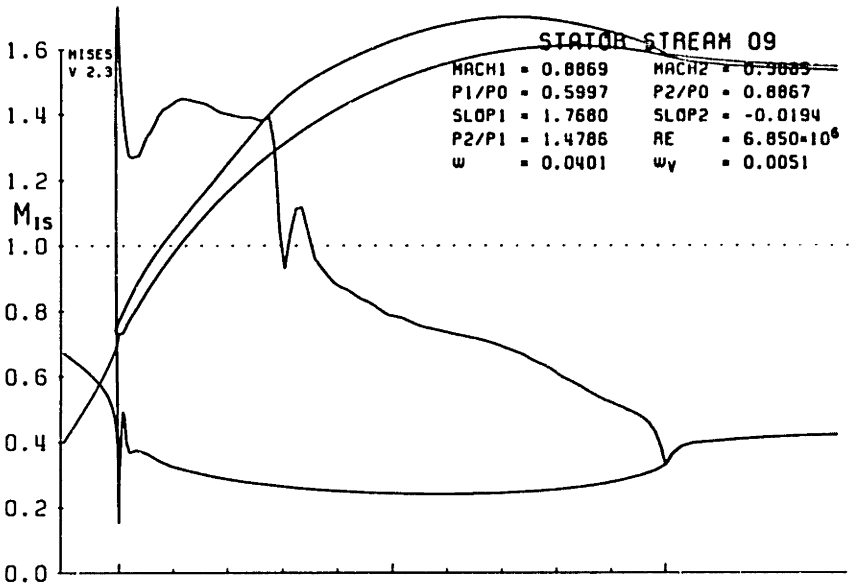

Figure B-8: Stator Section 9 Mach Contour Viscous Solution

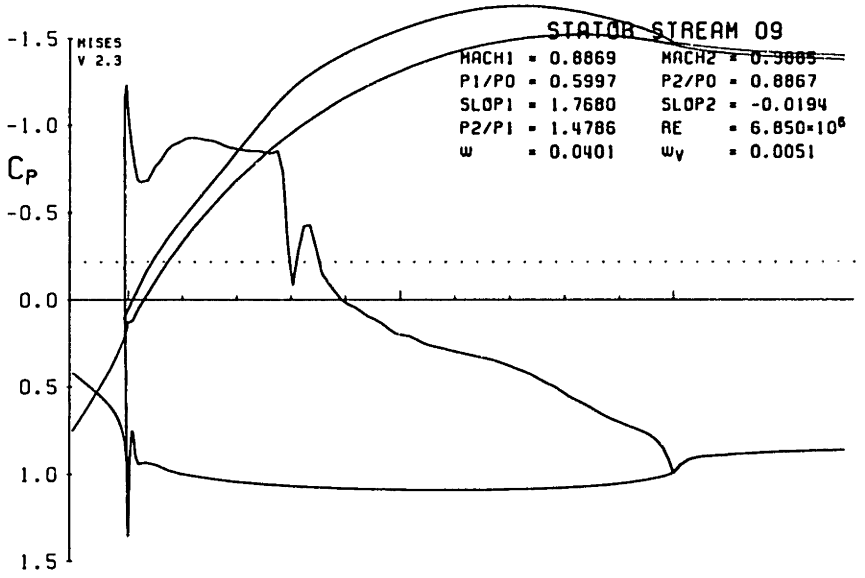

Figure B-9: Stator Section 9 Coefficient of Pressure Viscous Solution

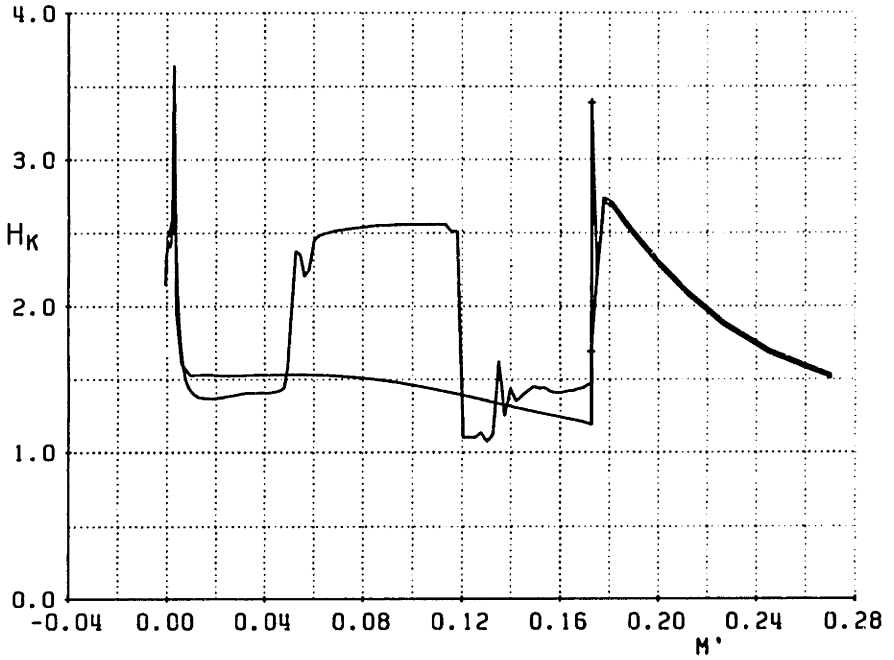

Figure B-10: Stator Section 9 Shape Factor

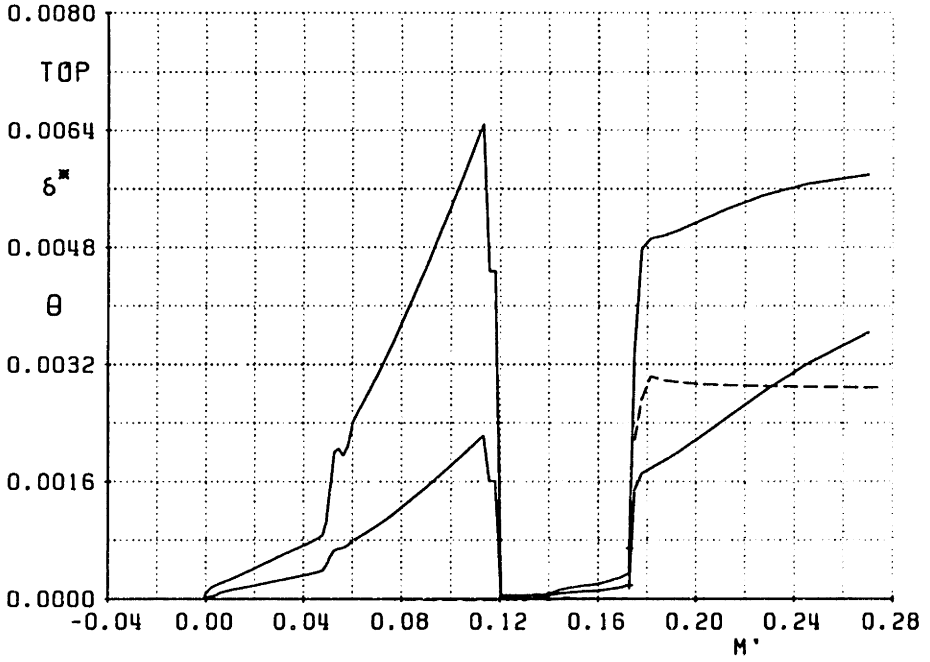

Figure B-11: Stator Section 9 Suction Surface Boundary Layer Profile

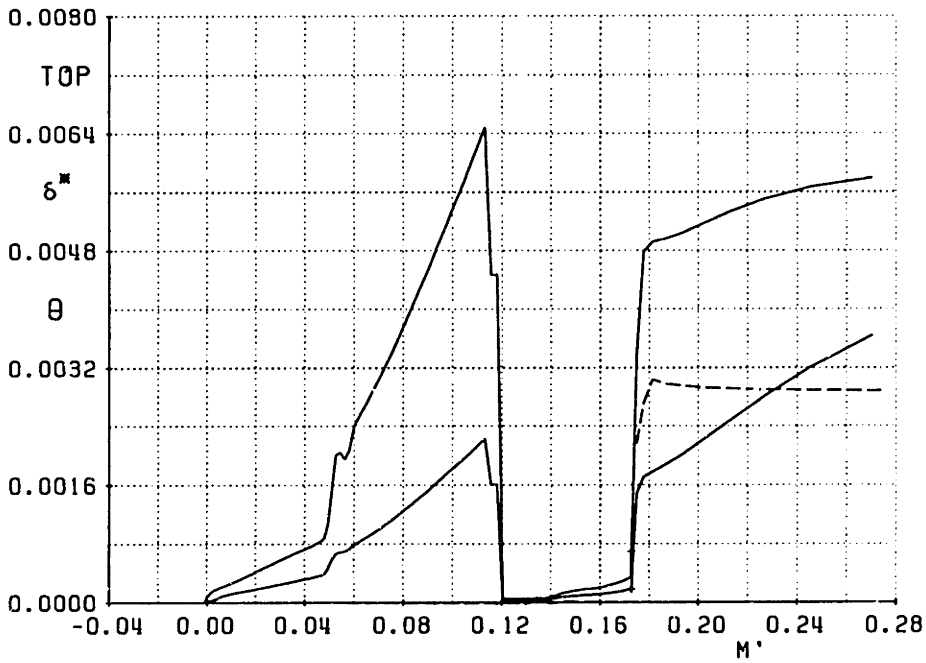

Figure B-12: Stator Section 9 Pressure Surface Boundary Layer Profile

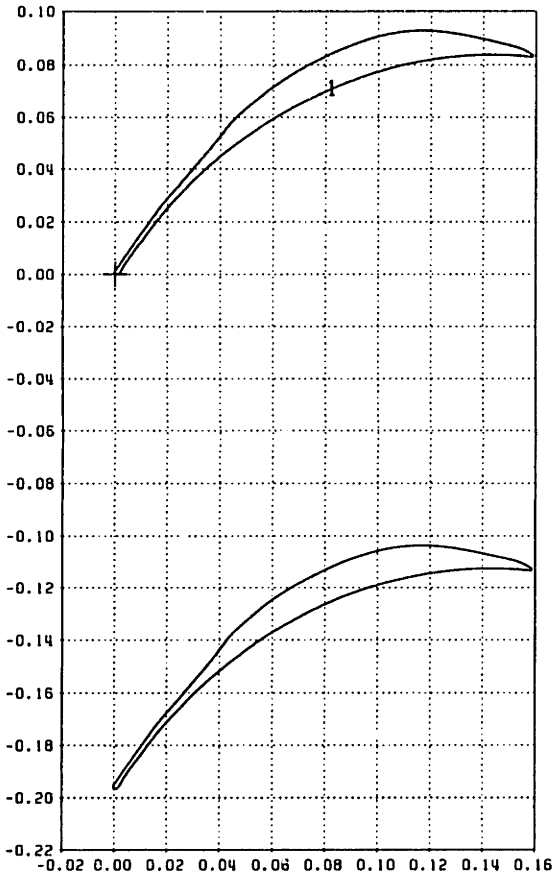

Figure B-13: Stator Section 15 MISES Coordinates

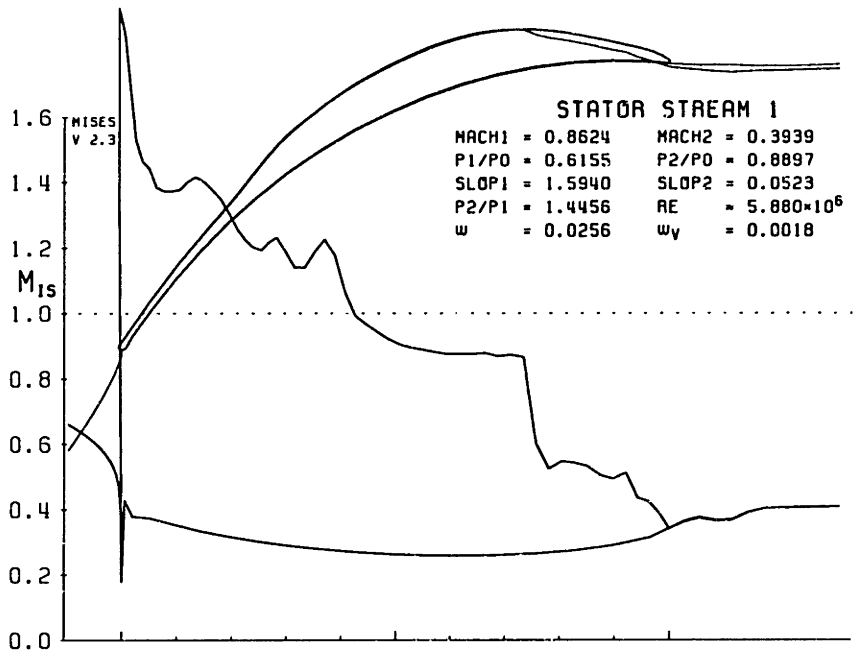

Figure B-14: Stator Section 15 Mach Contour Viscous Solution

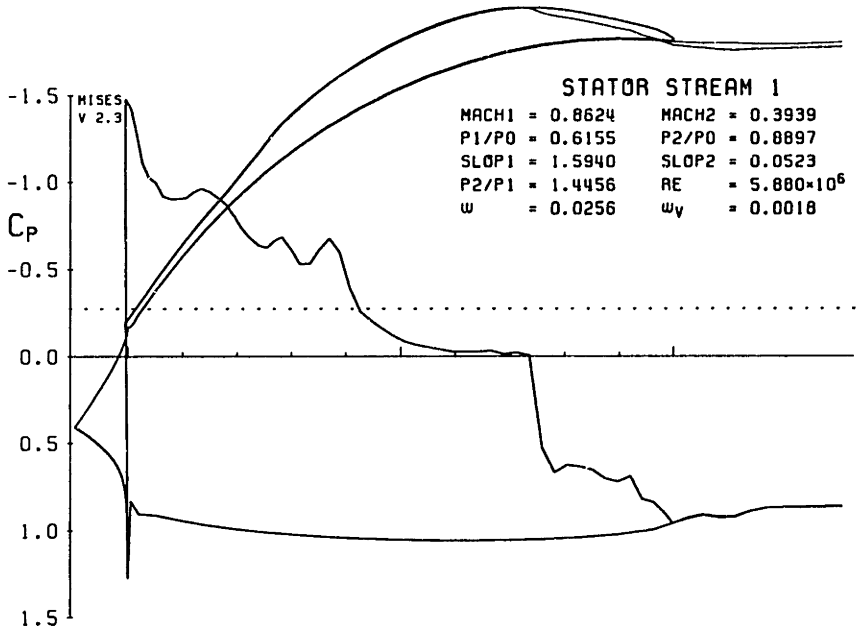

Figure B-15: Stator Section 15 Coefficient of Pressure Viscous Solution

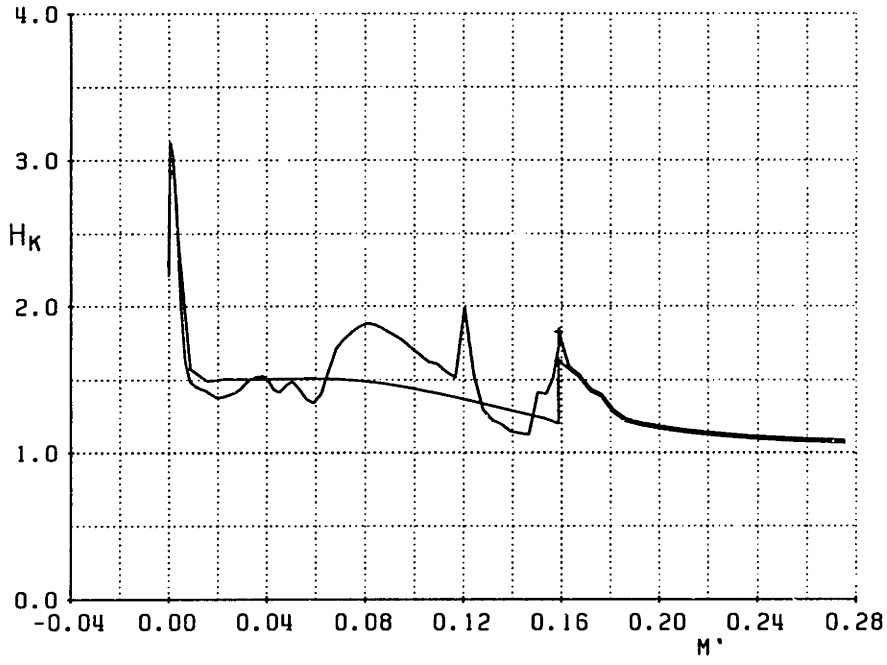

Figure B-16: Stator Section 15 Shape Factor

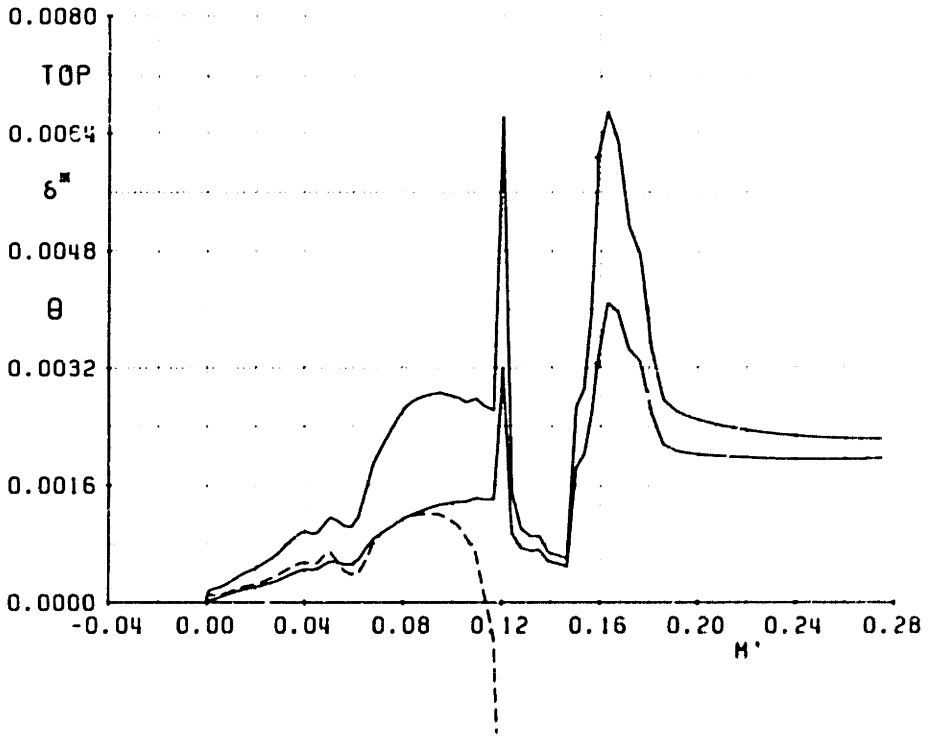

Figure B-17: Stator Section 15 Suction Surface Boundary Layer Profile

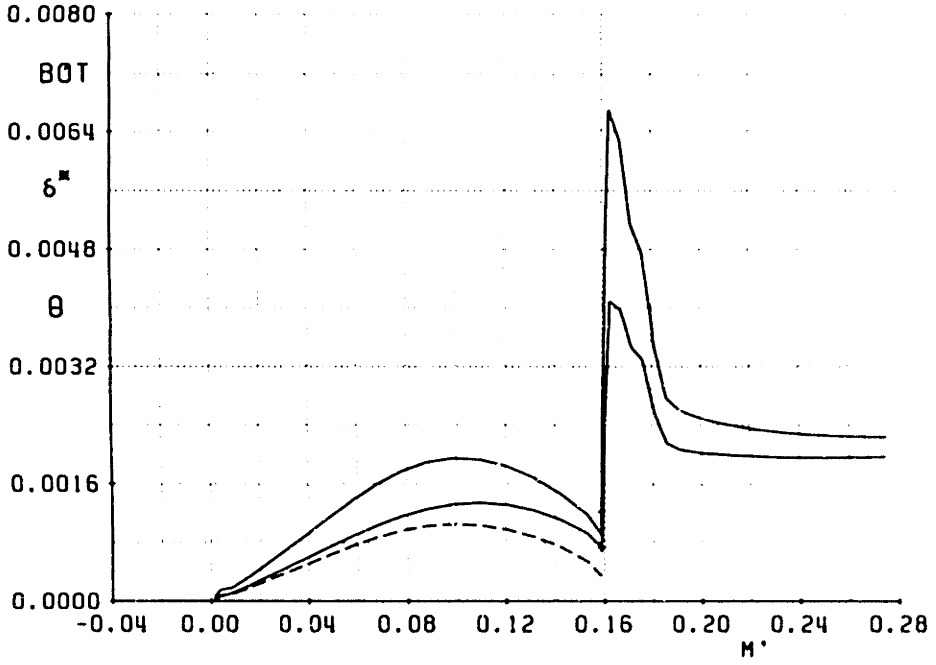

Figure B-18: Stator Section 15 Pressure Surface Boundary Layer Profile

Appendix C

Valve Drawings 1

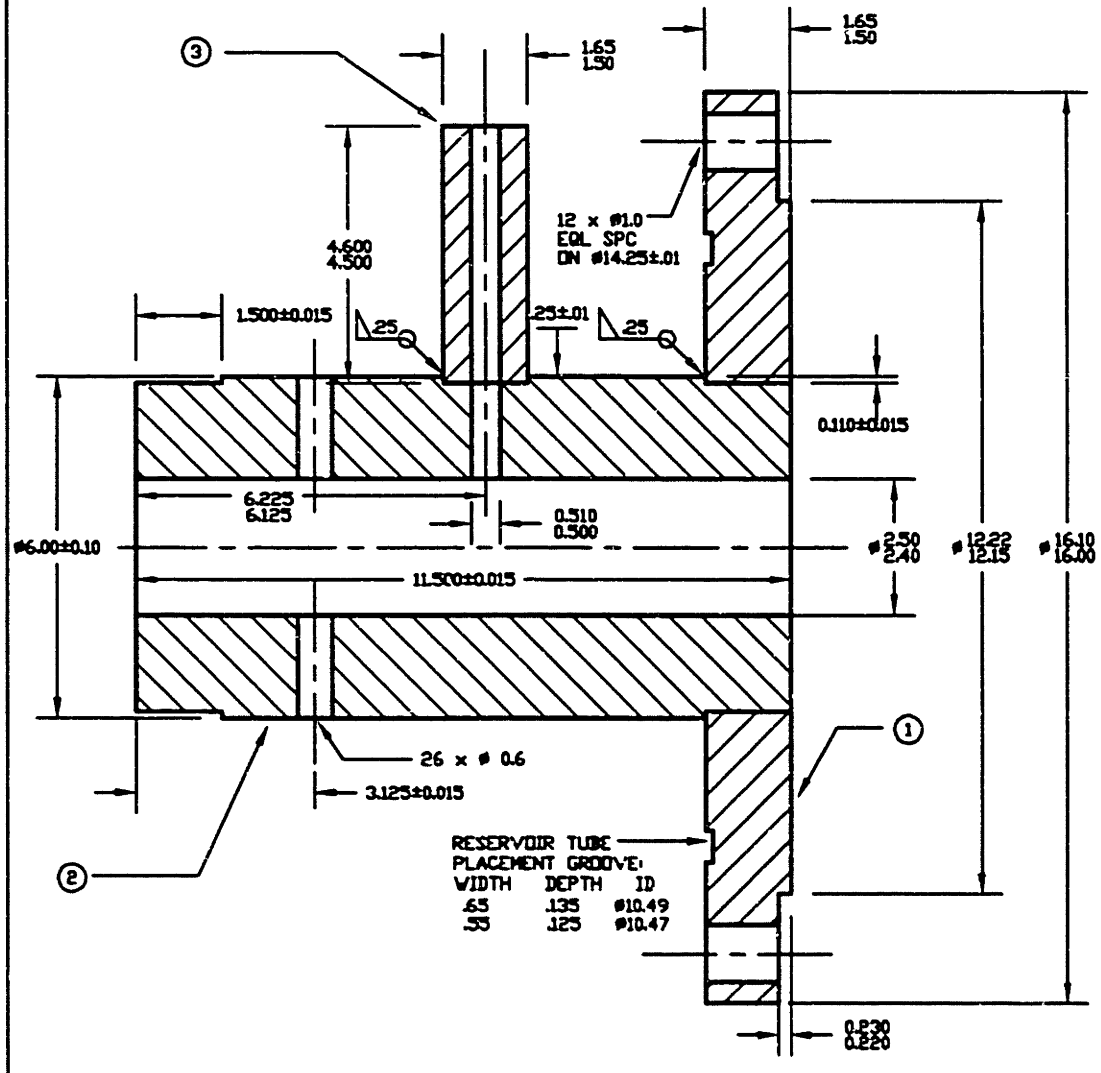

SHOWN ARE THREE PIECES WELDED TOGETHER:

① CIRCULAR FLANGE (1025 STEEL)
OD: 16.00 (+.10 -.00)
ID: 5.80 (+.01 -.00)
FEATURES: (1) 12 X ⌀1.0 BOLT HOLES
(2) PLACEMENT GROOVE

② LARGE TUBE (1025 STEEL)
OD: 6.05 ±.05
ID: 2.85 ±.05
FEATURES: (1) 30 X ⌀0.6 HOLES
(2) COUNTERBORED HOLE FOR SMALL TUBE
(3) .125 WELDING SHOULDERS FOR FLANGES

③ SMALL TUBE (1025 STEEL)
OD: 1.50±.01
ID: .5±.01
FEATURES: NONE

ALL SURFACES 32

ALL DIMENSIONS IN INCHES

NOTE: FACE FLANGE AFTER WELDING
ALL PARALLEL AND PERPENDICULAR TO ±.1°
ESPECIALLY THE FACE OF THE FLANGE
PERPENDICULAR TO THE AXIS OF LARGE TUBE

FLANGED POWER SHOT TUBE (FIRST STEP OF ASSEMBLY)

Zmansky-Brown

1

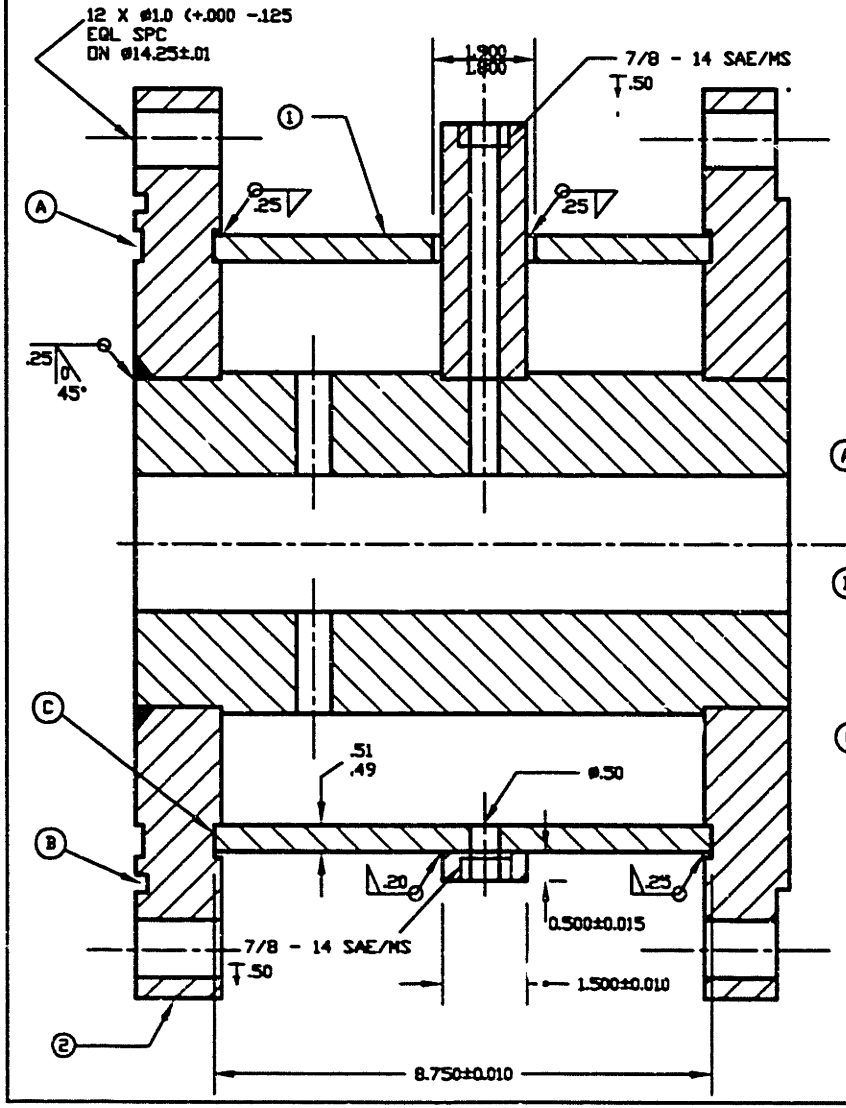

(A) MAIN TUBE LOCATION GROOVE

WIDTH	DEPTH	ID
.405	.140	ø10.4975
.395	.135	ø10.4940

(B) O-RING GROOVE

WIDTH	DEPTH	ID
.308	.205	ø11.975
+.002	+.006	±.060
-.003	-.004	

FOR DETAIL OF O-RING GROOVE SEE DATA SHEET FIG. A

(C) RESEVOIR TUBE PLACEMENT GROOVE

WIDTH	DEPTH	ID
.65	.135	ø10.490
.55	.125	ø10.470

(1) RESERVOIR TUBE:
ID: 10.5 (+.002 -.00)
OD: 11.5±.02
LENGTH: 8.25±.01
FEATURES: (i) THRU-HOLE FOR SMALL TUBE
(ii) THREADED STUD W/THRU-HOLE

(2) CIRCULAR FLANGE:
ID: 5.80±.01
OD: 16.0±.1
THICKNESS: 1.5±.01
FEATURES: (i) 12 X ø1.0 BOLT HOLES
(ii) MAIN TUBE LOCATION GROOVE
(iii) RESERVOIR LOCATION GROOVE
(iv) O-RING GROOVE

ALL DIMENSIONS IN INCHES

NOTES:

- THREAD SMALL TUBE WITH SAE/MS STRAIGHT THREADS AFTER WELDING RESERVOIR TUBE.
- WELD AND THREAD STUD ONTO RESERVOIR TUBE BEFORE WELDING RESERVOIR TUBE TO FLANGES.
- ALL SURFACES 3.2
- FACE OF FLANGE (2) SHOULD BE PERPENDICULAR TO THE AXIS OF THE LARGE TUBE TO ±.1°

FLANGED POWER SHOT TUBE (SECOND STEP OF ASSEMBLY)

Zawasky-Brown

2

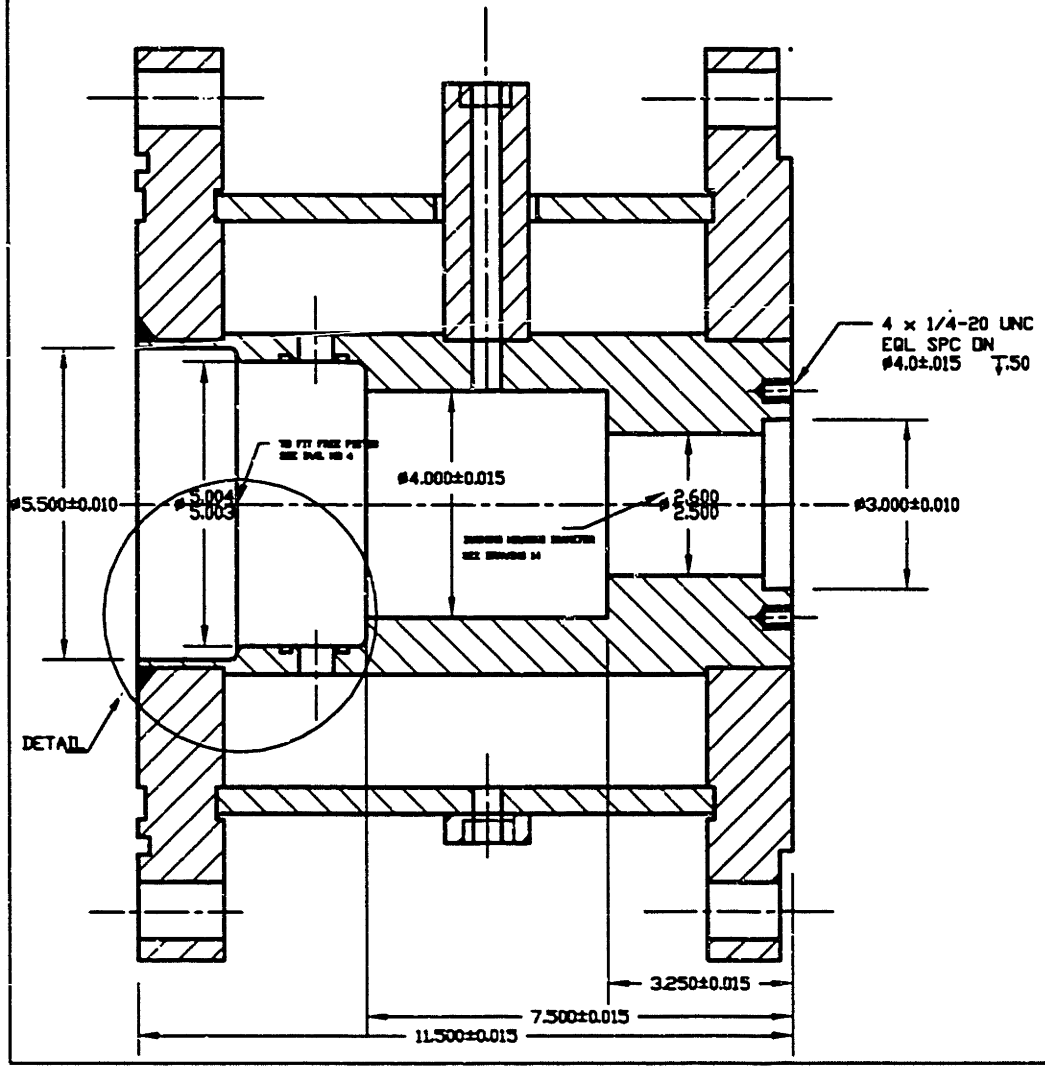

DETAIL
SCALE - 1:1
NOTE: RADIUS ON ALL CHAMFERS
IS .125

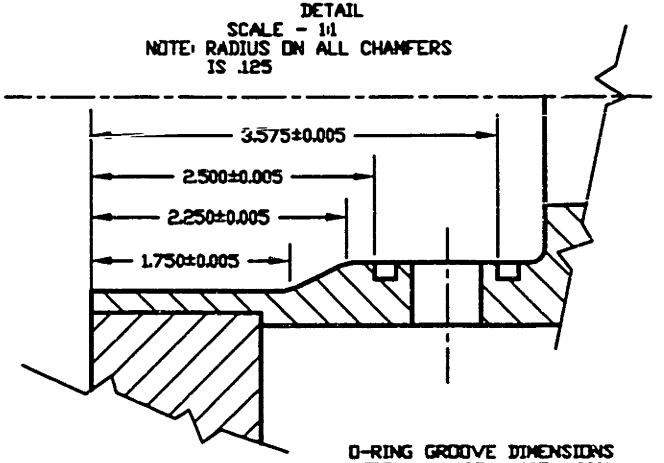

O-RING GROOVE DIMENSIONS
WIDTH .187 (+.005 -.000)
GROOVEø 5.222 (+.002 -.000)

FOR DETAIL OF O-RING GROOVE
SEE DATA SHEET FIG. B

ALL SURFACES 32

ALL DIMENSIONS IN INCHES

FLANGED POWER SHOT TUBE
FINAL STEP-BORING INNER TUBE

Zinnsky-Brown

3

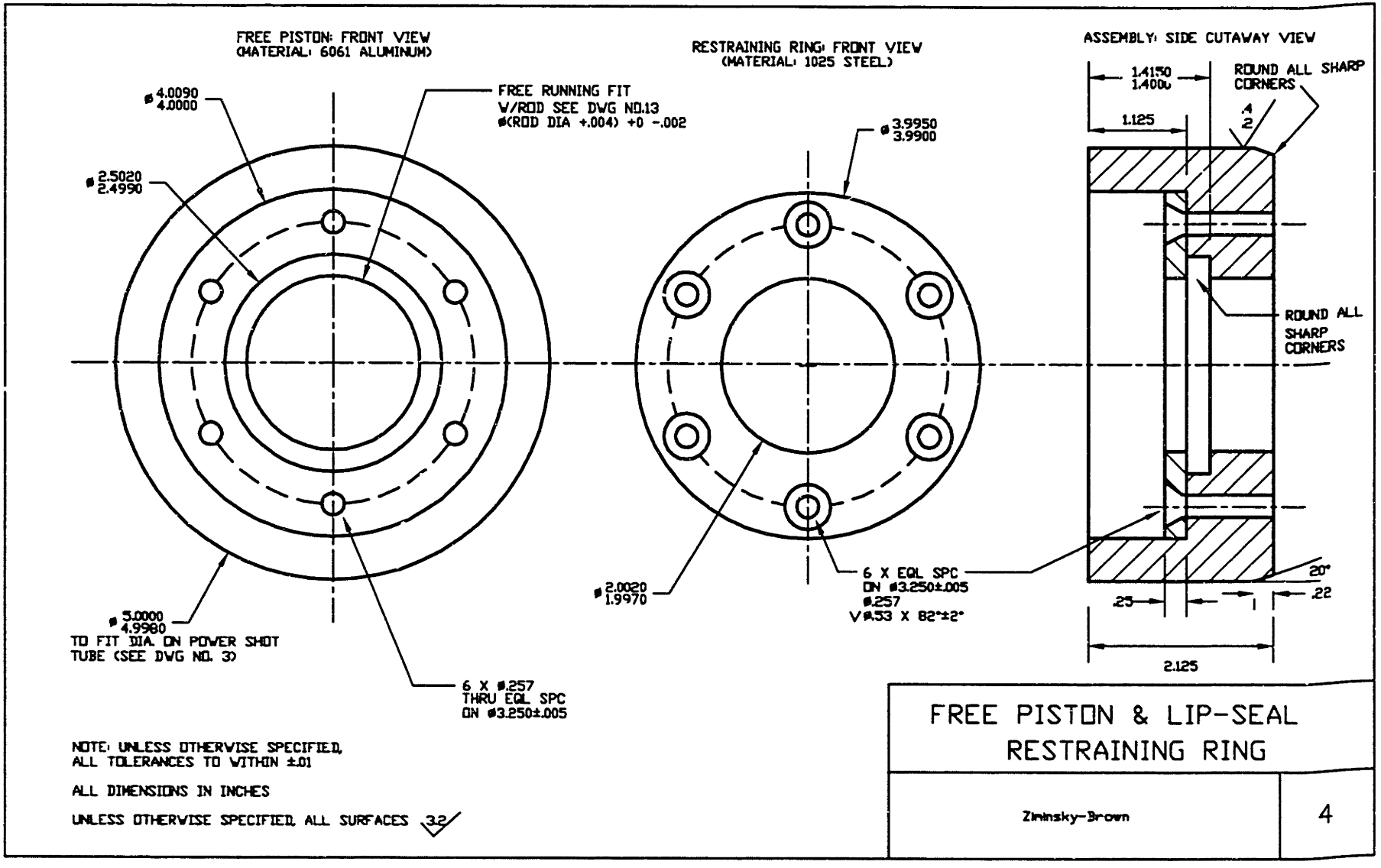
FREE PISTON: FRONT VIEW
(MATERIAL: 6061 ALUMINUM)
ø4.0090
4.0000
FREE RUNNING FIT
W/ROD SEE DWG NO.13
ø(ROD DIA +.004) +0 -.002
ø2.5020
2.4990
ø5.0000
4.9980
TO FIT DIA. ON POWER SHOT
TUBE (SEE DWG NO. 3)
6 X ø.257
THRU EQL SPC
ON ø3.250±.005
RESTRAINING RING: FRONT VIEW
(MATERIAL: 1025 STEEL)
ø3.9950
3.9900
ø2.0020
1.9970
6 X EQL SPC
ON ø3.250±.005
ø.257
V ø.53 X 82°±2°
ASSEMBLY: SIDE CUTAWAY VIEW
1.4150
1.4000
1.125
ROUND ALL SHARP
CORNERS
.4
.2
ROUND ALL
SHARP
CORNERS
20°
.25
1
.22
2.125
NOTE: UNLESS OTHERWISE SPECIFIED,
ALL TOLERANCES TO WITHIN ±.01
ALL DIMENSIONS IN INCHES
UNLESS OTHERWISE SPECIFIED, ALL SURFACES 32
FREE PISTON & LIP-SEAL
RESTRAINING RING
Zminsky-Brown
4

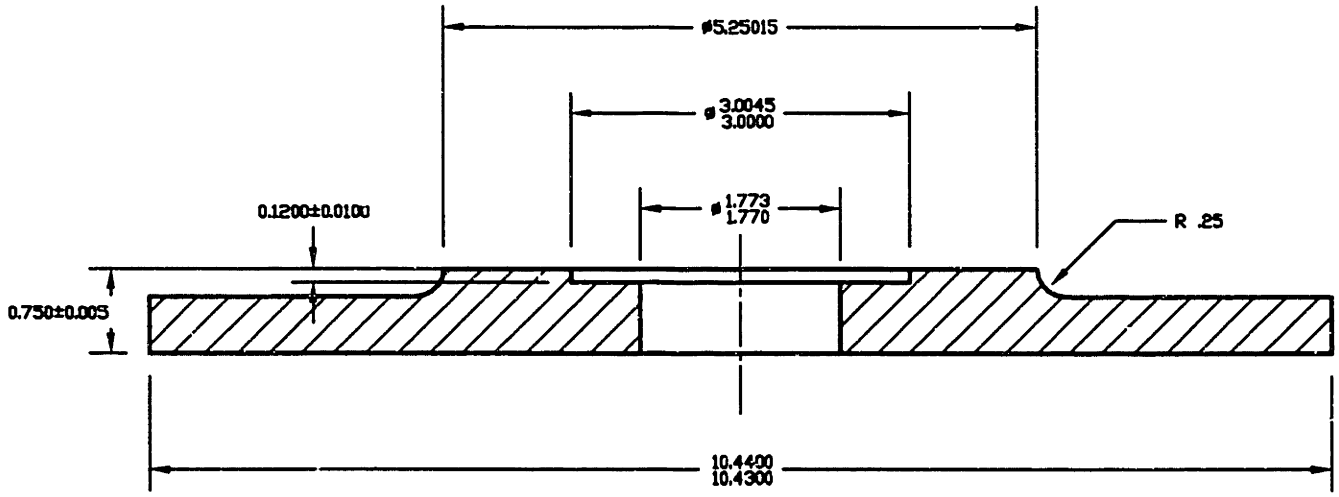

MATERIAL: 6061 ALUMINUM

ALL SURFACES 32

ALL DIMENSIONS IN INCHES

FIXED PISTON	
Zinnsky-Brown	5

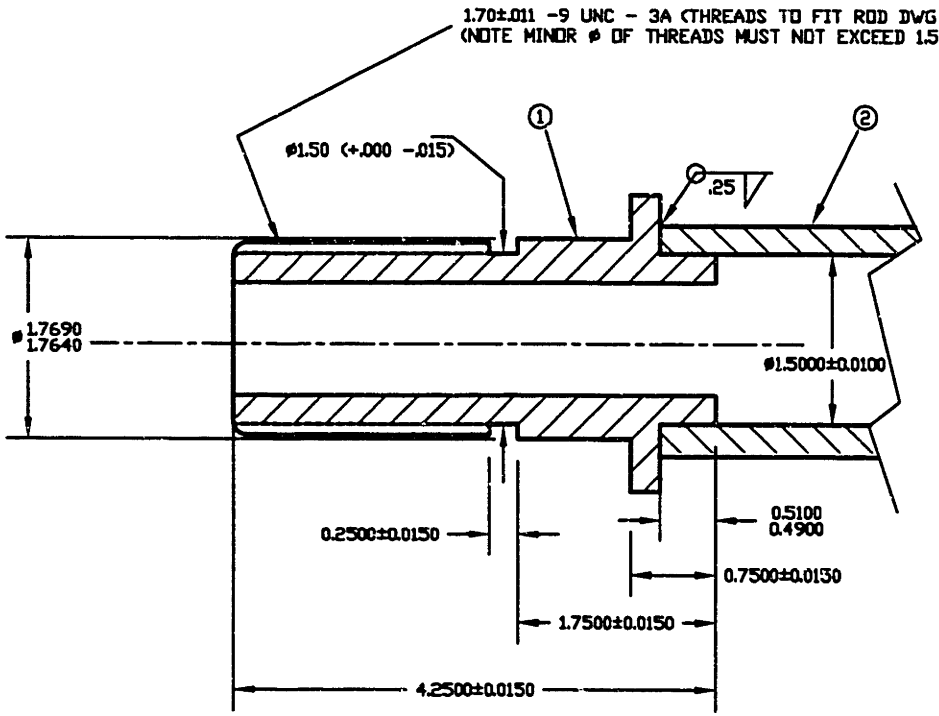

SECTION AA

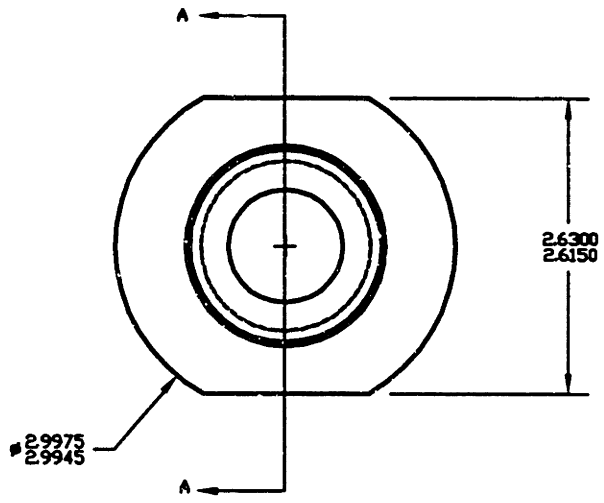

MATERIAL: 4140 STEEL

ALL DIMENSIONS IN INCHES

ALL SURFACES 32

① ROD-CONNECTING STUD: MACHINE AFTER WELDING TO ②

② FRONT END OF ROD: SEE DWG NO. 13

ROD-CONNECTION STUD

Zaninsky-Brown

6

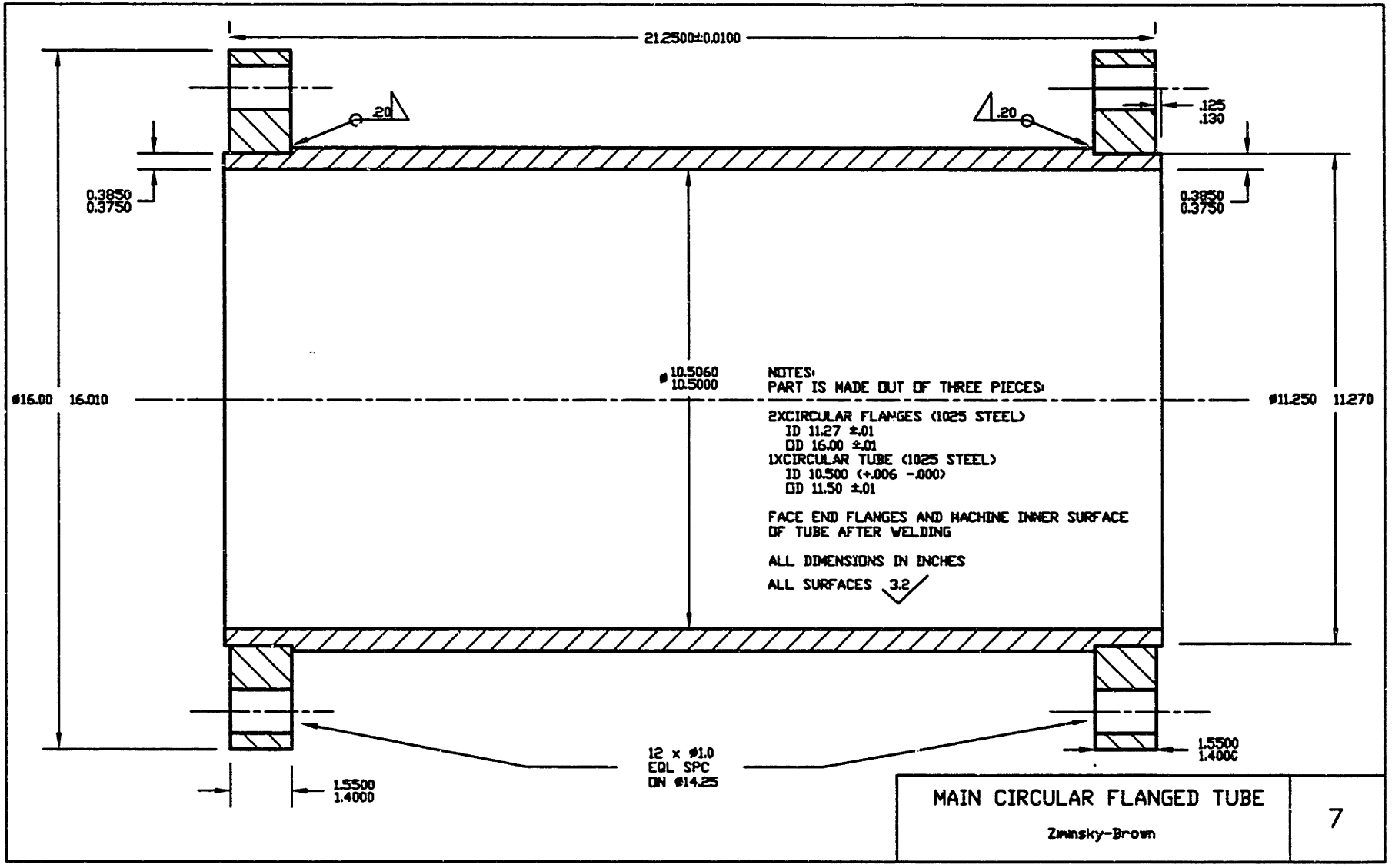
21.2500±0.0100
.20
.20
.125
.130
0.3850
0.3750
0.3850
0.3750
ø16.00
16.010
ø 10.5060
10.5000
ø11.250
11.270
NOTES:
PART IS MADE OUT OF THREE PIECES:
2XCIRCULAR FLANGES (1025 STEEL)
ID 11.27 ±.01
OD 16.00 ±.01
1XCIRCULAR TUBE (1025 STEEL)
ID 10.500 (+.006 -.000)
OD 11.50 ±.01
FACE END FLANGES AND MACHINE INNER SURFACE
OF TUBE AFTER WELDING
ALL DIMENSIONS IN INCHES
ALL SURFACES 3.2
12 x ø1.0
EQL SPC
ON ø14.25
1.5500
1.4000
1.5500
1.4000
MAIN CIRCULAR FLANGED TUBE
Zimsky-Brown
7

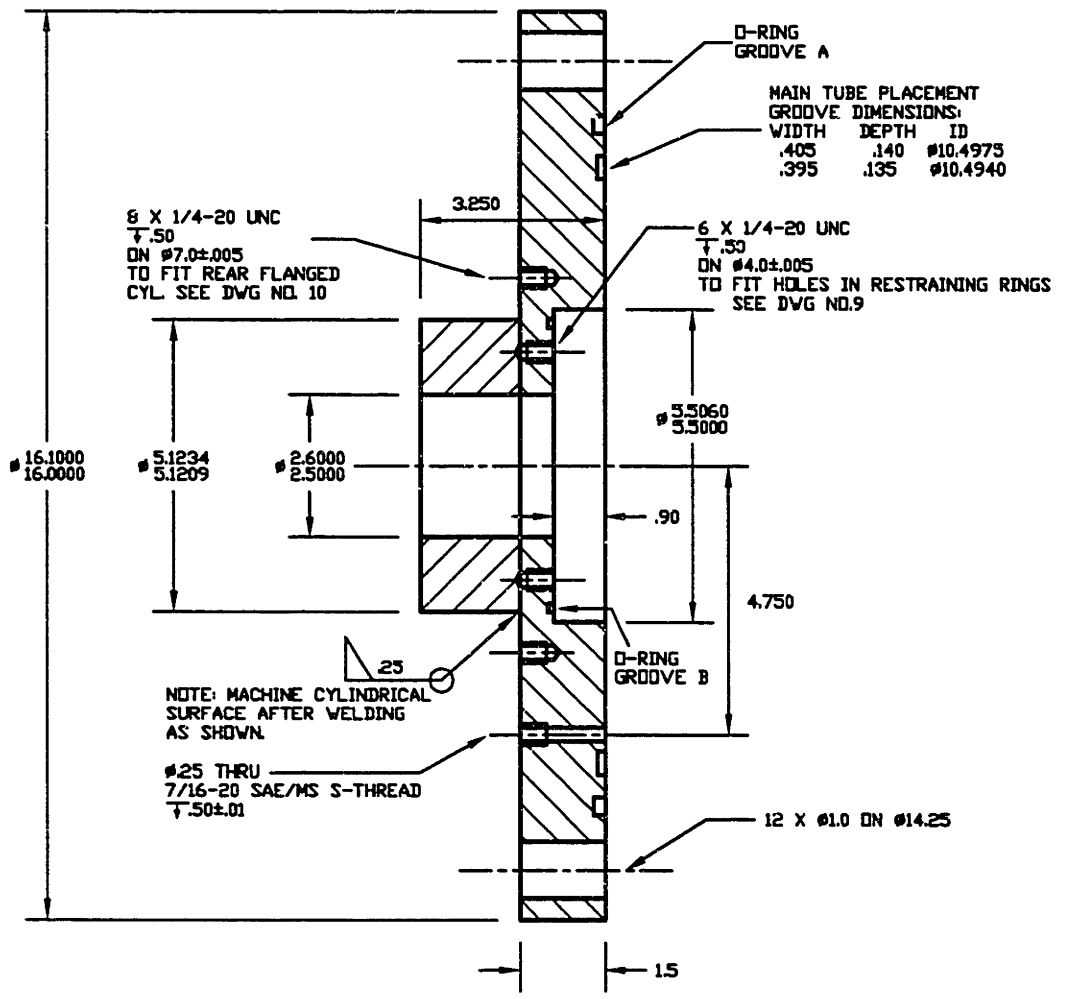

O-RING GROOVE	WIDTH	DEPTH	ID
A	.308 +.002 -.003	.205 +.006 -.004	ø11.975 ±.060
B	.160 ±.003	.104 ±.003	ø4.984 ±.035

FOR DETAIL OF O-RING GROOVE:
SEE DATA SHEET FIG. A FOR GROOVE A
AND FIG. B FOR GROOVE B.

NOTE: UNLESS OTHERWISE INDICATED,
ALL TOLERANCES TO ±.010

ALL DIMENSIONS IN INCHES

ALL MACHINING SHOULD BE DONE
AFTER WELDING.

ALL SURFACES 3.2

REAR CIRCULAR FLANGE

Zwinsky-Brown

8

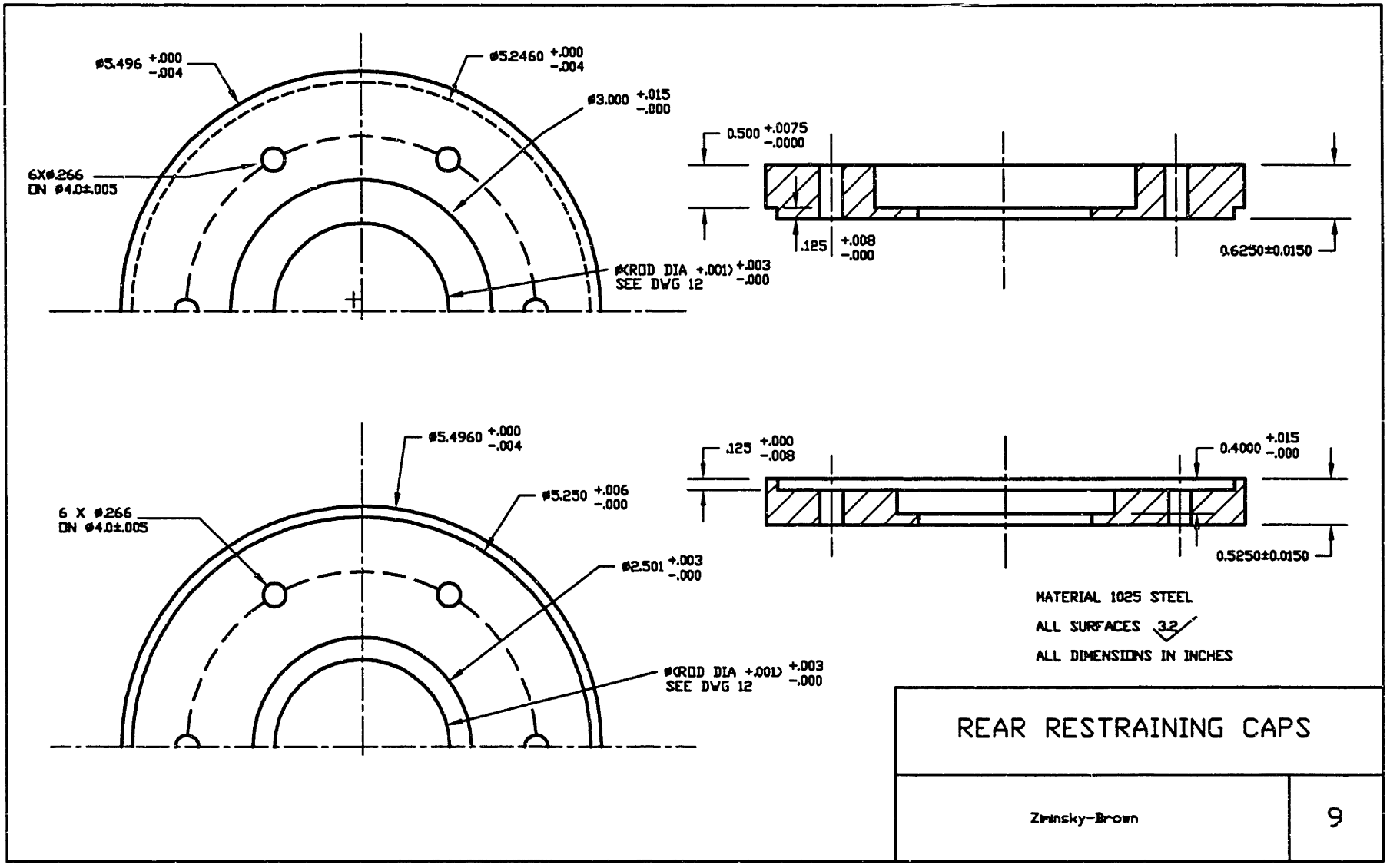
ø5.496 +.000 -.004
ø5.2460 +.000 -.004
ø3.000 +.015 -.000
6Xø.266 ON ø4.0±.005
ø(ROD DIA +.001) +.003 -.000 SEE DWG 12
0.500 +.0075 -.0000
.125 +.008 -.000
0.6250±0.0150
ø5.4960 +.000 -.004
ø5.250 +.006 -.000
6 X ø.266 ON ø4.0±.005
ø2.501 +.003 -.000
ø(ROD DIA +.001) +.003 -.000 SEE DWG 12
.125 +.000 -.008
0.4000 +.015 -.000
0.5250±0.0150
MATERIAL 1025 STEEL
ALL SURFACES 3.2
ALL DIMENSIONS IN INCHES
REAR RESTRAINING CAPS
Zmmsky-Brown
9

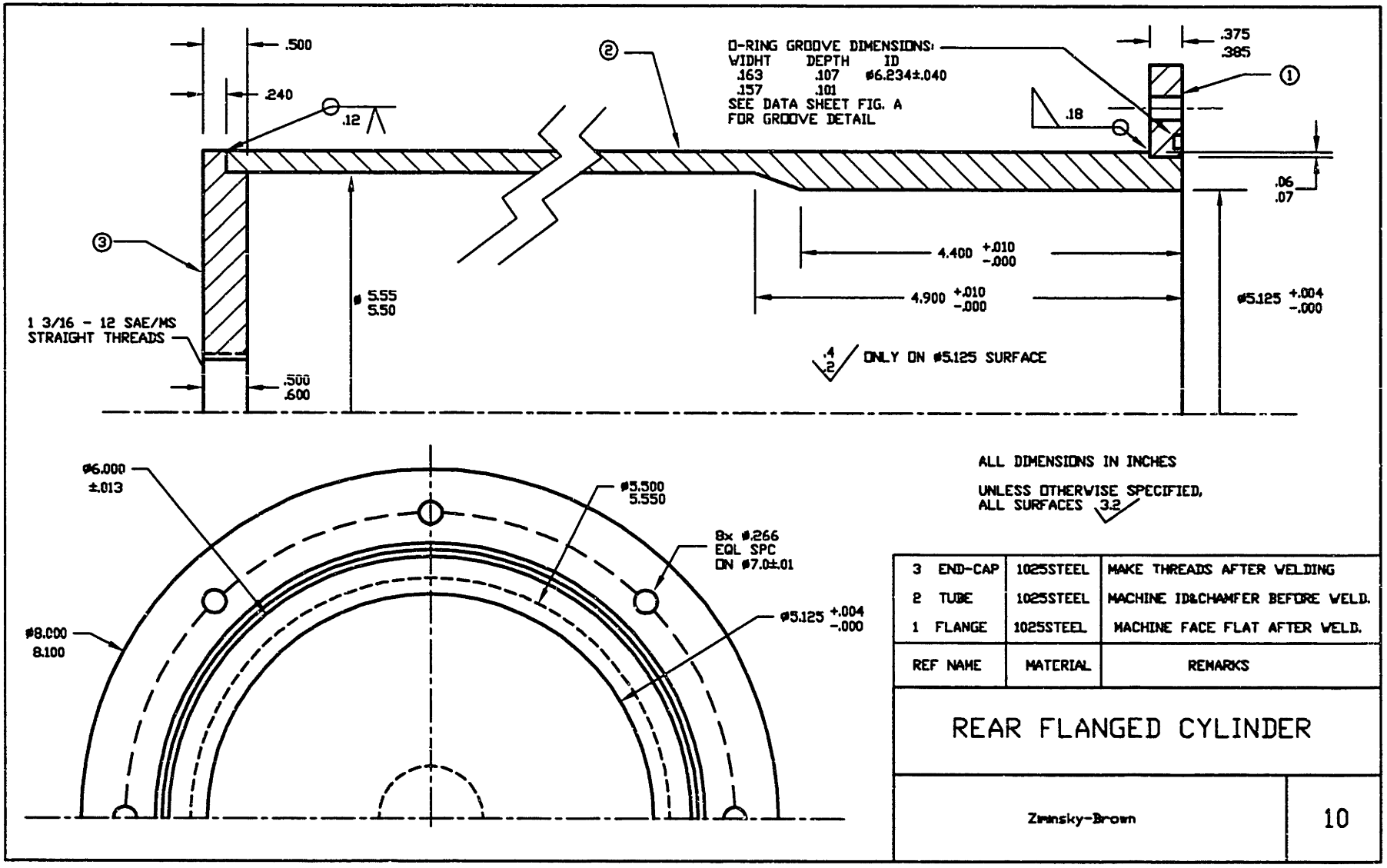

REF NAME	MATERIAL	REMARKS
3 END-CAP	1025STEEL	MAKE THREADS AFTER WELDING
2 TUBE	1025STEEL	MACHINE ID&CHAMFER BEFORE WELD.
1 FLANGE	1025STEEL	MACHINE FACE FLAT AFTER WELD.

REAR FLANGED CYLINDER

Zimsky-Brown

10

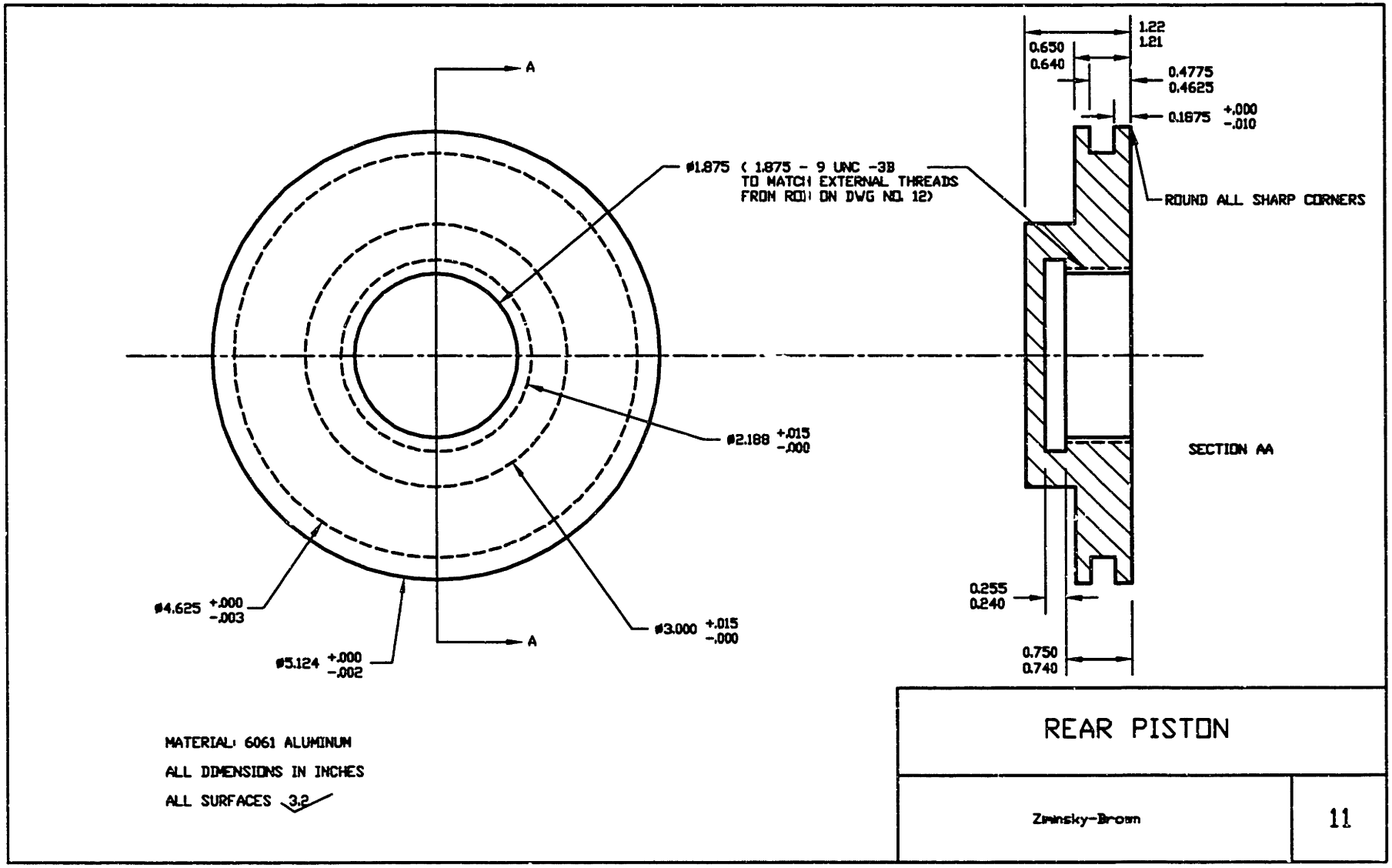
A
A
ø1.875 (1.875 - 9 UNC -3B
TO MATCH EXTERNAL THREADS
FROM ROD ON DWG NO. 12)
ø2.188 +.015 -.000
ø4.625 +.000 -.003
ø5.124 +.000 -.002
ø3.000 +.015 -.000
1.22
1.21
0.650
0.640
0.4775
0.4625
0.1875 +.000 -.010
ROUND ALL SHARP CORNERS
SECTION AA
0.255
0.240
0.750
0.740
MATERIAL: 6061 ALUMINUM
ALL DIMENSIONS IN INCHES
ALL SURFACES 3.2
REAR PISTON
Zmmsky-Brown
11

SECTION BB

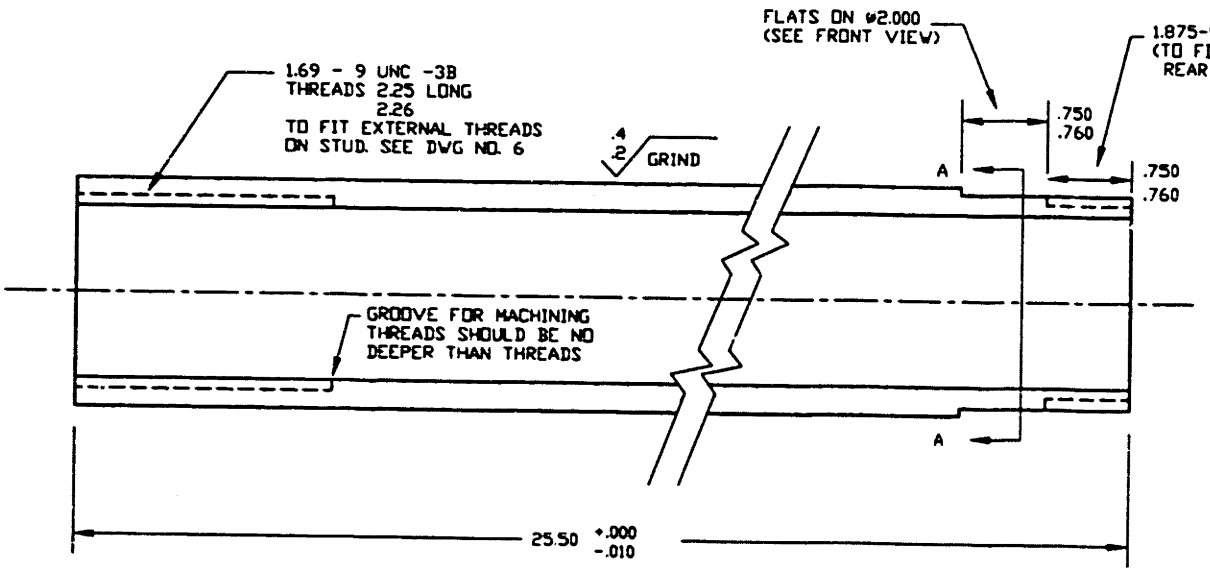

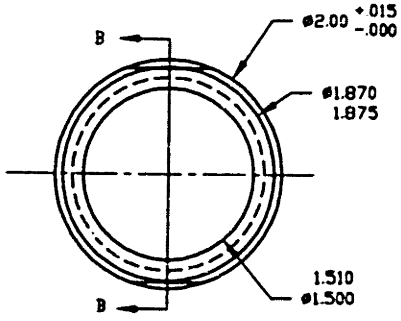

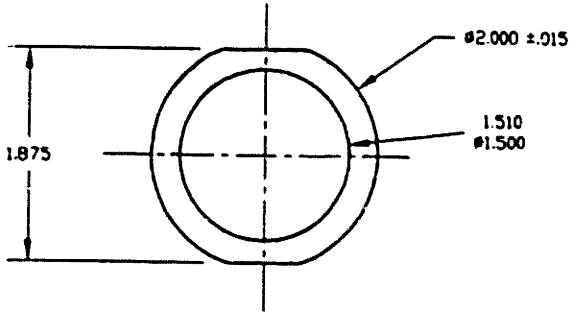

SECTION AA

MATERIAL: 4130 ASTM STEEL

ALL DIMENSIONS IN INCHES

OUTER SURFACE SHOULD BE
GROUND AFTER MACHINING THREADS

REAR SECTION ACTUATOR ROD	
Zmnsky-Brown	12

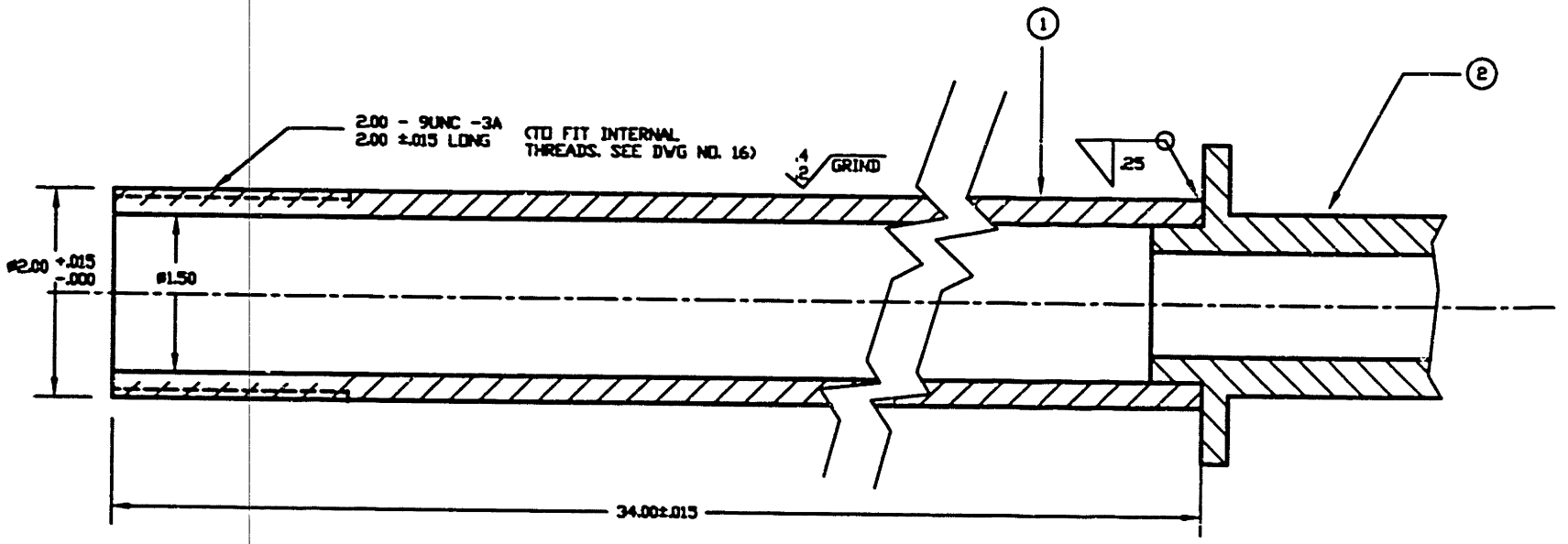

① FRONT END OF ROD
OD ø2.000±.001
ID ø1.50±.01

② ROD CONNECTING STUD
SEE DWG NO. 6

ALL DIMENSIONS IN INCHES

WELD SUTD TO ROD BEFORE MACHINING EITHER

FRONT SECTION ACTUATOR ROD	
Zwansky-Brown	13

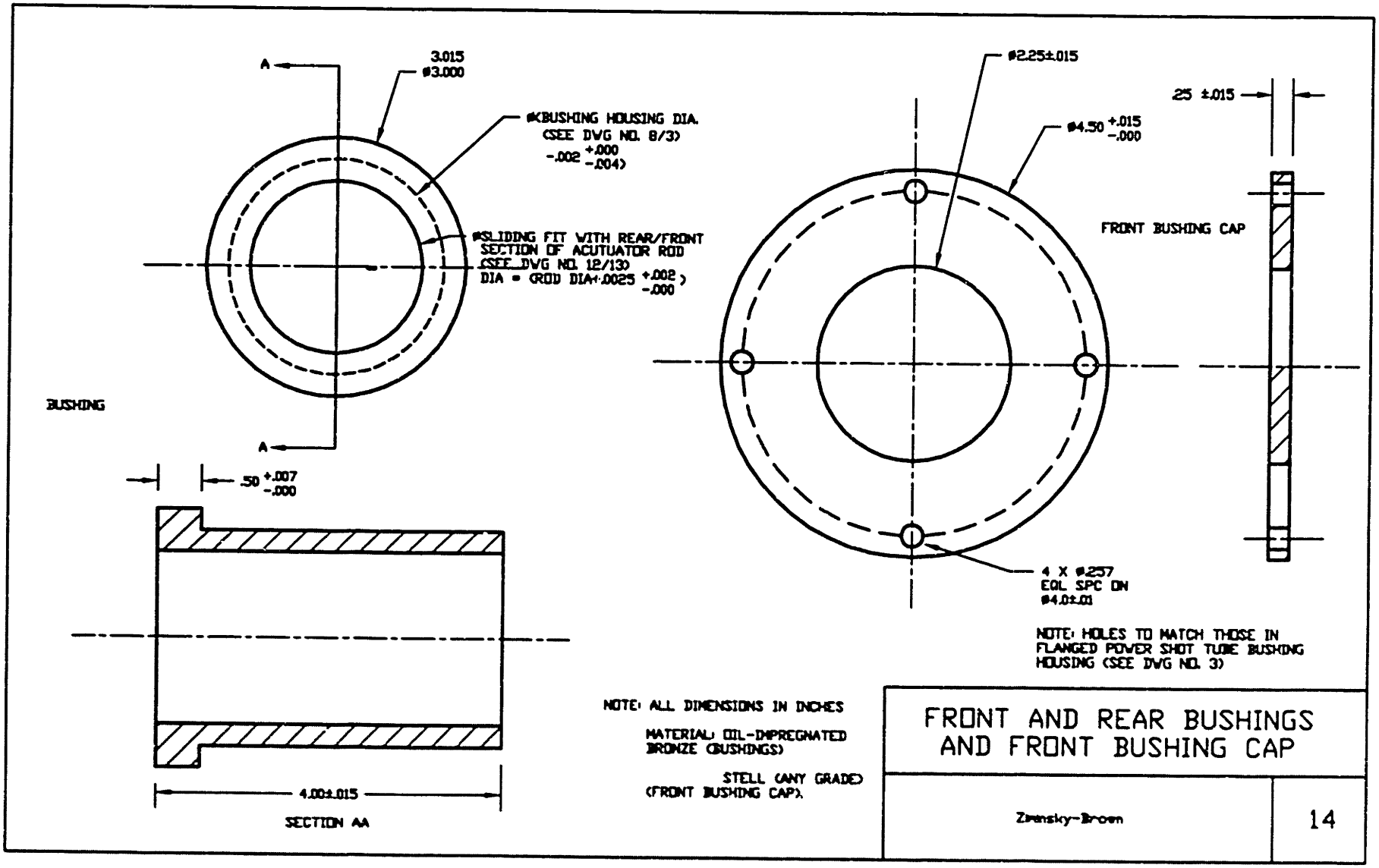
3.015
ø3.000
A
ø(BUSHING HOUSING DIA.
(SEE DWG NO. 8/3)
-.002 +.000
-.004)
ø(SLIDING FIT WITH REAR/FRONT
SECTION OF ACUTUATOR ROD
(SEE DWG NO. 12/13)
DIA = (ROD DIA+.0025 +.002
-.000)
BUSHING
A
.50 +.007
-.000
4.00±.015
SECTION AA
ø2.25±.015
ø4.50 +.015
-.000
.25 ±.015
FRONT BUSHING CAP
4 X ø.257
EQL SPC ON
ø4.0±.01
NOTE: HOLES TO MATCH THOSE IN
FLANGED POWER SHOT TUBE BUSHING
HOUSING (SEE DWG NO. 3)
NOTE: ALL DIMENSIONS IN INCHES
MATERIAL: OIL-IMPREGNATED
BRONZE (BUSHINGS)
STELL (ANY GRADE)
(FRONT BUSHING CAP).
FRONT AND REAR BUSHINGS
AND FRONT BUSHING CAP
Zwansky-Brown
14

Appendix D

Valve Drawings 2

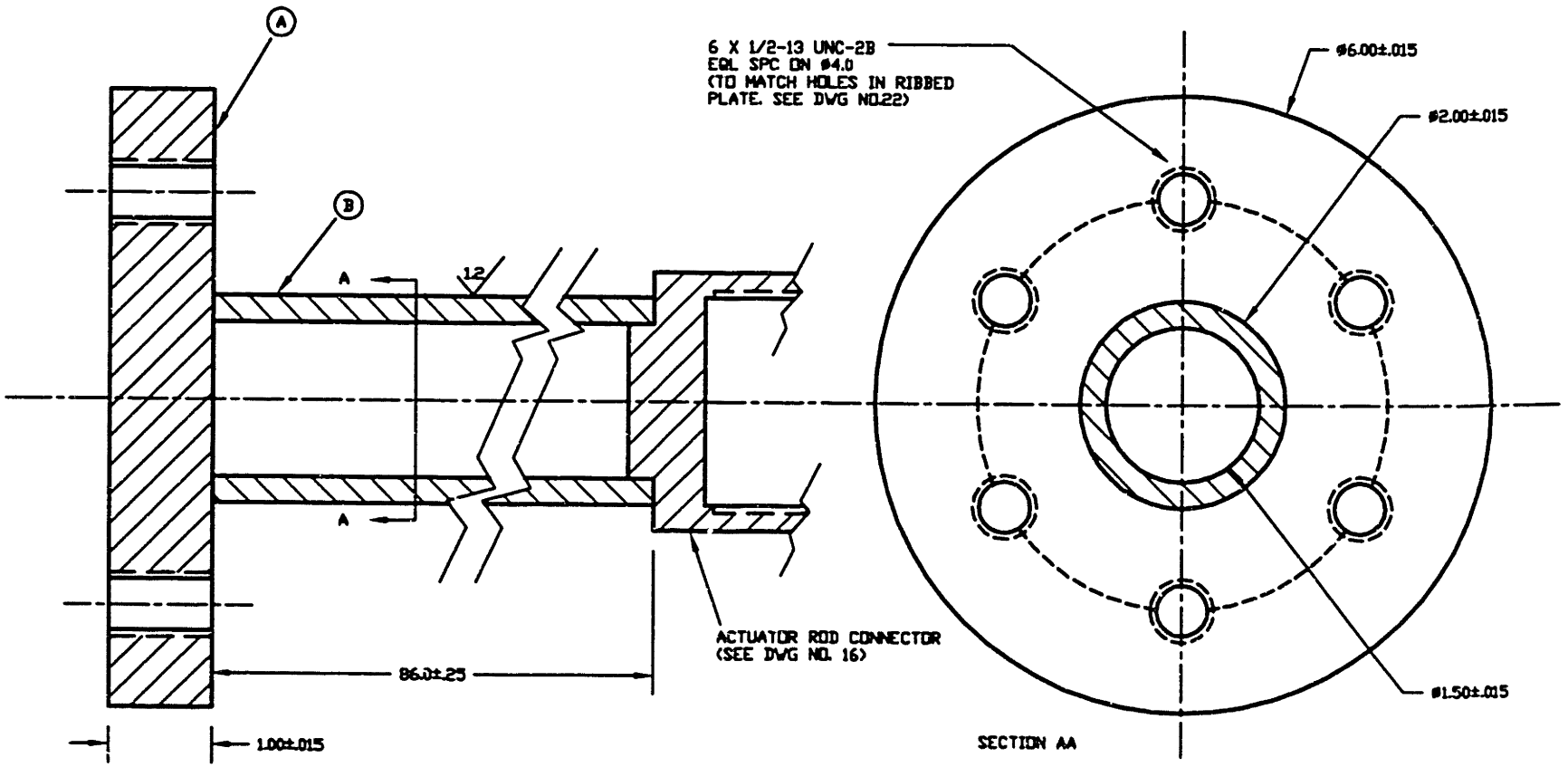

ALL DIMENSIONS IN INCHES

ALL SURFACES 32 UNLESS OTHERWISE SPECIFIED

MATERIAL: STEEL (ANY GRADE WELDABLE TO PROVIDED ROD)

NOTE: DO NOT WELD PART A TO PART B. MAKE FLANGE (PART A) SUPPLY TANK ROD (PART B) SEPARATELY.

SUPPLY TANK ROD: FLANGE END

Zmansky-Brown

15

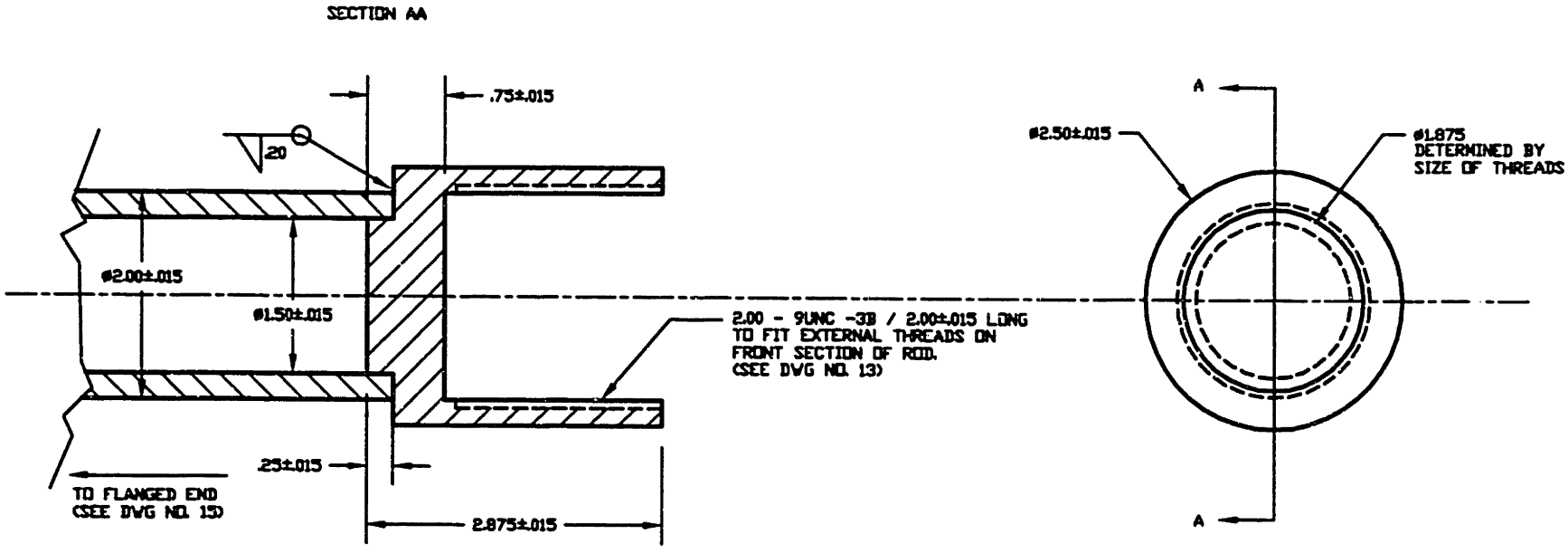

ALL DIMENSIONS IN INCHES

ALL SURFACES 32

MATERIAL: 1025 STEEL

ACTUATOR ROD CONNECTOR END	
Zmansky-Brown	16

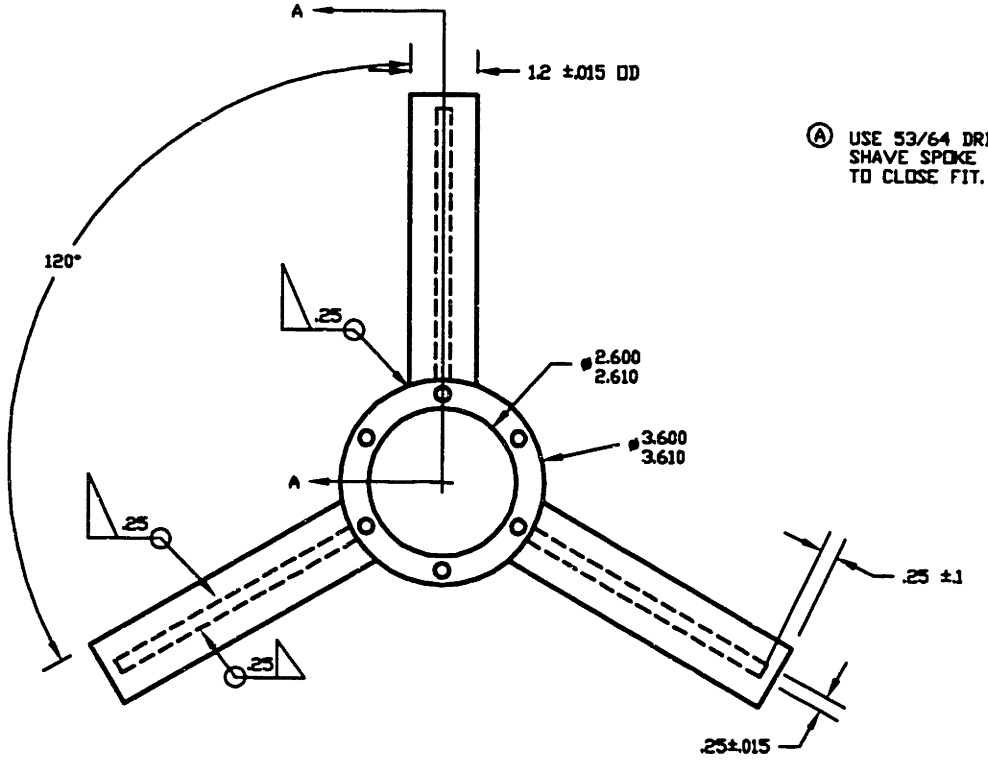

Ⓐ USE 53/64 DRILL SIZE (.8281) SHAVE SPOKE (DWG NO. 20) TO CLOSE FIT.

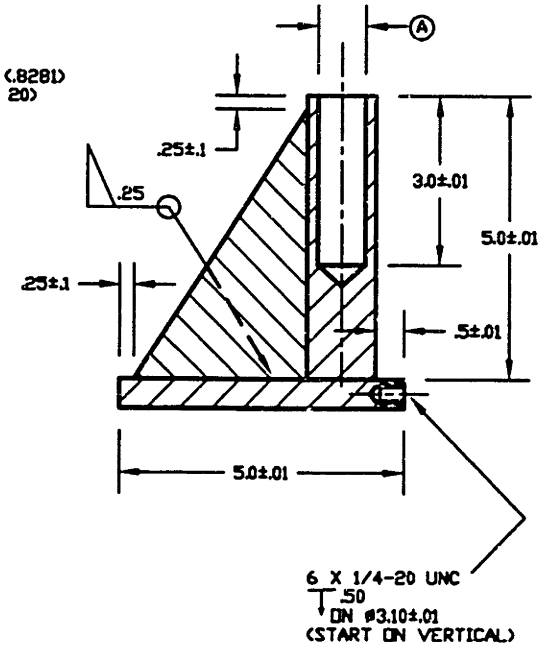

ALL DIMENSIONS IN INCHES

ALL SURFACES 3.2

MATERIAL: 1025 STEEL

SUPPORT EYE	
Zimmsky-Brown	17

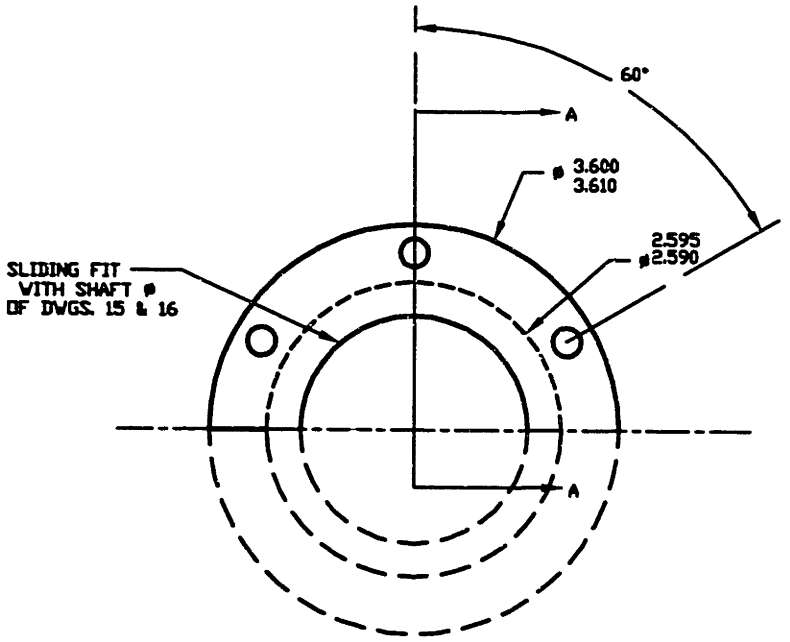

BUSHING FITS SUPPORT EYE
SEE DWG NO. 17

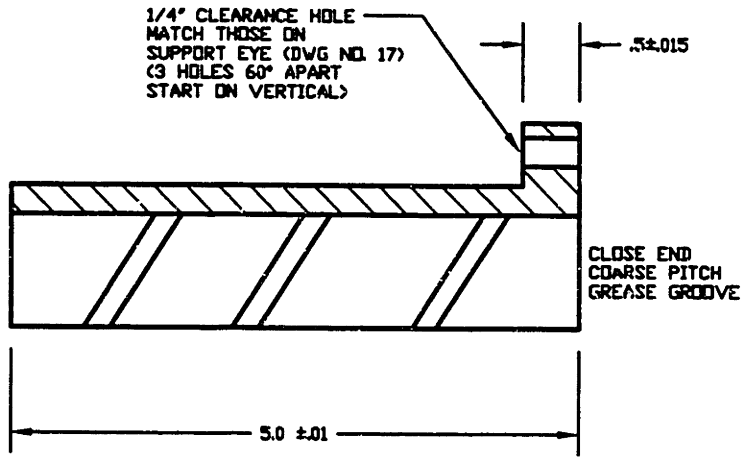

SECTION AA

QUANTITY: 2

ALL DIMENSIONS IN INCHES

ALL SURFACES 3.2

MATERIAL: 1025 STEEL

SPLIT BUSHING

Zimansky-Brown

18

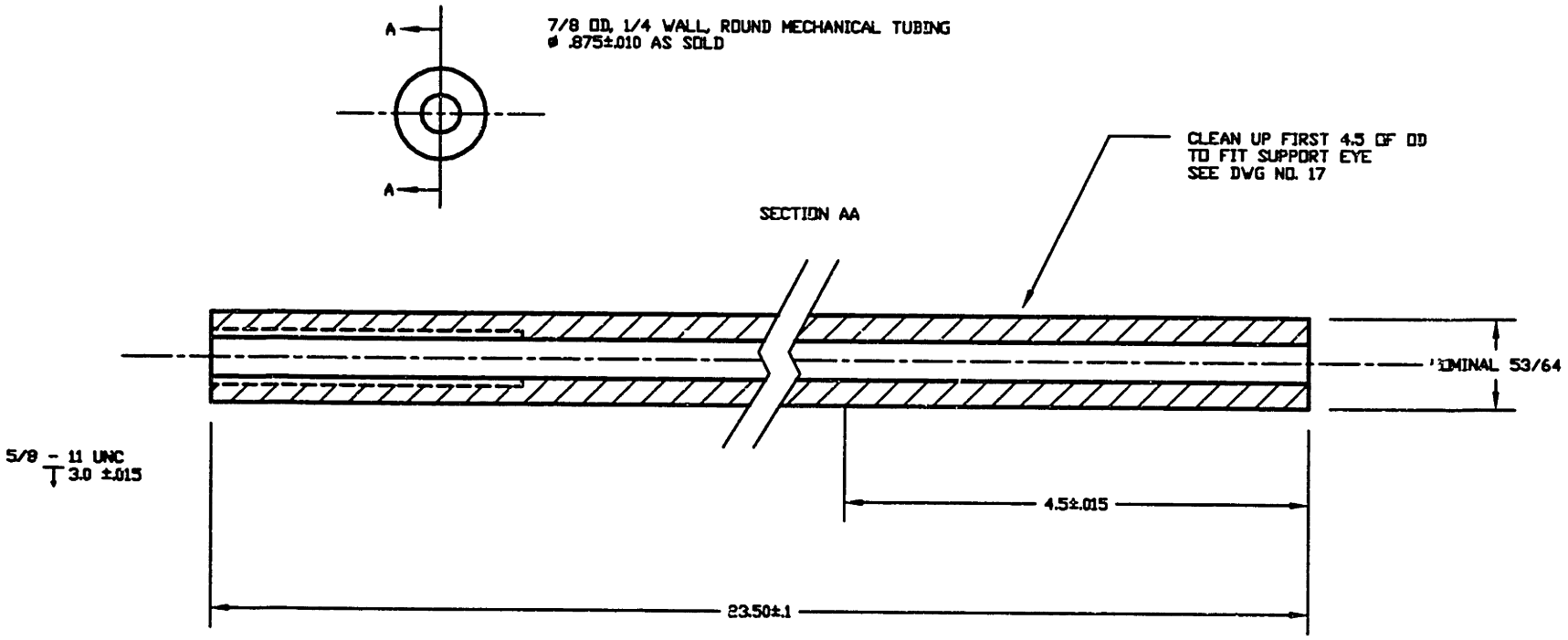

QUANTITY 3

ALL DIMENSIONS IN INCHES

ALL SURFACES 3.2

MATERIAL: 1025 STEEL

SUPPORT SPOKE	
Zmansky-Brown	19

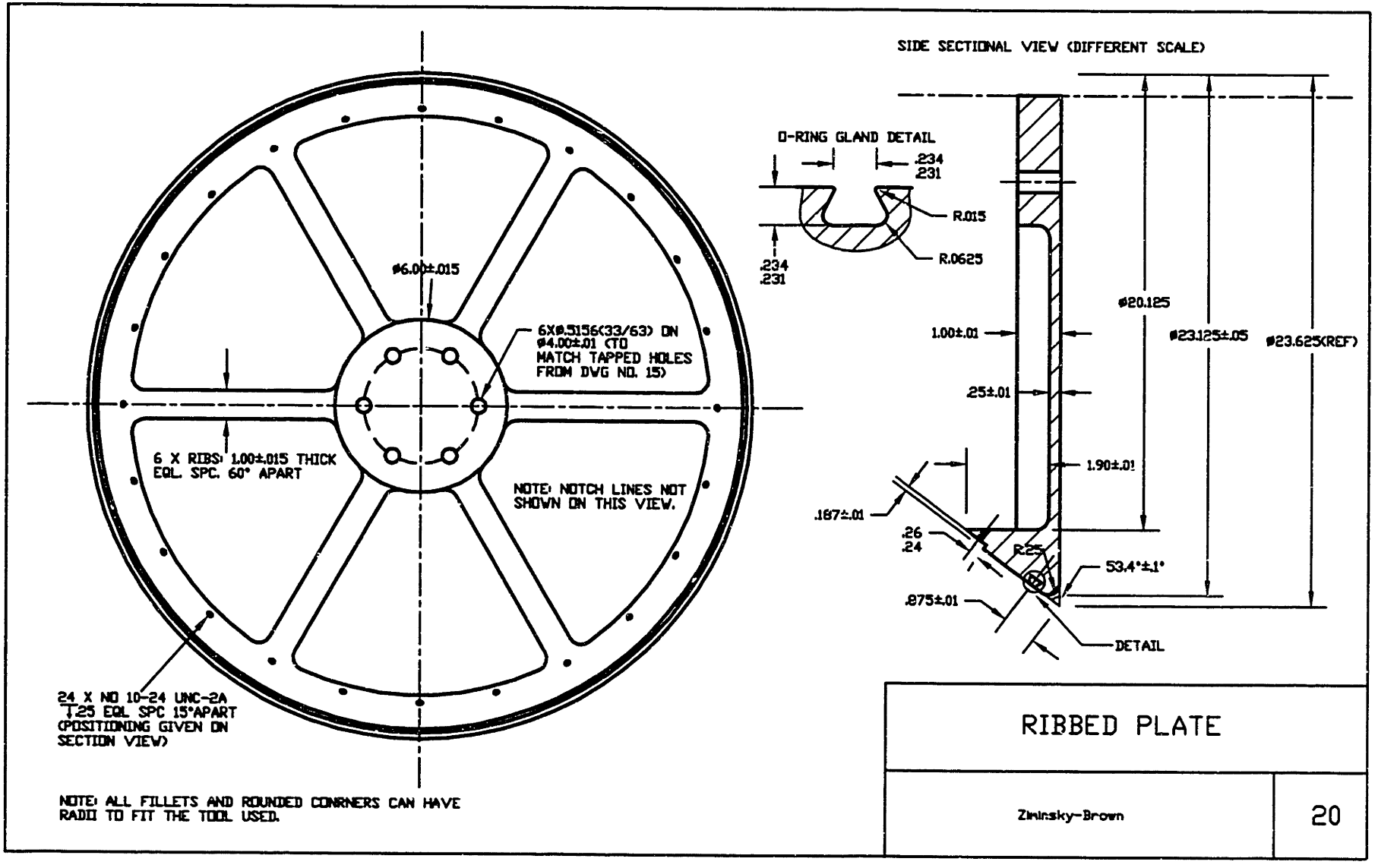
SIDE SECTIONAL VIEW (DIFFERENT SCALE)
O-RING GLAND DETAIL
.234
.231
R.015
R.0625
.234
.231
ø6.00±.015
6XØ.5156(33/63) ON
ø4.00±.01 (TO
MATCH TAPPED HOLES
FROM DWG NO. 15)
6 X RIBS: 1.00±.015 THICK
EQL. SPC. 60° APART
NOTE: NOTCH LINES NOT
SHOWN ON THIS VIEW.
24 X NO 10-24 UNC-2A
T.25 EQL SPC 15°APART
(POSITIONING GIVEN ON
SECTION VIEW)
NOTE: ALL FILLETS AND ROUNDED CORNERS CAN HAVE
RADII TO FIT THE TOOL USED.
ø20.125
ø23.125±.05
ø23.625(REF)
1.00±.01
.25±.01
1.90±.01
.187±.01
.26
.24
R.25
53.4°±.1°
.875±.01
DETAIL
RIBBED PLATE
Zminsky-Brown
20

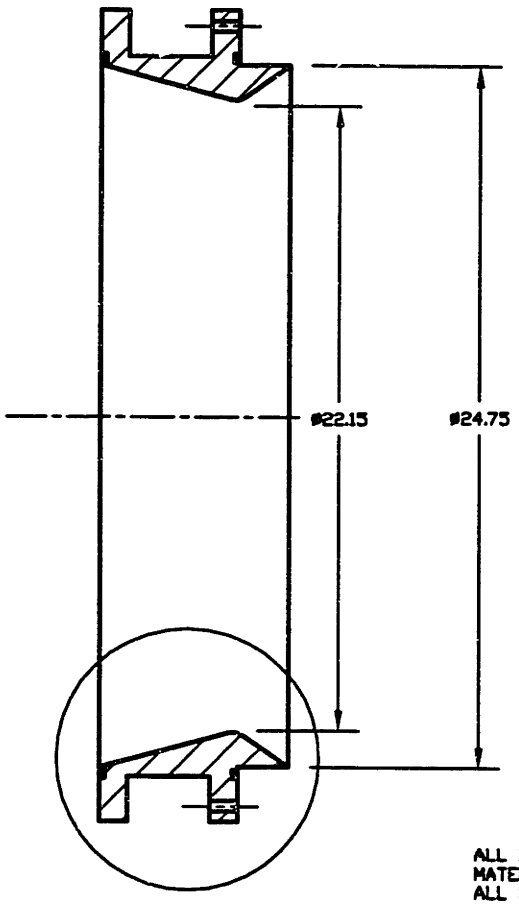

DETAIL A

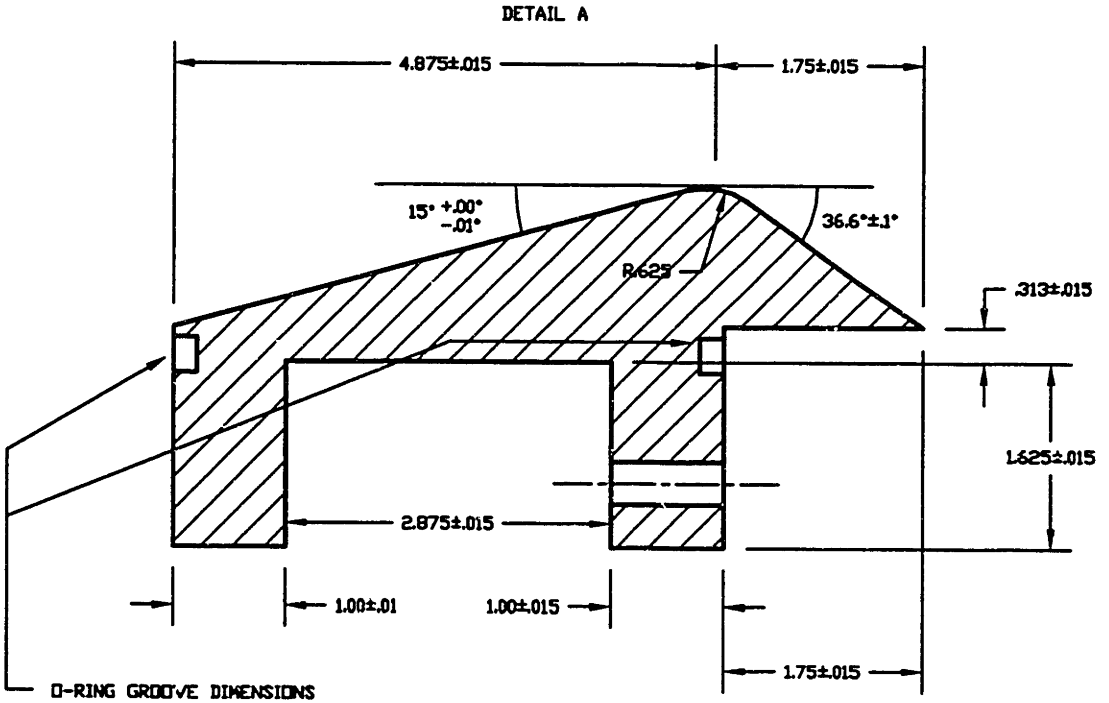

O-RING GROOVE DIMENSIONS

ID	WIDTH	DEPTH
24.940 +.060 -.000	.310	.211 .201

ALL DIMENSIONS IN INCHES
MATERIAL: 6061 ALUMINUM
ALL SURFACES 3.2

THROAT CONTRACTION RING

Zwinsky-Brown

21